Understanding of Cutting Tool Edge Preparations and their Impacts on Machining Process Performance

by

Zakaria AHMED M TAGIURI

MANUSCRIPT-BASED THESIS PRESENTED TO ÉCOLE DE TECHNOLOGIE SUPÉRIEURE IN PARTIAL FULFILLEMENT OF THE REQUIREMENTS FOR THE DEGREE OF DOCTOR OF PHILOSOPHY PH.D.

MONTRÉAL, AUGUST 23 th, 2024

ECOLE DE TECHNOLOGIE SUPÉRIEURE
UNIVERSITÉ DU QUÉBEC

BOARD OF EXAMINERS THESIS PH.D.

THIS THESIS HAS BEEN EVALUATED

BY THE FOLLOWING BOARD OF EXAMINERS

Mr. Victor Songmene, Thesis Supervisor
Department of Mechanical Engineering at École de Technologie Supérieure

Mr. Thien -My. Dao, Thesis Co-Supervisor
Department of Mechanical Engineering at École de Technologie Supérieure

Mr. Michel Rioux, President of the Board of Examiners
Department of Systems Engineering at École de Technologie supérieure

Mr. Lucas Hof, Member of the jury
Department of Mechanical Engineering at École de Technologie Supérieure

Mr. Nabil Nahas, External Evaluator
Department of Administration at Université de Moncton

THIS THESIS WAS PRENSENTED AND DEFENDED

IN THE PRESENCE OF A BOARD OF EXAMINERS AND PUBLIC

MONTRÉAL, AUGUST 6 th, 2024

AT ÉCOLE DE TECHNOLOGIE SUPÉRIEURE

ACKNOWLEDGMENT

First, I would like to express my sincere gratitude to the director and supervisor of my doctoral research, the professor Victor Songmene for his guidance, support and availability during my research study. Moreover, sincere appreciation is also expressed to my co-supervisor, the professor Thien-My Dao for his relevant advises and encouragements.

I would also like to thank the members of my jury committee, Professor Michel Rioux Professor Lucas Hof, Professor Nabil Nahas for their acceptance to valuate my present thesis.

I also wish to thank the Ministry of Higher Education and Scientific Research in Libya in collaboration with the Canadian Bureau for International Education (CBIE) for their financial support as Ph.D. scholarship.

Finally, and most importantly, special thanks to my family. Words cannot express how grateful I am to my beloved mother, brothers and sisters for their affection, endless love and encouragement. They have always been incenting me to strive towards my goal and have been supporting me, unconditionally and continuously, throughout my life.

Understanding of Cutting Tool Edge Preparations and Their Impacts on Machining Process Performance

Zakaria AHMED M TAGIURI

RESUMÉ

La préparation des arêtes des outils de coupe est considérée comme l'une des technologies importantes récemment développées pour le micro-usinage en raison de son impact sur les forces et les contraintes de coupe, la durée de vie de l'outil, la distribution de la température et l'intégrité de la surface. Les préparations d'arêtes d'outils les plus fréquentes sont les arêtes rondes, les arêtes chanfreinées et les arêtes vives. Il n'est pas facile de déterminer, pour un matériau de pièce donné, la préparation appropriée de l'arête de l'outil ou les paramètres d'usinage à utiliser, car ils sont interdépendants et affectent conjointement plusieurs indicateurs de performance de l'usinage. L'objectif de cette thèse est de mener une étude sur les effets de trois géométries d'arêtes de coupe et des paramètres de coupe sur les caractéristiques d'usinage telles que la température de coupe, la contrainte effective, l'épaisseur du copeau et l'usure de l'outil. Les géométries d'arêtes de coupe étudiées sont le rond, le chanfrein et le tranchant. Cette étude a consisté à simuler le processus de coupe orthogonale de l'acier AISI 1045 à l'aide du logiciel DEFORM à éléments finis 2D. Les tests de simulation numérique ont été réalisés à l'aide d'un plan d'expériences (DOE) basé sur un réseau orthogonal de Taguchi qui comprenait différents paramètres de l'arête de l'outil tels que le rayon du nez, la largeur du chanfrein, l'angle du chanfrein, l'angle vif et les paramètres de coupe tels que la vitesse de coupe, la vitesse d'avance.

Ce travail de recherche est divisé en trois étapes. Dans la première étape, un modèle de simulation 2D basé sur l'analyse par éléments finis a été développé pour prédire les effets du rayon du nez de l'outil avec de petites et grandes échelles et des paramètres de coupe sur la température de coupe, la contrainte de coupe et l'usure de l'outil. Les résultats obtenus ont montré que la température de coupe, la contrainte et l'usure de l'outil présentaient une dépendance approximativement linéaire avec le rayon du nez de l'outil.

Dans un deuxième temps, des tests numériques ont été réalisés pour étudier les effets de la largeur du chanfrein, de l'angle du chanfrein, de l'angle vif, de la vitesse de coupe, de la vitesse d'avance et de leurs interactions sur la température de coupe, la contrainte effective et la profondeur d'usure. Les résultats obtenus ont été évalués statistiquement à l'aide de l'analyse de la variance (ANOVA).

Enfin, dans la troisième étape, les facteurs significatifs de la géométrie des arêtes et leurs interactions avec les paramètres d'usinage ont été déterminés ; ensuite, des comparaisons par simulation numérique ont été effectuées afin de déterminer les paramètres optimaux pour obtenir une bonne préparation de l'outil de coupe entre les arêtes rondes, les arêtes chanfreinées et les arêtes vives, afin d'améliorer les performances du processus de coupe.

Mots clés: Usinage, coupe orthogonale, préparation de l'arête de l'outil, simulation, performance du procédé, acier AISI 1045.

Understanding of Cutting Tool Edge Preparations and Their Impacts on Machining Process Performance

Zakaria AHMED M TAGIURI

ABSTRACT

The cutting tool edge preparation is considered as one of the important technologies that were recently developed for micro-machining due to its impact on cutting forces and stresses, tool life, temperature distribution and surface integrity. The most frequent tool edge preparations include round edge, chamfered edge and sharp edge. It is not easy to determine, for a given workpiece material, the appropriate tool edge preparation or the machining parameters that should be used, as they are interrelated and affect jointly several machining performance indicators. The objective of this thesis is to conduct a research study on the effects of three cutting tool edge geometries and the cutting parameters on the machining characteristics such as cutting temperature, effective stress, chip thickness and tool wear. The cutting tool edge geometries studied are round, chamfer and sharp. This study consisted of simulating the orthogonal cutting process of AISI 1045 steel using 2D finite elements DEFORM software. The numerical simulation tests were performed using a design of experiments (DOE) based on Taguchi orthogonal array design which included different tool edge parameters such as nose radius, chamfer width, chamfer angle, sharp angle and the cutting parameters such as cutting speed, feed rate.

This research work is divided into three stages. In the first stage, a 2D simulation model based on finite element analysis was developed to predict the effects of the tool nose radius with small and large scales and cutting parameters on cutting temperature, cutting stress and tool wear. The obtained results showed that cutting temperature, stress and tool wear presented approximately linear dependency with tool nose radius.

In the second stage, numerical tests were performed to investigate the effects of chamfer width, chamfer angle, sharp angle, cutting speed, feed rate and their interactions on cutting temperature, effective stress and wear depth. The obtained results were evaluated statistically using analysis of variance (ANOVA).

At the end, in the third stage, significant edge geometry factors and their interactions with machining parameters were determined; then, numerical simulation comparisons were made in order to determine the optimal parameters in order to get good cutting tool preparation between round, chamfer and sharp edges for a better cutting process performance.

Keywords: Machining, orthogonal cutting, tool edge preparation, simulation, process performance, AISI 1045 steel.

TABLE OF CONTENTS

Page

INTRODUCTION ……..1

CHAPTER 1 LITERATURE REVIEW 5
1.1 Introduction.....5
1.2 Cutting tool edge preparation overview.....5
1.2.1 Cutting tool edge preparation definition 5
1.2.2 Classification of tool edge preparation geometries..... 6
1.2.3 Factors influencing the cutting-edge geometry..... 7
1.2.4 Influence of cutting-edge preparation method on machining performance 9
1.2.5 Machining process performance evaluation methods..... 11
1.2.6 Summary of previous works on the impacts of cutting-edge preparation on machining process characteristics..... 17
1.3 Conclusion 19

CHAPTER 2 METHODOLOGY 23
2.1 Introduction.....23
2.2 Material of study 25
2.3 Design of experiment.....25
2.4 Numerical modeling.....25
2.5 Numerical simulations for optimal responses.....28
2.6 Conclusion 29

CHAPTER 3 A NUMERICAL MODEL FOR PREDICTING THE EFFECT OF TOOL NOSE RADIUS ON MACHINING PROCESS PERFORMANCE DURING ORTHOGONAL CUTTING OF 1045 STEEL 33
3.1 Introduction.....34
3.2 Numerical simulation model for orthogonal cutting analysis.....36
3.2.1 Material characterization 37
3.2.2 Numerical design planning 41
3.3 Numerical simulation results 42
3.3.1 Comparison of results between numerical simulations and experimental data from literature..... 51
3.3.2 Interactive effects between the cutting parameters and the tool geometries 53
3.4 Conclusions.....69

CHAPTER 4 NUMERICAL PREDICTION OF THE PERFORMANCE OF CHAMFERD AND SHARP CUTTING TOOLS DURING ORTHOGONAL CUTTING OF AISI 1045 STEEL.....71
4.1 Introduction.....72

4.2 Materials and methods 76
4.2.1 Material and machining process characterization 77
4.2.2 Finite element simulation model 77
4.2.3 Design of experiments 80
4.3 Results and discussion 85
4.3.1 Influence of Tool Geometry on Machining Process Performance 85
4.3.2 Analysis of variance (ANOVA) 94
4.3.3 Response surface analysis 99
4.3.4 Validation of Results 104
4.4 Conclusions 106

CHAPTER 5 COMPARATIVE EVALUATION OF THE PERFORMANCES OF HONED, CHAMFERED AND SHARP TOOLS IN ORTHOGONAL CUTTING OF AISI 1045 STEEL 109
5.1 Introduction 110
5.2 Materials and Methods 112
5.2.1 Cutting tool and workpiece materials 112
5.2.2 Cutting tool and workpiece designs 113
5.2.3 Numerical simulation tests characterization 114
5.2.4 Validation results 124
5.2.5 ANOVA and regression analysis 125
5.2.6 Response surface method analysis 147
5.3 Numerical determination of best output responses 151
5.4 Conclusions 153

GENERAL CONCLUSION 157

CONTRIBUTION ……..161

RECOMMENDATION 163

ANNEX I FACTORIAL DESIGN FOR ROUND GEOMETRY CUTTING TOOL 165

ANNEX II FACTORIAL DESIGN FOR CHAMFER GEOMETRY CUTTING TOOL ……..167

ANNEX III FACTORIAL DESIGN FOR SHARP GEOMETRY CUTTING TOOL.....169

APPENDIX I PUBLICATION LIST 171

LIST OF BIBLIOGRAPHICAL REFERENCES 173

LIST OF TABLES

Page

Table 1.1	Summary of research studies on influences of different tool edge geometries on orthogonal machining processes	18
Table 2.1	Typical chemical composition of AISI 1045 steel AZOM (2000)	25
Table 3.1	Thermal and physical properties of workpiece and tool materials	38
Table 3.2	Mechanical properties of workpiece and tool materials Zakaria (2019)	38
Table 3.3	Design for numerical simulations	42
Table 3.4	Comparison of numerical and experimental results for small tool nose radius	52
Table 3.5	Numerical and experimental results comparison for large tool nose radius	52
Table 4.1	Thermal properties of workpiece and tool materials	78
Table 4.2	Mechanical properties of workpiece and tool materials	78
Table 4.3	The constants of Johnson–Cook material model for AISI 1045 steel Jaspers et al (1998)	80
Table 4.4	Parametric design plan for the chamfer tool geometry numerical simulations	81
Table 4.5	Parametric design plan for the sharp tool geometry numerical simulations	81
Table 4.6	Design of experiments for the chamfer tool	95
Table 4.7	Design of experiments for the sharp tool	95
Table 4.8	Analysis of variance for temperature as a function of cutting speed (V), feed rate (f) and tool geometry (γ_n and w_n) when using a chamfered tool	96
Table 4.9	Analysis of variance for stress as a function of cutting speed (V), feed rate (f) and tool edge chamfer with (w_n)	97

Table 4.10 Analysis of variance for temperature as a function of cutting speed (V), feed rate (f) and sharp tool angle (θ_t)— Original model before suppression of factors 97

Table 4.11 Analysis of variance for stress as a function of cutting speed (V), feed rate (f) and sharp tool angle (θ_t) 98

Table 4.12 Summary of most influential parameters in terms of importance (1 = most, 4 = least) 99

Table 4.13 Comparison of numerical and experimental results for chamfer tool.....105

Table 4.14 Comparison of numerical and experimental results for sharp tool 106

Table 5.1 Thermal and mechanical properties of workpiece and tool materials 112

Table 5.2 Validation results for the round, chamfer and sharp tools……125

LIST OF FIGURES

Figure 1.1 Typical cutting edge preparation designs 6

Figure 1.2 Influencing factors for selecting appropriate cutting-edge geometry Rodríguez (2009) 8

Figure 1.3 Variation of the tool life travel path as a function of the cutting edge rounding parameter in orthogonal turning AISI 1045.....10

Figure 1.4 Influence of cutting-edge microgeometry on process forces.....11

Figure 1.5 The three deformation zones during orthogonal cutting process 12

Figure 1.6 Mechanics of orthogonal cutting 15

Figure 2.1 Research study framework.....24

Figure 2.2 The pre-processing step. 26

Figure 2.3 post-processing step. 27

Figure 3.1 Tool model geometry (r_c, α, γ are the nose radius, the clearance angle and the rake angle, respectively) 37

Figure 3.2 Workpiece model geometry.....37

Figure 3.3 Meshing of the model for cutting simulation at V_c = 104 m/min, f = 0.1 mm/rev.....39

Figure 3.4 Transient force simulations during machining process at V = 400 m/min, r_c = 0.3 mm, f = 0.1mm/rev, γ = 5° 43

Figure 3.5 Distribution of cutting temperature in the workpiece and cutting tool at V = 400 m/min, f = 0.1mm/rev, γ = 5° for the nose radii r_c: (a) 0.3 mm, (b) 0.5 mm (c) 0.7 mm and (d) 0.9 mm.....44

Figure 3.6 Distribution of effective stress in the workpiece and cutting tool at V = 400m/min, f = 0.1mm/rev, γ = 5° for the nose radii r_c: (a) 0.3 mm, (b) 0.5 mm (c) 0.7mm and (d) 0.9 mm.....45

Figure 3.7 Distribution of effective strain in the workpiece and cutting tool at V = 400 m/min, f = 0.1mm/rev, γ = 5° for the nose radii r_c: (a) 0.3 mm, (b) 0. 5 mm (c) 0.7 mm and (d) 0.9 mm.....46

Figure 3.8 The simulation results for tool wear rate at V = 400 m/min, f = 0.1 mm/rev, ...47

Figure 3.9 Distribution of cutting force for different tool nose radii at 49

Figure 3.10 Distribution of thrust force for different tool nose radii at 49

Figure 3.11 Distribution of tool wear for different tool nose radii at.....51

Figure 3.12 Variation of cutting temperature with small tool nose radius for different feed rates at V = 400 m/min, γ = 5º.....53

Figure 3.13 Variation of cutting temperature with large tool nose radius for different feed rates at V = 400 m/min, γ = 5º 54

Figure 3.14 Variation of cutting stress with small tool nose radius for different feed rates at V = 400 m/min, γ = 5º 55

Figure 3.15 Variation of cutting stress with large tool nose radius for different feed rates at V = 400 m/min, γ = 5º 56

Figure 3.16 Variation of maximum temperature with small tool nose radius for different cutting speeds at f = 0.1 mm/rev, γ = 5º 57

Figure 3.17 Variation of maximum temperature with large nose radius for different cutting speeds at f = 0.1 mm/rev, γ = 5º 58

Figure 3.18 Variation of cutting stress with small tool nose radius for different cutting speeds at f = 0.1 mm/rev, γ = 5 59

Figure 3.19 Variation of cutting stress with large tool nose radius for different cutting speeds at f = 0.1 mm/rev, γ = 5 60

Figure 3.20 Variation of maximum temperature with small tool nose radius for different rake angles at V = 104 m/min, f = 0.1 mm/rev 61

Figure 3.21 Variation of cutting temperature with large tool nose radius for different rake angles at V = 400 m/min, f = 0.1 mm/rev 62

Figure 3.22 Variation of cutting stress with small tool nose radius for different rake angles at V = 104 m/min, f = 0.1 mm/rev 63

Figure 3.23 Variation of cutting stress with large tool nose radius for different rake angles at V = 104 m/min, f = 0.1 mm/rev 64

Figure 3.24 Variation of tool wear width with small nose radius for different cutting speeds at f = 0.1 mm/rev, γ = 5º 65

Figure 3.25 Variation of tool wear width with large nose radius for different cutting speeds at f = 0.1 mm/rev, $\gamma = 5^{o}$ 66

Figure 3.26 Variation of tool wear width with nose radius for different rake angles at V = 104 m/min, f = 0.1 mm/rev.....68

Figure 3.27 Variation of tool wear width with large tool nose radius for different rake angles at V = 104 m/min, f = 0.1 mm/rev 69

Figure 4.1 Two-dimensional (2D) models of the cutting tools studied: 76

Figure 4.2 The workpiece model geometry.....77

Figure 4.3 Chamfer cutting tool geometries with different chamfer widths w_n: a) 0.1 mm b) 0.4 mm c) 0.6 mm d) 0.75 mm.....82

Figure 4.4 Chamfer cutting tool geometries with different chamfer angles γ_n :.....83

Figure 4.5 Sharp cutting tool geometries with different sharp angles θ_t : 84

Figure 4.6 Variation in force versus time during cutting process for.....85

Figure 4.7 Variation in maximum temperature versus time during cutting process ...86

Figure 4.8 Distribution of cutting temperature in the model at V = 150 m/min, f = 0.2 mm/rev, γ_n = 10° for the chamfer widths w_n: (a) 0.1 mm, (b) 0.4 mm, (c) 0.6 mm, (d) 0.75 mm 87

Figure 4.9 Distribution of effective stress in the model at V = 150 m/min, f = 0.2 mm/rev and γ_n =10° for the chamfer widths w_n: (a) 0.1 mm,.....88

Figure 4.10 Distribution of tool wear in the model at V = 150 m/min, f = 0.2 mm/rev and γ_n =10° for the chamfer widths w_n: (a) 0.1 mm, (b) 0.4 mm, (c) 0.6 mm, (d) 0.75 mm, (e) zoomed of (b) 89

Figure 4.11 Distribution of cutting temperature in the model at V = 150 m/min, f = 0.3 mm/rev and w_n = 0.1 mm for the chamfer angles γ_n: (a) 15°, (b) 25°, (c) 35°, (d) 45°.....90

Figure 4.12 Distribution of effective stress in the model at V = 150 m/min, f = 0.3 mm/rev and w_n = 0.1 mm for the chamfer angles γ_n: (a) 15°, (b) 25°, (c) 35°, (d) 45° 91

Figure 4.13 Distribution of cutting temperature at V = 150 m/min and f = 0.3 mm/rev for the sharp angles θ_t: (a) 35°, (b) 45°, (c) 55°, (d) 65° ...92

Figure 4.14 Distribution of effective stress in the model at V = 150 m/min and f = 0.3 mm/rev for the sharp angles θ_t: (a) 35°, (b) 45°, (c) 55°, (d) 65° 93

Figure 4.15 Distribution of tool wear depth in the model at V = 150 m/min and f = 0.3 mm/rev, for the cutting tool angles: (a) sharp edge; θ_t = 45°, (b) sharp edge; θ_t = 55°, (c) chamfered edge; γ_n = 25°, (d) chamfered edge; γ_n = 35° 94

Figure 4.16 Comparison of predicted and simulated temperatures: (a) chambered tool and (b) sharp tool 100

Figure 4.17 Comparison of predicted and simulated stress: (a) chambered tool and (b) sharp too 100

Figure 4.18 3 D Surface plots of parametric effects of cutting speed, feed rate and chamfered tool angle (γ_n) on temperature (°C) when using a chamfered tool (w_n = 0.34 mm) 102

Figure 4.19 3D Surface plots of parametric effects of cutting speed, feed rate and chamfered tool length (w_n) on temperature (°C) when using a chamfered tool (γ_n = 35°) 102

Figure 4.20 3D Surface plots of parametric effects of cutting speed, feed rate and chamfered tool length (w_n) on the stress when using a chamfered tool (γ_n = 35°) 103

Figure 4.21 3D Surface plots of parametric effects of cutting speed, feed rate and sharp tool angle (θ_t) on the temperature (°C) when using a sharp tool (γ_n = 35°).....104

Figure 4.22 3D Surface plots of parametric effects of cutting speed, feed rate and sharp tool angle (θ_t) on the stress (MPa) when using a sharp tool (γ_n = 35°) 104

Figure 5.1 The 2D model design of cutting tool: (a) round (b) chamfer (c) sharp....113

Figure 5.2 Chamfer cutting tool geometries with different chamfer width and angles (a) $\gamma_n = 10^o$; w_n = 0.15mm (b) $\gamma_n = 10^o$; w_n = 0.45mm (c) $\gamma_n = 40^o$; w_n = 0.15mm (d) $\gamma_n = 40^o$; w_n = 0.45mm 113

Figure 5.3 Distributions of machining forces at V = 200/min, f = 0.2 mm/rev, α = 15° for different cutting tool geometries: (a) Round (b) Chamfer (c) Sharp.....115

Figure 5.4 Variation of residual stresses with workpiece depth for different rake angles γ (15°, 25°, 35°, 45°); (Edge radius r_c = 0.03 mm).116

Figure 5.5 Variation of residual stresses with workpiece depth for different chamfer angles γ_n (15°, 25°, 35°, 45°) 117

Figure 5.6 Variation of residual stresses with workpiece depth for different sharp angles θ_n (10°, 15°, 20°, 25°) 118

Figure 5.7 Distributions of residual stresses for various tool edge radii r_c: 119

Figure 5.8 Distributions of residual stresses for different 120

Figure 5.9 Distributions of residual stresses for different sharp angles γ_n : (a) 10°, (b) 15°, (c) 20°, (d) 25° 121

Figure 5.10 Distribution of cutting temperature for different tool edge radii: 122

Figure 5.11 Distribution of cutting temperature for different chamfer angles γ_n : (a) 15˚, (b) 25˚, (c) 35˚, (d) 45˚ 123

Figure 5.12 Distribution of cutting temperature for various sharp angles θ_t :.....124

Figure 5.13 Pareto diagram of standardized effects for cutting round tool: (a) temperature; 131

Figure 5.14 Pareto diagrams of standardized effects for chamfer cutting tool: (a) temperature 138

Figure 5.15 Pareto diagram of standardized effects for sharp cutting tool: (a) temperature (b) effective stress (c) chip thickness (d) wear depth (e) residual stress.....144

Figure 5.16 3D Surface plots of parametric effects on (a) temperature, (b) stress, (c) chip thickness and (d) wear depth for round cutting tool (Edge radius : 0.03 mm).....148

Figure 5.17 3D Surface plots of parametric effects on (a) temperature, (b) stress , (c) chip thickness and (d) wear depth (e) residual stress for cutting chamfer cutting tool (Chamfer width: 0.35 mm, Chamfer angle: 20º) 149

Figure 5.18 3D Surface plots of parametric effects on (a) temperature, (b) stress, (c) chip thickness and (d) wear depth (e) residual stress for sharp cutting tool 150

LIST OF ABREVIATIONS

ANOVA	Analysis of variance
BUE	Build-Up Edge
C	Carbon
CM	Conventional Machining
DOE	Design of experiment
FEM	Finite Element Method
Fe	Iron
HB	Brinell Hardness
HRC	Rockwell Hardness
HSM	High-speed machining
Mn	Manganese
P	Phosphorus
RSM	Response surface methodology
S	Sulfur
SSD	Sum of squared deviations
SSE	Sum of squared error
TSS	Total sum of squares
VMG	Variable Microgeometry

LIST OF SYMBOLS AND UNIT OF MEASUREMENTS

A	Initial yield strength (MPa)
B	Hardening modulus (MPa)
C	Strain rate sensitivity coefficient
C_T	Volume heat capacitance
A_γ	Tool face (mm)
A_s	Area of the shear plane (m^2)
A_α	Tool flank (mm)
F_c	Cutting force (N)
F_f	Feed force (N)
F_n	Normal force in shear plane (N)
F_s	Shear force in shear plane (N)
F_u	Friction force on rake face (N)
F_x	Cartesian force in X direction (N)
F_y	Cartesian force in Y direction (N)
f	Feed rate (mm/rev)
h	Uncut chip thickness (mm)
h_∞ , h_c	Convection heat transfer coefficient
k_i	Thermal conductivity for material i
K_T	Thermal conduction matrice

m	Thermal softening coefficient
n	Hardening coefficient
N	Normal force on rake face (N)
P	Interface pressure (Pa)
$\dot{Q}_g$	Generated total heat
R	Cutting ratio
R_{ext}	Vector of external force
R_{int}	Vector of internal force
r_c	Nose, edge radius (mm)
R^2	Correlation coefficient (%)
S_α	Cutting edge segment on flank face
S_β	Profile flattening
S_γ	Cutting edge segment on rake face
T	Temperature (°C)
T_{air}	Ambient temperature (°C)
T_c	Cutting temperature (°C)
T_{melt}	Melt temperature (°C)
T_{room}	Room temperature (°C)
ΔT	Temperature gradient (°C)
τ_s	Shear stress (MPa)
t_o	Depth of cut (mm)
t_1	Undeformed chip thickness (mm)
t_c	Chip thickness (mm)
dt	Time increment (s)

U	Material displacement vector (m)
$\ddot{U}$	Material acceleration vector (m/s^2)
V_c	Cutting speed (m/min)
Vx	Cutting speed in x-axis direction (m/min)
Vy	Cutting speed in y-axis direction (m/min)
V	Sliding velocity (m/min)
v	Relative velocity between object surface and air (m/min)
W	Tool wear
W	Width of cut (mm)
W_d	Wear depth (mm)
w_n	Chamfer width (mm)
α	Clearance angle (deg)
γ, γ_c	Rake angle (deg)
γ_n	Chamfer angle (deg)
θ	Rotation angle (deg)
θ_t	Sharp angle (deg)
ε	Plastic strain
$\dot{\varepsilon}$	Plastic strain rate (s^{-1})
$\dot{\varepsilon}_0$	Reference plastic strain rate (s^{-1})
ϕ	Shear angle (deg)
σ_c	Cutting stress (MPa)

INTRODUCTION

The demands of producing quality structural machined parts are increasing continuously. The manufacturing of such particular parts which are used for different applications need to be done by machinists. They work with designers to get good quality such as the better surface finish, good geometrical tolerance, accuracy and to obtain high resistance to wear. The scientific research and the technological development have pointed out that two important properties have the influence and the impact on the machining process performance during the cutting process: machining conditions and the cutting tool geometry. They affect the most the machining process performance outputs. This tool geometry includes the following: the edge radius, rake angle and the chamfer angle.

It was stated that failure and damage of cutting tool are generally caused by high thermo-mechanical loads at tool-workpiece contact are and at tool-chip contact area (Javidikia et al., 2020). Moreover, the machining field is facing a challenge of shaping advanced and complex difficult-to cut workpiece. Thus, requires long cycle time and high manufacturing costs. So, in order to solve these machining problems and satisfy the requirements it is necessary to call for cutting edge preparation by generating a specific geometry around the cutting tool edge (round, chamfer, sharp or their combinations) in order to improve the resistance of cutting edge to tool wear and chipping (Shnfir, 2020). Recently, the cutting tool edge preparation method was applied in different previous research works especially for micro-machining applications. However, these applications were almost based on round tool edge geometries. Moreover, there is still a lack of understanding on cutting edge geometry and its effects on the performance of machining processes due to many interactions existing between the workpiece material properties, the cutting tool geometry and the machining process parameters. Also, the machining operations are varied and involve specific and complex mechanisms. Experimental cutting tests could be used to determine the best settings but such experiments are time consuming and there too many parameters to control. Simulations could help in such cases. This research work is characterized by numerical studies validated by experimental data from literature.

Scope and research objectives

The present research work investigates numerically the effects of tool-edge designs and machining parameters on the machining process performance during orthogonal cutting of AISI 1045 steel.

The main objectives of the research study are:

- To predict the influence of tool nose radius and cutting process parameters on machining characteristics including cutting force, cutting stress, tool wear and temperature.
- To evaluate the interactive effects of chamfered and sharp cutting tools and cutting parameters on cutting temperature, effective stress, tool wear, chip thickness and residual stress.
- To optimize the tool edge geometry (round, chamfered or sharp) and the cutting process parameters, with specific attention to cutting temperature, cutting stresses and tool wear.

Research study concept

In order to realise these objectives, it is important to develop suitable process, material and tool models that will help to perform the simulations. The orthogonal cutting simulations were conducted using the DEFORM 2D Finite Element Method software. The machining characteristics that are simulated are the cutting force, effective stress, strain, chip thickness and the tool wear. For this study, three tool edge geometries: round, chamfer and sharp. The numerical simulations tests are planned using the design of experiment technique. Each test is designed by the cutting parameters (cutting speed and feed rate) and the cutting tool edge geometrical parameters such nose radius, chamfer width, chamfer angle, sharp angle. After the experimental validation of the numerical simulations, the obtained results are investigated statistically using analysis of variance ANOVA. These analysis show, on one hand, the

interactive effects between cutting parameters and cutting tool edge geometries on different machining characteristics. On the other hand, the optimal cutting conditions using the optimization approach based on ANOVA.

Structure of the thesis

The present research thesis consists of five chapters. An introduction presents the context, the research study concept, the problem statement to be addressed, the principal goal and the objectives. Outline of the different chapters is discussed below:

Chapter 1 is devoted to the literature review on cutting edge preparation overview including the various edge tool preparation geometries, factors influencing edge tool geometry, effects of edge tool preparation on machining performance, optimization methods of cutting-edge geometry and the previous research works realised on the impacts of cutting-edge preparation of machining process characteristics.

Chapter 2 presents the methodology used to realise the mentioned research objectives: design planning, numerical simulation modeling.

Chapter 3 is dedicated to numerical study of the effects of tool nose geometries and their interactions with cutting parameters on cutting temperature, effective stress, cutting forces and tool wear during orthogonal cutting of AISI 1045 steel.

Chapter 4 presents numerical investigation on the performance of chamfered and sharp cutting tools during orthogonal cutting of AISI 1045 steel.
Chapter 5 focuses on the numerical comparison study of machining conditions and cutting-edge tool geometry in orthogonal cutting of AISI 1045 steel.

Finally, a general conclusion outlines the important results obtained in this research study, highlights the contributions and proposes recommendations to be considered for research works.

CHAPTER 1

LITERATURE REVIEW

1.1 Introduction

This section is devoted to the literature review on cutting edge preparation overview including the edge tool preparation definition, classification of edge tool preparation geometries, factors influencing edge tool geometry, effects of edge tool preparation on machining performance, optimization methods of cutting-edge geometry and finally on summary of previous research works on the impacts of cutting-edge preparation on machining process characteristics.

1.2 Cutting tool edge preparation overview

As mentioned previously, the cutting-edge geometry preparation plays a significant role on the cutting tool performance particularly for machining difficult-to cut workpiece. Tool edge preparation can help to improve the cutting tool life and quality of the part, to eliminate irregularities and defects of cutting edge. Moreover, the characteristics of cutting-edge geometry preparation associated with cutting edge design and microtopography of tool surfaces produce accurate and precise tool edge geometries.

1.2.1 Cutting tool edge preparation definition

The cutting-edge preparation is defined as generation of a specified radial form along the cutting edge, changing the micro topography of the edge and its tool surface finish by eliminating defects and irregularities in order to improve the performance of cutting tool and the quality of the machined part.

1.2.2 Classification of tool edge preparation geometries

In order to meet the industrial cutting tool-edge specifications, tool makers and designers prepared different tool-edge geometries based on different criteria. Among these criteria are the material removal quantities for eliminating edge defects and improving the tool strength and the workpiece quality. Moreover, such tool-edge shapes are convenient for many machining purposes due to the high stability against the strong mechanical loads. The common and important cutting-edge preparation designs commercially available are sharp, rounded, chamfered forms and the combination between rounded and chamfered edge shape. Figure 1.1 shows typical cutting edge preparation designs.

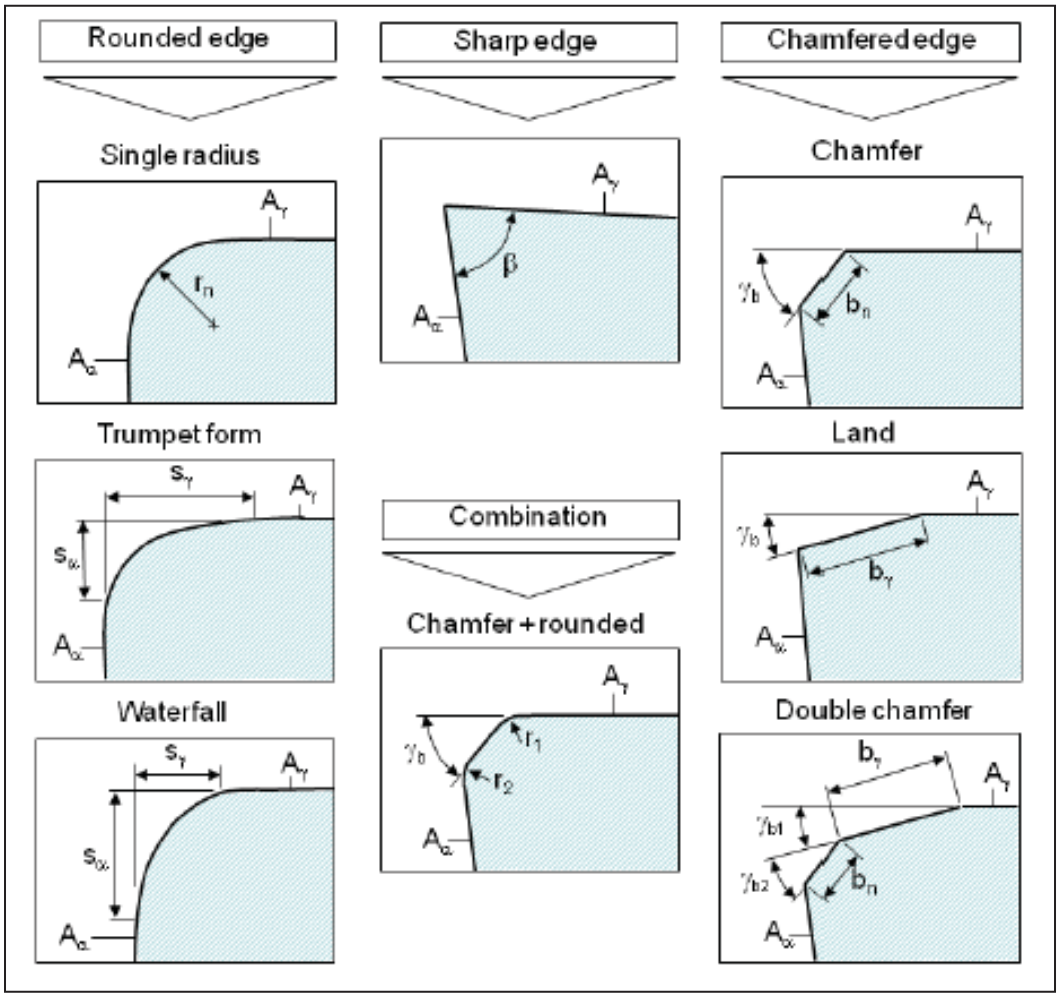

Figure 1.1 Typical cutting edge preparation designs
Rodríguez (2009)

Sharp cutting edge

The sharp cutting-edge geometry is designed by the intersection of the tool face A_γ and the tool flank A_α delimited by an angle β. The sharp form is characterized by an irregular and chipped aspect having no specified parameters. Sharp cutting edge presents difficult compatibility to all machining applications as long as it can not be resisted to some mechanical stresses (Rodríguez 2009).

Round cutting edge

The rounded cutting edge is defined by a circle with constant radius r_n joining rake face and flank face. The round edge can be combined with the chamfered edge producing a geometry specified with a chamfer angle γ_b and two edge radii r_1 and r_2 . This round edge presents complex geometries with several parameters to be determined and different curvature variations that depend on the form of the joining profile.

The rounded edge has two curvature variations generating two different geometries: waterfall and trumpet. These two edge geometries are delimited by the rounding lengths S_α (cutting edge segment on flank face) and S_γ (cutting edge segment on rake face) to join the rake and flank surface.

Chamfered cutting edge

The chamfered cutting edge is made by the junction of rake face and flank face with a length b_n and the angle γ_b in the plane surface. There is also the combination of two chamfered edges specified by two lengths b_n and b_γ and two angles γ_{b1} and γ_{b2} . The chamfer shapes can be prepared mainly under symmetrical and asymmetrical geometries using hard turning, interrupted cutting and heavy rough cutting methods.

1.2.3 Factors influencing the cutting-edge geometry

The influencing factors for selecting appropriate cutting-edge geometry are illustrated in Figure 1.2.

There are various factors that affect and influence the selection of cutting-edge design preparation in order to obtain a required geometry. Among them: the machining process, initial condition of existing edge, parameters of the process, material of workpiece, tool material, required coating and micro and macro machining conditions. Each cutting-edge design is selected based on the initial conditions of the cutting edge to be prepared such as the surface defects, irregularities and material quantity to be removed. Moreover, the designing of cutting-edge contour should be adapted on one hand to the process type and the used cutting parameters and on the other hand, to the tool material characteristics and workpiece material machinability. The friction mechanism, the interfaces of tool-chip and of tool-workpiece depend on the microstructure of the flank and rake faces. The angles of the edge geometry should be adequately designed for the appropriate load distribution on the cutting edge. The dimensional tolerance of the edge contour is defined by the coating structure of the layers , the coating thickness and its composition.

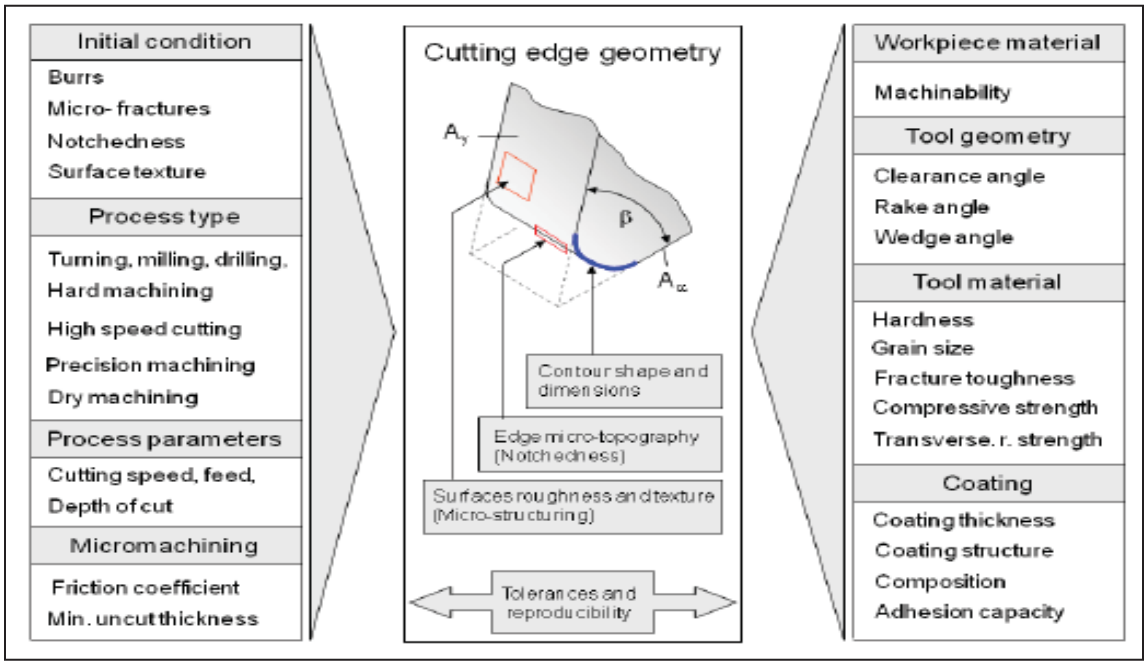

Figure 1.2 Influencing factors for selecting appropriate cutting-edge geometry
Rodríguez (2009)

1.2.4 Influence of cutting-edge preparation method on machining performance

As discussed before, the importance of cutting-edge preparation method and its influence on improving machining process especially on the orthogonal machining can be presented under different aspects. The tool performance and the desired machined part are obtained as results and consequences. To illustrate the impacts of this method, Figures 1.3 and 1.4 show respectively the variation of the tool life in terms of travel path as a function of the edge rounding parameter during orthogonal turning AISI 1045 and the influence of cutting-edge microgeometry on process forces (Bassett et al, 2012). The different thermomechanical aspects that are influenced by the cutting-edge preparation are:

- Distribution of cutting temperature
- Distribution of cutting forces and cutting stresses
- Deformation

Consequently, they will have effects on:

- Tool resistance to wear
- Part roughness and surface finish
- Chip formation

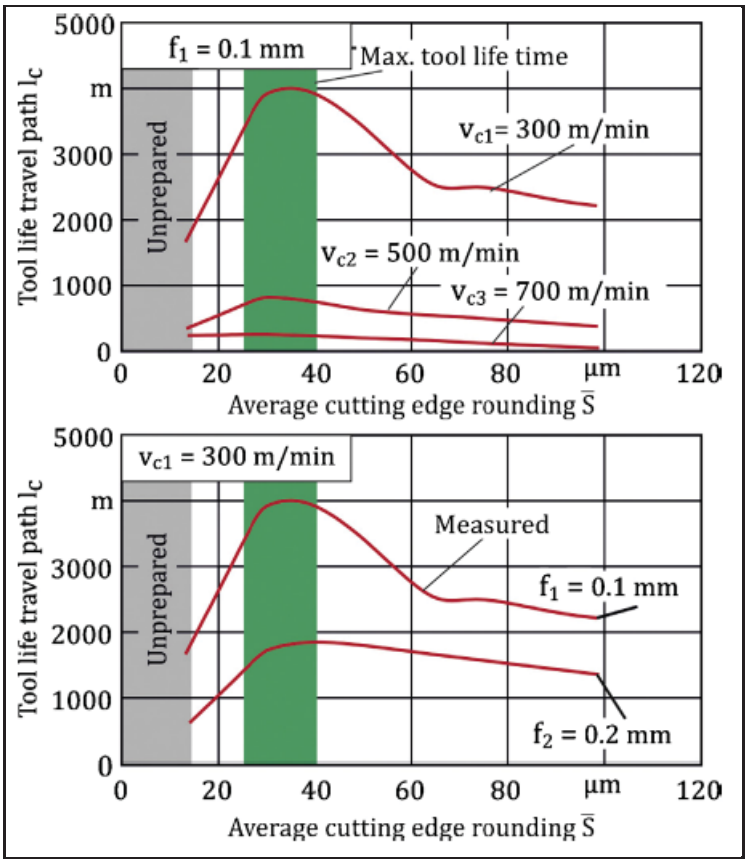

Figure 1.3 Variation of the tool life travel path as a function of the cutting edge rounding parameter in orthogonal turning AISI 1045 Bassett et al, (2012)

From Figure 1.3 it is noted that the cutting speed and the feed rate both influence the tool life. There is a best edge rounding parameter range (25-40) for which the maximum tool life are obtained.

From Figure 1.4 it is observed that there is symmetrical variation of cutting edge rounding with with $\overline{S_\alpha} = \overline{S_\gamma}$ = 12 mm and 100 mm. The Cutting and thrust forces increase with increasing on the cutting-edge rounding or in the chip thickness.

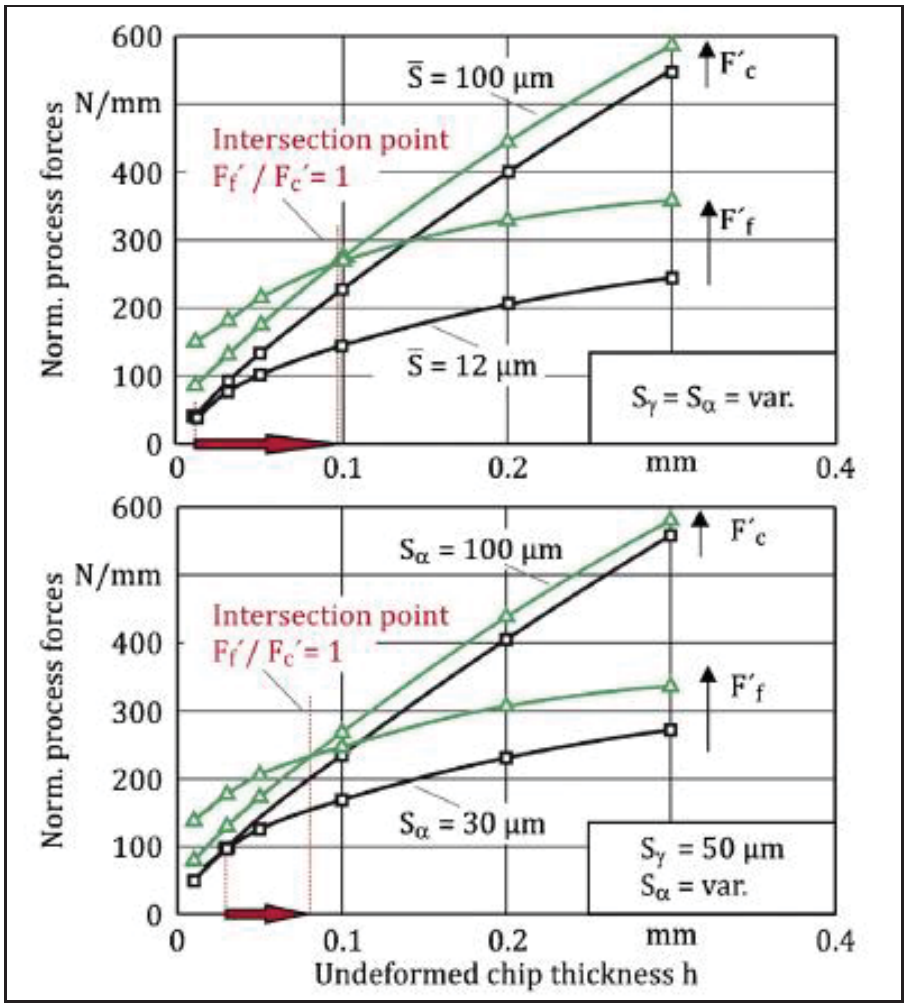

Figure 1.4 Influence of cutting-edge microgeometry on process forces
Bassett et al, (2012)

1.2.5 Machining process performance evaluation methods

If the desired part is not obtained during machining process, the independent variables have to be investigated and modified systematically in order to identify the interactions effects between them. The understanding of different phenomena occurred calls for cutting mechanics theory.

Cutting process mechanics

During cutting process, the important deformations occur in three locations near to the cutting tool edge during: primary shear zone, secondary shear zone and third deformation zone. Figure 1.5 shows the three deformation zones during orthogonal cutting process. The primary shear zone is attributed to chip formation location caused by plastic deformation of the workpiece. The second deformation zone is located in the rake contact area between cutting tool and chip where the friction phenomenon occurs. Whereas the third or tertiary deformation zone is attributed to the deformation of the workpiece (Özlü., 2008).

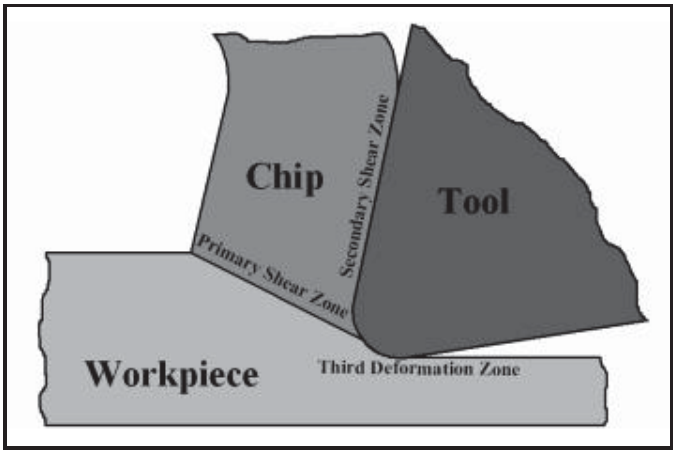

Figure 1.5 The three deformation zones during orthogonal cutting process
Özlü (2008)

Chip formation

During machining processes, there is a waste of material under chips form which may have adverse impacts on produced surface quality. So, it is necessary to study the mechanics of chip formation and to develop machining models such as merchant model known as orthogonal cutting model, where two-dimensional forces are perpendicular to each other. Thus, can definite the positive rake angle γ and the clearance angle α. The chips are produced due to shearing mechanism that occurred in the shear zone (referred to shear plane) at the shear angle (φ). This model is expressed by the following formulas (Kalpakjian & Schmid., 2009):

$$\tan\phi = \frac{r\cos\alpha}{1 - r\sin\alpha} \tag{1.1}$$

$$r = \frac{t_o}{t_c} = \frac{\sin\phi}{\cos(\phi - \alpha)} \tag{1.2}$$

Where t_c , t_o and r are respectively the chip thickness, the depth of cut and the cutting ratio. The previous studies have shown that when the rake angle decreases (the friction increases at the contact of tool-chip), the shear angle increases, thus producing thicker chips then increasing heat and rising temperature consequently. The non-orthogonal chips formation is not considered in the present research.

Cutting forces

Collecting data on cutting forces involved are important in machining process in order to design properly the machine tool for reducing distortion and keeping the required geometry accuracy for the parts to be machined and choosing adequate toolholders (Kalpakjian & Schmid., 2009).

The cutting force depends strongly the power involved during cutting process. It is needed to use enough power for separating the formed chip from the workpiece. The cutting forces are measured by the dynamometer. They are calculated according to the Cartesian system. Generally, lower cutting forces are due to high cutting speed by considering the used material and the cutting conditions.

In the two dimensional (2D) orthogonal cutting the material removal is done by the cutting tool edge in perpendicular position to the workpiece plane. Thus means the cutting-edge tool is also located perpendicular to the direction of the cutting speed (V_c).
It is assumed that the cutting is to be uniform and two cutting forces are defined: the cutting forces (or tangential forces) are acting on the direction of the cutting speed (V_c) and the feed forces (or thrust forces) are acting in the direction of the uncut chip thickness.

By associating the rotation and translation movement, the cutting force F_c and the feed force F_f can be determined by calculating the cartesian forces F_x and F_y according to the following equations (Shnfir, 2020):

$$F_c = F_x \sin\theta + F_y \cos\theta \quad (1.3)$$

$$F_f = F_x \sin\theta - F_y \cos\theta \quad (1.4)$$

The undeformed chip thickness t_1 is proportional to feed rate and it is expressed as follows:

$$t_1 = f \sin\theta \quad (1.5)$$

Where θ is the rotation angle and f is the feed rate (mm/tooth)

Based on the equilibrium theory of the forces the resultant cutting force F_r is determined from the cutting force and the feed force as expressed by Equation (1.6).

$$F_r = \sqrt{F_t^2 + F_f^2} + \quad (1.6)$$

In order to highlight the mechanics of the orthogonal cutting, the merchant cycle diagram is used showing the cutting forces and the cutting speed diagrams (see Figure 1.6).

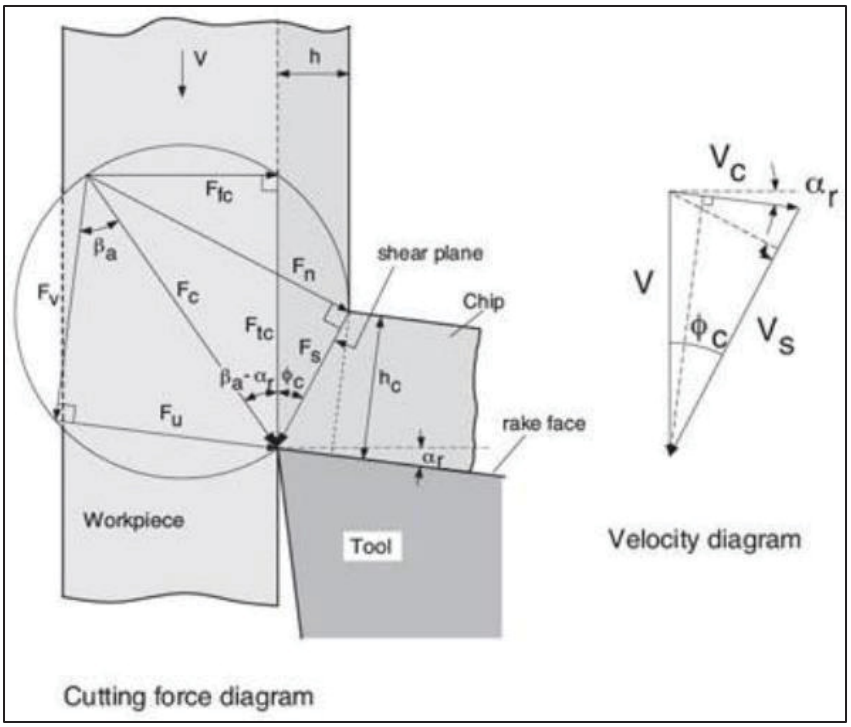

Figure 1.6 Mechanics of orthogonal cutting
Altintas (2012); Umbert (2017)

From the cutting force diagram (Figure 1.6) the Shear force (F_s) and the normal force (F_n) are defined as the force acting in the shear plane. These forces are determined respectively in equations (1.7) and (1.8) as follows (Altintas, 2012):

$$F_s = F_c \cos(\Phi_c + \beta - \alpha_r) \tag{1.7}$$

$$F_n = F_c \sin(\Phi_c + \beta - \alpha_r) \tag{1.8}$$

The two cutting forces acting on the rake face of the cutting tool in the secondary shear zone are the normal force (N) and the friction force (F_u). They are expressed respectively by equations (1.9) and (1.10)(Altintas, 2012):

$$N = F_t \cos \alpha_r - F_f \sin \alpha_r \tag{1.9}$$

$$F_u = F_t \sin \alpha_r - F_f \cos \alpha_r \tag{1.10}$$

Shear stress

As the shear force is acting in shear plane, the shear stress (τ_s) is coplanar with the shear plane surface and it can be calculated by the Equation (1.11):

$$\tau_s = \frac{F_s}{A_s} \tag{1.11}$$

Where A_s is the Area of the shear plane given Equation (1.12)(Altintas, 2012):

$$A_s = w \cdot \frac{h}{sin\,(\Phi)} \tag{1.12}$$

w, h and Φ are respectively the width of cut, the uncut chip thickness and the shear angle.

Wear and tool life

The tool life is the period of time during which the cutting tool is used until failure. The tool life is influenced by cutting edge geometry in particular cutting-edge radius. The previous research results showed proportional effects of cutting-edge radius on tool life. It is very important to make a good choice of material tool and cutting-edge geometry during tool selection process in order to extend the tool life by increasing the wear resistance and then improving productivity consequently. The tool wear mechanisms can be divided into two main modes: flank wear and crater wear.

Flank wear is taking place on the flank face of cutting tool, due to the presence of friction or abrasive action of microchips or powdered particles present at the tool work interface.

Crater wear is taking place on the rake face of cutting tool, due to the presence of friction or abrasive action of microchips at the chip-tool interface.

In order to show the effect of cutting speed on tool life, a model was developed by Taylor. The Taylor's tool life T is expressed in Equation (1.13) as follows (Childs et al., 2000):

$$VT^n = C \tag{1.13}$$

Where V is the cutting speed C is cutting speed that specifies the lifetime unity, n is an exponent indicating that life is sensitive to change of speed.

Temperature distribution

Previous numerical results analysis confirmed, on one hand, the effects of cutting-edge geometry on tool-chip interface temperature. It was shown that maximum temperatures were determined on tool edge and the high temperature position are due to increasing cutting edge radius. On the hand, the influence of cutting-edge preparation on process machining especially orthogonal high-speed steel machining. It was concluded that honed tools generate higher temperature and chamfered tools produce lower temperature at the rake face area (Childs et al.,2000). The temperature distribution simulation model will be treated later in simulation design section through this document.

1.2.6 Summary of previous works on the impacts of cutting-edge preparation on machining process characteristics

In the literature there are several research works realised on the effects of the cutting-edge tool geometry preparations on the performance of machining. Among these researches there was a study of the effects of chamfer and honed edge geometry preparation of ceramic tools on the tool life, surface finish and cutting forces in hard turning of DF-3 tool steel under different cutting experimental conditions by using ANOVA. The results showed that chamfered edge geometry demonstrated longer machining length in all cutting condition (longer tool life), low roughness was recorded with chamfered edge design and honed tools geometry produced higher forces (Davoudinejad & Noordin, 2014). Another research study was conducted with different tests investigating the effects of different cutting-edge preparation methods on micro milling performance. They found that magnet finishing, and immersed tumbling yielded lower resultant forces (Fz) and lower tool wear. Moreover, the surface quality is slightly improved by using tools prepared with magnet finishing (Uhlmann et al., 2016). (Bordin & Zeilman ,2014) investigated the effects of the cutting-edge preparation on the surface integrity of the

hole after dry drilling. They found that the sharpened condition results in higher roughness and the highest temperatures highest values of the affected layer were obtained for the conditions sharpened and drag finished. (Denkena et al.,2010) used the abrasive brushing tools for cutting edge preparation in order to study and understand the influence of brushing process parameters on the size and the form of produced cutting edge rounding geometries. The results showed that the tool life was improved the quality-oriented cutting tool preparation and the productivity of the machining process. Table 1.1 presents the previous research works on the influences of different tool edge geometries on orthogonal machining processes.

Table 1.1 Summary of research studies on influences of different tool edge geometries on orthogonal machining processes

References	Main Objective	Results
Denkena et al. 2021	To investigate the performance of Polycrystalline cubic boron nitride (PCBN) on thermomechanical load using finite element method.	By enlarging the cutting-edge microgeometry, the thermal loads acting on the tool are increased and the mechanical stress on the tool are significantly reduced.
Binxun et al. 2022	To study the cutting performance and surface integrity considering tool edge micro-geometry in metal cutting process	-Micro-geometry changes the contact condition and friction behavior between cutting edge and workpiece. -Cutting forces components increase with increasing uniform edge hone radius or chamfer length.
Marcos et al. 2021	To investigate the influence of cutting- edge preparation and cutting parameter during milling process.	Cutting tool with edge preparation generate less surface roughness and reduce cutting tool wear
Shnfir et al. 2019	To investigate the effects of edge preparation (honed, chamfered), workpiece hardness and machining parameters on milling od AISI-1045 steel.	-When machining harder 1045 steel using honed edges inserts, the use of high feed rates resulted in higher cutting forces. -The use of inserts with chamfered tool-edge preparation greatly reduced tool wear

References	Main Objective	Results
Shnfir et al. 2020	To study the effects of cutting tool edge preparation, speed, feed rate, and hardness of workpiece material on ultrafine particles (UFP) emissions during a face milling process	-The workpiece hardness has the greatest influence on ultrafine particle (UFP) emission for honed and T-land edge preparations. -The use of honed edge at moderate speed and higher feed rate reduces UFP emission during milling operations
Weiwei et al. 2020	To make analysis of the effects of cutting-edge microgeometry on surface roughness and white layer formation	-Enlarging chamfer width can improve surface roughness -increasing chamfer angle do not have significant effects on surface roughness - Large, rounded edge and large chamfered edge can contribute to white layer formation
Yussefian 2018	To apply the design of manufacturing concept for creating variable microgeometry (VMG) cutting tools by conventional edge preparation processes	-Hard part turning of AISI 4140 (42 HRC), VMG1 variant had an improved tool life of 100% compared to a uniformly honed standard reference tool. -Surface roughness was enhanced by almost 30% in the case of VMG2 tool. - As edge radius and wedge angle decrease there is maximum temperature on the chip tool interface

1.3 Conclusion

From the presented literature review the following points were concluded:

- Many applications of the cutting tool edge preparation method were limited to analysis of the effects of tool edge geometry on the tool wear resistance (tool life). These

applications were done without good understanding of this method and its influence on the machining performance in order to avoid the cutting tool failure problems.

- No research work was found on the interactive effects between the parameters of different tool edge designs and the machining parameters on the machining characteristics such as cutting temperature, machining forces, effective stress, residual stress, chip thickness and tool wear depth.

- The cutting tool and the different tool edge geometrical parameters were not yet optimized from the interactive effects for improving the machining characteristics during orthogonal cutting of AISI 1045 steel.

So, it is needed to perform numerical simulations and statistical studies on the different machining characteristics considering the different interactions between the machining and the various available tool edge geometrical parameters to complete the lack of the industrial data on tool edge preparations and machining performance.

CHAPTER 2

METHODOLOGY

2.1 Introduction

This chapter presents the methodology that was used during different research project steps. The description is detailed in Chapter 3 (Papers I) and Chapter 4 (Paper II). these descriptions include the workpiece and the tool materials utilized, design of experiment (DOE), numerical simulation design planning and statistical analysis. The present research work consists to perform numerical stimulations of orthogonal cutting of AISI 1045 steel using 2D Deform Software. These numerical stimulations are designed using Design of Experiment (DOE). The simulated tests are the combination of different tool and cutting process parameters. The 2D Deform program calculates different machining characteristics: cutting temperature, stress chip thickness, wear depth and residual stress. The obtained interactive effects numerical results were studied and analysed statistically using a statistical analysis software to identify the influencing parameters during the cutting process. These results were optimised to determine the configurations corresponding to minimum machining properties.

Figure 2.1 presents the research study framework. This research study was based on numerical simulations without any experimental testing for economical and temporal reasons. The numerical simulations results were validated experimentally using data found in the literature for the same material, the same tool-edge geometries and the same cutting conditions. The calculated error was determined by the following Equation:

$$\Delta = \frac{|X_{exp} - X_{num}|}{X_{exp}} \quad (2.1)$$

Where X_{exp}, X_{num} and Δ are respectively the experimental value, the numerical value and the calculated error.

For the experimental validation, the calculated errors are considered acceptable when they are less than 10%. This is the generally accepted in the field.

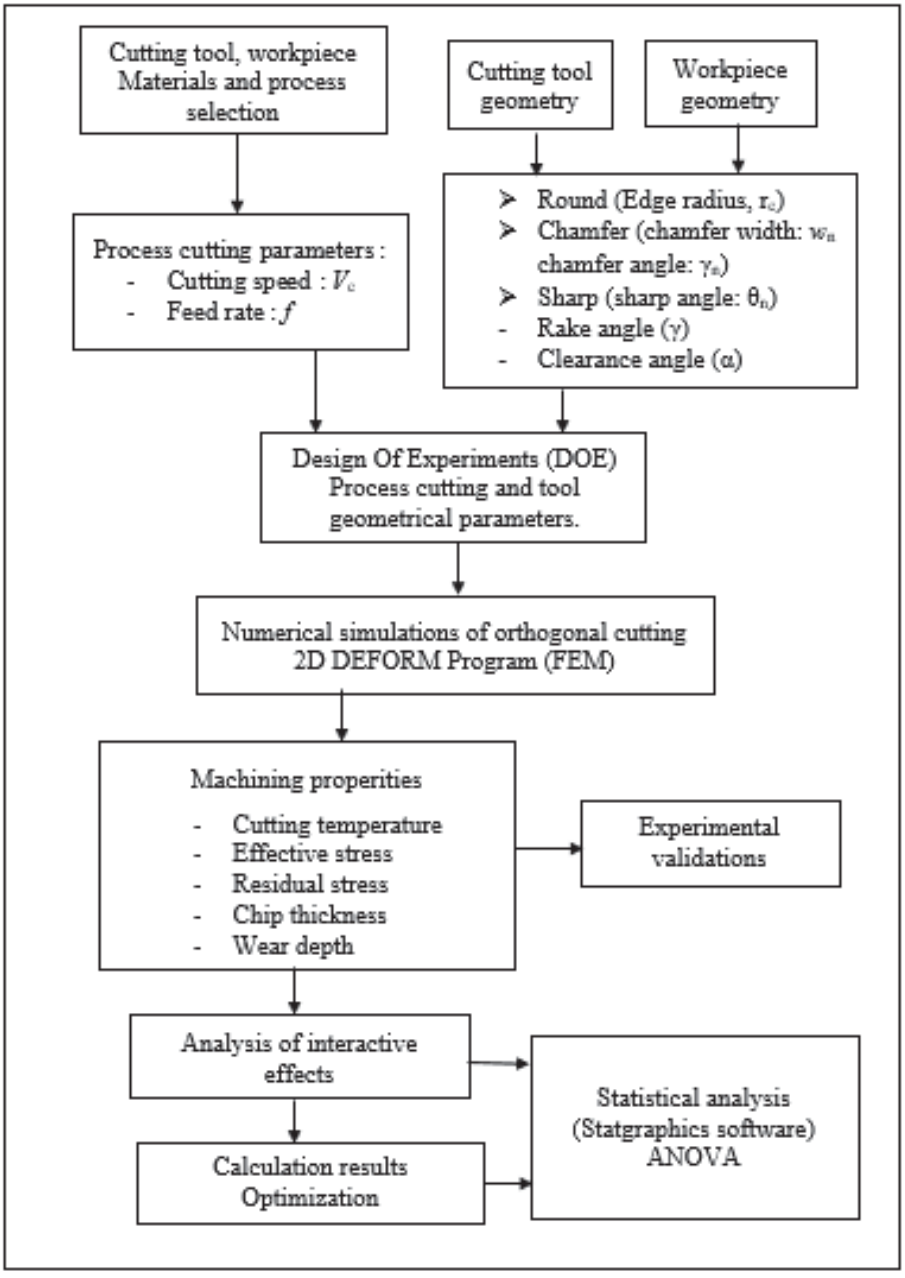

Figure 2.1 Research study framework

2.2 Material of study

In the present study, the workpiece material selected is AISI 1045 steel. It is used to manufacture machine parts with high strength requirements such as gears, piston pins, shafts. AISI 1045 steel consists of various chemical elements. Table 2.1 presents the typical chemical composition of AISI 1045 steel. The tool material used is uncoated cemented carbide.

Table 2.1 Typical chemical composition of AISI 1045 steel AZOM (2000)

Element	C	Mn	S	P	Fe
Content (%)	0.43-0.50	0.60-0.90	0.05 (max)	0.04 (max)	Balance

2.3 Design of experiment

To determine the influence of cutting tool and machining variables on the output of cutting process, design of Experiment (DOE) was used. This systematic method consists to perform different sets of tests called design planning. In each set of test, one tool edge geometry and one cutting parameter will be varied. Whereas the other parameters will be kept constant. The design planning is an established matrix with tool edge geometrical and cutting factors at different levels.

2.4 Numerical modeling

To study the effects of different tool edge preparations and the specified cutting parameters on output responses, various numerical tests based on the design of experiment (DOE) were performed using Two-dimensional (2D) orthogonal cutting simulations. The software used was DEFORM-2D R V 11.3. The 2D orthogonal cutting numerical modeling was selected because it provides conservative results with simplicity and faster computation. The mentioned simulated machining characteristics were determined by solving the corresponding equations integrated in DEFORM program. The transient temperatures and forces were calculated numerically using transient heat transfer and motion modules. In the heat transfer modeling,

there are two types of mechanisms: conductive and convective modes. The conductive mode occurred between tool and workpiece. Whereas the convective mode occurred between tool, workpiece and the ambient air. The simulation steps including boundary conditions are explained in next chapters three and four. The cutting geometry model consisted of the cutting tool and the workpiece which are meshed automatically with two-dimensional (2D) quadrilateral elements.

The numerical modeling process includes three steps: pre-processing, simulation processing and post-processing. The pre-processing step consists to enter the input and the data such as cutting parameters and boundary conditions, the cutting tool and workpiece materials and their geometries. The simulation processing step is to control the numerical calculations in the time. The post-processing step is to exploit the simulation results for analysis. Figures 2.2 and 2.3 illustrate the different simulations steps of the orthogonal cutting process.

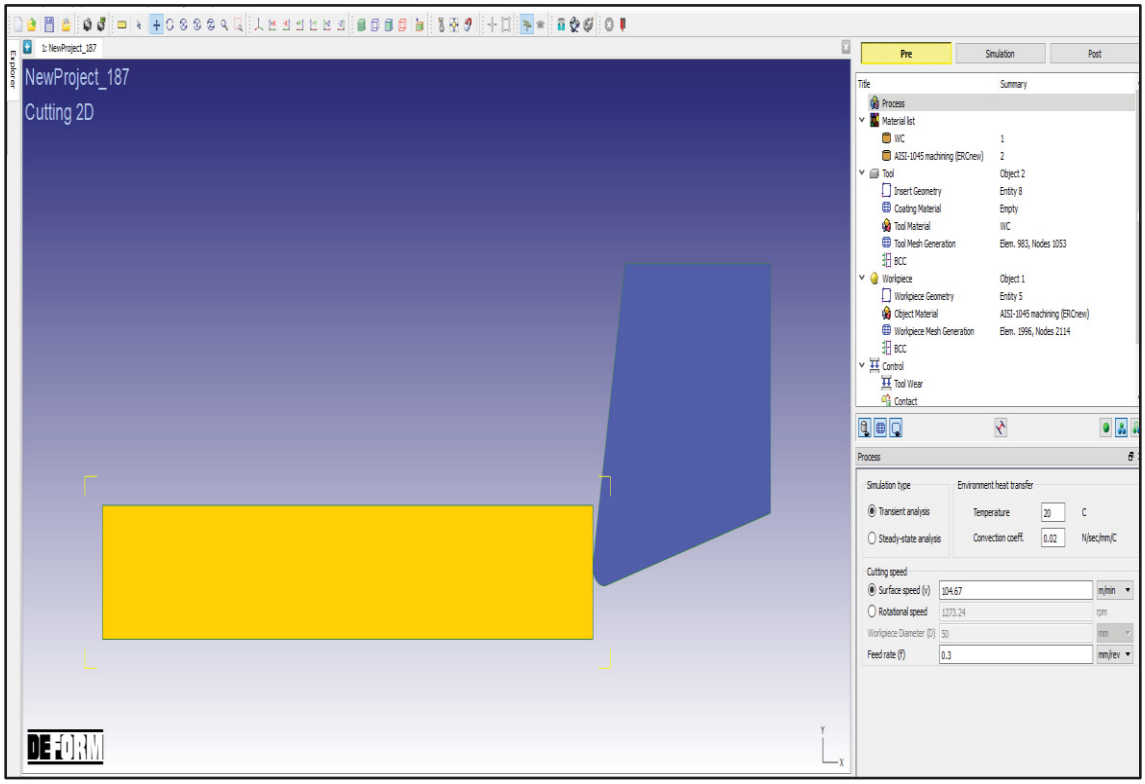

Figure 2.2 The pre-processing step.

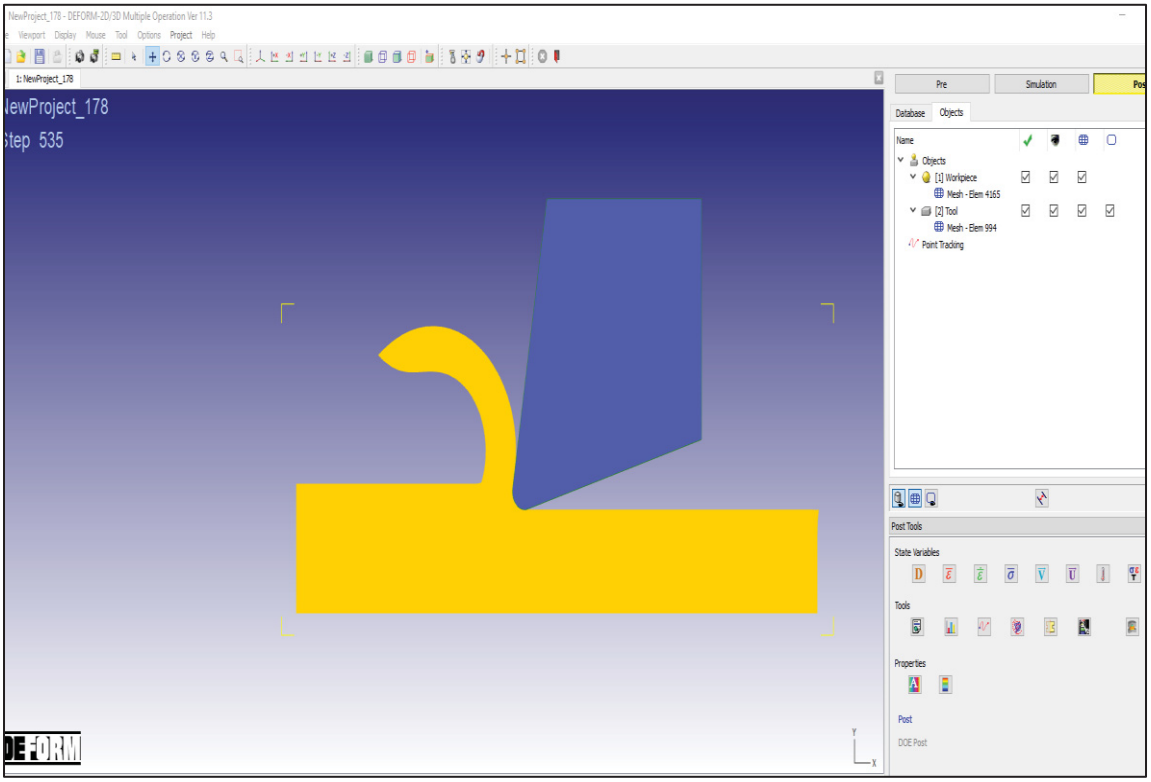

Figure 2.3 post-processing step.

In this research, the design of simulations and the statistical analysis were performed using the Statgraphics XVII.I centurion software. The developed design of experiments (DOE) will be set by selecting the studied factors with different levels. Th number of tests is set with different nonrandomized combinations and can be calculated by L^F (L stands for number of levels and F stands for number of factors). The total number of the simulation test can be reduced by the Statgraphics program. The designed number of levels is based on effect variability of the factors for each level on output response of the cutting process. The multifactorial analysis is designed to build a statistical model describing the effect of two or more factors (independent variable) on dependent variable (output response). The numerical tests realised in DEFORM software are run and analysed by ANOVA to determine the significant differences between the means of the output response at the different levels of the factors and the interactions force between these factors. The obtained results will be presented in Tables and displayed graphically in means plots and interaction plots.

According to Stagrahphics XVII.I Software analysis, tables decompose the total variability among the measurements into separate components that correspond to different source of variations: main effect, interaction and residual component. P-values stands for the statistical measurement for performing significant tests. P-values that are less than 5% correspond to significant effects at the 95.0% confidence level.
The numerator term stands for the sum of squares of deviations of all the measurements from the mean. Whereas the denominator term is the degrees of freedom.
The total sum of squared deviations (TSS) includes two components: the first one is sum of squares of deviations due to each factor and the interaction effects with other factors (SSD), the second one is the sum of squared error (SSE). TSS is expressed by the algebraic formula:

$$TSS = SSD + SSE \tag{2.2}$$

The F-tests called in honor of Sir Ronald Aylmer Fisher are used to evaluate the equality of means and to test the overall the significance of the regression model. It is about calculating the probability of observing F-statistics allowing to determine if the F-values under the null hypothesis is true. At high F-values, the results are statistically significant.
In case of existing significant interactions, they can be analysed together using the interaction Plot. The interaction plot displays the least squared means at all combinations of two factors. If the factors interact, the effect of one factor depends upon the level of the other. If they do not, the lines on the plot are approximately parallel.

The statistical results can be displayed in pareto diagrams with the effects of the parameters and their interactions obtained by ANOVA showing the most significant terms.

2.5 Numerical simulations for optimal responses

The study of the optimization of tool edge geometry and the cutting parameters will be realized using the analysis of variance (ANOVA). The response surface method will be used to develop and to predict the regression models that are expressed by response functions fitting to data. The most significant parameters will be identified. The optimization model consists to

determine the edge tool geometrical and cutting parameters in such way to minimize the studied machining characteristics (cutting temperature, cutting stress, chip thickness and wear depth) as formulated bellow:

$$\text{Find } V, f, r_c, w_n, \gamma_n \text{ and } \theta_n \xrightarrow{\text{Minimize}} T_c, \sigma_c, t_c \text{ and } w_d$$

$$\frac{d\,(T_c,\ \sigma_c,\ t_c, W_d)}{d\,(V, f,\ r_c, w_n, \gamma_n, \theta_n)} = 0 \tag{2.3}$$

Where:

T_c, σ_c, t_c and W_d are cutting temperature, cutting stress, chip thickness and wear depth

2.6 Conclusion

The present work study was conducted using the following tools:

- The 2D Deform software for performing numerical stimulations of orthogonal cutting of AISI 1045 steel.
- The numerical stimulations are designed under different tests form by applying Design of Experiment (DOE). The tests are made by the selected cutting process and tool parameters.
- The obtained machining characteristics numerical results were studied statistically based on ANOVA using a stratigraphic software to determine the influencing parameters et their interactive effects.
- Using ANOVA from stratigraphic software the simulated results were optimized to identify the configuration of the cutting and tool parameters producing the minimum machining properties.

CHAPTER 3

A NUMERICAL MODEL FOR PREDICTING THE EFFECT OF TOOL NOSE RADIUS ON MACHINING PROCESS PERFORMANCE DURING ORTHOGONAL CUTTING OF 1045 STEEL

Zakaria Ahmed M. Tagiuri[1], Thien-My Dao[1], Agnes Marie Samuel[1], and Victor Songmene[1]

[1]Department of Mechanical Engineering, École de Technologie Supérieure (ÉTS)
1100 Notre-Dame Street West, Montréal, QC H3C 1K3, Canada

Paper published in Materials, May 2022, 3369; doi:10.3390/ma15093369

Abstract

This paper presents the development of a numerical model for predicting and studying the effects of tool nose geometries and its interactions with cutting parameters during orthogonal cutting of AISI 1045 steel. The process performance characteristics studied were cutting temperature, effective stress, cutting forces and tool wear. The cutting simulations were done using the commercial DEFORM-2D R V 11.3 software, based on the finite element method (FEM). The cutting tool used had a round nose with various nose radii (0.01– 0.9 mm), while the machining parameters tested were the feed rate (0.1– 0.3 mm/rev), the cutting speed (100–500 m/min) and the rake angle (–5º to +10º). The interactions between the tool nose radius and the cutting parameters (speed, feed) were found to affect mostly the cutting stress and, slightly, the tool wear rate. These interactions did not much influence the cutting temperature, that was found to be high when the tool nose radius and/or the cutting speed were high. The maximum temperature was found to occur at the middle of the tool-chip contact length and at the interaction of nose radius and flank face of the tool. Except for some fluctuations, there was no significant difference in tool wear rate between small and large nose radius scales.

Keywords: tool nose radius; orthogonal cutting; AISI 1045; cutting forces; temperature; stress; tool wear

3.1 Introduction

One of the major problems commonly met on a continual basis during cutting processes in different machining industries is failure of the cutting tool, due to excessive mechanical forces, higher temperatures and gradual tool wear. Gradual tool wear occurs on the cutting tool edge, especially for complex parts that may be difficult to cut, leading to short tool life, and, consequently, increasing cycle time and machining costs. To enable machining companies to become more competitive, there is an imminent need to incorporate cutting-edge preparation as a new concept in the context of cutting tools, by generating a specific geometry around the cutting tool edge, so as to improve tool life, part quality, and reduce cycle time and machining cost (Rodríguez.,2009; Wang et al., 2020). In literature, few research studies have been conducted on machining operations by adopting cutting edge preparation approaches that show their advantages in different machining applications. (Denkena & Biermann., 2014) reported that a good selection of cutting tool edge geometry influences machining process performance. It improves tool wear resistance, and tool life, as well as having effects on chip formation, and mechanical and thermal stresses. (Tiffe et al., 2019) proposed a finite element analysis-based methodology of the optimization of prepared cutting-edge micro forms that reduce tool wear during the machining of Inconel 718. They found that an asymmetrical micro shape is the optimal cutting-edge profile, by investigating cutting-edge parameters S_α, S_β and S_γ. In fact, (Shnfir et al.,2019) investigated the machinability of hardened steel AISI 1045 during face milling using cutting tools with tool edge preparation, in order to identify the effects of cutting parameters, milling configuration, edge preparation and work material hardness on cutting force, power consumption and flank tool wear. Their results showed that lower feed rates and increased workpiece hardness resulted in decreasing cutting forces with honed edge inserts. At low cutting speeds and high feed rates, flank wear was increased, and the use of tools with chamfered tool-edge preparation greatly improved tool wear.(Zhuang et al., 2020) analysed the effects of cutting-edge micro-geometry on surface roughness and white layer formation in turning AISI 52100 steel. They found that increasing chamfer width improved surface roughness, but increasing the chamfer angle did not have any significant effect. Moreover, large rounded and chamfered edges could contribute to white layer formation. Despite the

increase in application of cutting tools with round geometry preparation techniques in current developments, previous research investigations on cutting edge geometry preparation, and its effect on the performance of machining processes are very limited. (Javidikia et al., 2020) studied interactive impacts between cutting-edge radius and cutting speed, feed rate, and rake angle on machining forces, cutting temperature, and chip thickness during turning of aluminium alloy 6061-T6. In fact, by comparing conventional machining (CM) with high-speed machining (HSM), the obtained results showed that both cutting force and feed force are increased when the cutting-edge radius is increased at low cutting speeds (related to conventional machining (CM)) and at a negative rake angle. For the thermal aspect, the maximum cutting temperatures remain almost constant with increasing cutting speed but they increase with increasing edge radius for all the cutting speeds considered, whereas an increase in the average temperatures of the tool tip is observed in the case of high-speed machining (HSM). Moreover, the maximum cutting temperature was found to depend mostly on cutting conditions and tool geometry for the workpiece and tool materials tested. In terms of chip formation, the authors found no significant variation of chip thickness with cutting-edge radius in high-speed machining (HSM) in their study. (Zhuang et al., 2018) proposed a numerical simulation model to predict the impacts of chamfer angle, chamfer length and feed rate on the machining force of Ti6Al4V. The obtained results showed a significant influence was exhibited by chamfer length and angle on cutting force. However, few studies have been realised on the interaction between cutting speed, edge radius, feed rate and rake angle and their effects on the machining properties of steel, in particular, carbon steel materials. A numerical study was conducted by (Cheng et al.,2016) on the influence of tool edge radius and rake angle during orthogonal cutting of Fe-Cr-Ni stainless steel on machining performance. They found that stress was more affected than temperature by edge radius, and with increasing rake angle there were fluctuations in terms of stress and a gradual increase in higher temperature and force increased on the rake face. (Jiang & Wang., 2019) performed a numerical research, based on the finite element method, investigating effects of different wiper tool edge designs on temperature and force during orthogonal cutting of AISI 4340 steel. They found that the tool temperature of the flank face is more reduced with wiper tools than with round conventional tools, whereas temperature and force increased on the rake face.

It is stated that on one hand, only the impact of cutting tool radius on different machining output variables was assessed, showing interactive behaviour with various cutting speeds, rake angles, and feed rates. On the other hand, only round edge geometry was considered, and other edge geometries were ignored. Moreover, the study was limited to small tool edge radius. Thus, large tool edge radius has not yet been studied, which points to another lack of data for the macro machining industry.

Based on the above details of the available data, the need to study more interactions between tool geometry and machining parameters for available cutting tool edge preparations is justified. This approach could help tool designers, and guide manufacturing engineers, in selecting a process with optimal geometrical parameters, and establish standard and accurate tool edge preparation procedures applicable in the machining industry.

The objective of the present research is to study the interactive effects of cutting tool geometrical parameters and different machining process conditions for designed tool nose geometry on cutting force, cutting stress, tool wear and temperature distribution. A numerical model, based on finite element analysis, was developed to predict the effects of interactions between cutting nose geometry and machining parameters of feed rate and cutting speed on machining process performance indicators; namely, cutting forces, temperature, tool wear and cutting stress.

3.2 Numerical simulation model for orthogonal cutting analysis

The objective of the present simulation study is to predict the effects of cutting tool nose geometries for different edge preparations on machining process performance in terms of temperature distribution, tool wear, effective stresses and strains. Two-dimensional (2D) orthogonal external cutting simulations, with plain strain condition, were conducted using the commercial Finite Element Method (FEM) DEFORM-2D R V 11.3 software. This software program is based on the Lagrangian formulation for plastic deformation analysis. The material of the workpiece is modelled as a plastic material, whereas the cutting tool is considered as an elastic material. The simulations are limited to round tool geometry. Chip formation is simulated by plastic flow, whereas separation of formed chips from the workpiece is completed

by continuous remeshing. It is assumed that there is no crack initiation detected in the tool tip during the cutting process. In the present study, for cutting nose preparation, only round nose geometry was proposed. Figures 3.1 and 3.2 show the workpiece and the tool model designs, respectively.

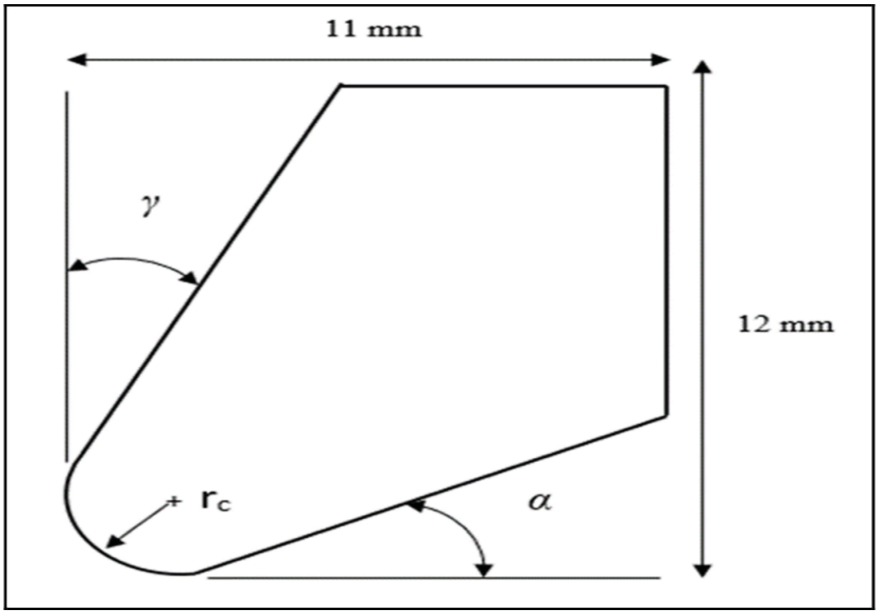

Figure 3.1 Tool model geometry (r_c, α, γ are the nose radius, the clearance angle and the rake angle, respectively)

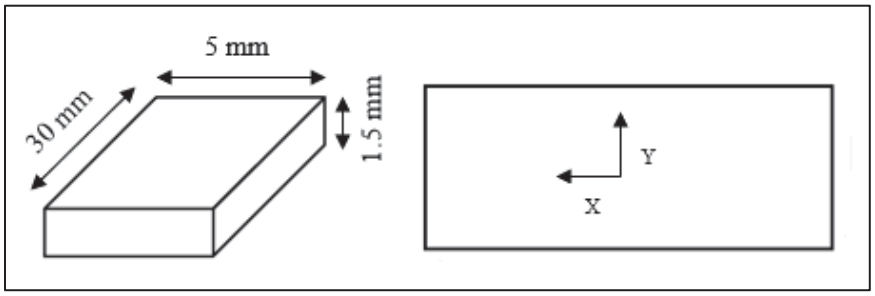

Figure 3.2 Workpiece model geometry

3.2.1 Material characterization

The selected workpiece material used for the present study is AISI 1045 steel. For the cutting tool, the material used is uncoated cemented carbide. The cutting process occurred in a very

short time (around ms), so that the temperature reached the steady state very quickly, thereby causing little variation in thermal conductivity with temperature. So, these properties are supposed constant. Table 3.1 presents the thermal and physical properties, while Table 3.2 presents the mechanical properties of the workpiece and tool materials.

Table 3.1 Thermal and physical properties of workpiece and tool materials
Adapted from Yen et al. (2004); Zakaria (2019)

Item	**Tool**	**Workpiece**
Properties	Uncoated cemented carbide	AISI 1045
Density (kg/m^3)	11900	7870
Thermal conductivity (W/m°C)	50	45
Specific heat (J/kg°C)	375	590

Table 3.2 Mechanical properties of workpiece and tool materials Zakaria (2019)

Item	**Tool**	**Workpiece**
Properties	Uncoated cemented carbide	AISI 1045
Young's modulus (GPa)	620	200
Poisson ratio	0.26	0.29
Hardness (HB)	93	163

The numerical model consists of conducting the orthogonal cutting simulations using the commercial DEFORM 2D Finite Element Method software. The cutting geometry model is meshed with two-dimensional (2D) quadrilateral elements. The Finite Element Method (FEM) mesh was based on quadrilateral elements because they can be used with adaptive mesh refinement. This approach generates simple meshes and ensures good control of the density of the elements. Each element has four nodes and can be generated automatically by a default algorithm for solid modeling. Figure 3.3 shows the meshing of the model for cutting

simulation, where V_c, f and h are the cutting speed, the feed rate and the depth of cut, respectively.

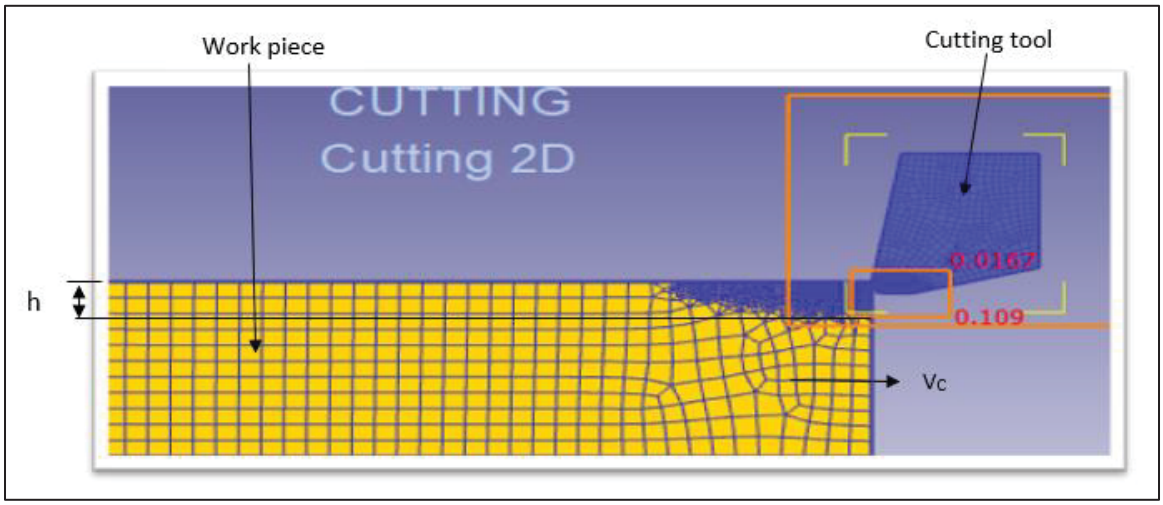

Figure 3.3 Meshing of the model for cutting simulation
at V_c = 104 m/min, f = 0.1 mm/rev

The transient heat transfer and motion equations used by the DEFORM software during the cutting process may be expressed by the following equations (Javidikia et al., 2020):

$$[C_T]\{\dot{T}\} + [K_T]\{T\} = \{\dot{Q}_g\} \tag{3.1}$$

$$[M]\{\ddot{U}\} + \{R_{int}\} = \{R_{ext}\} \tag{3.2}$$

where $[C_T]$ is the volume heat capacitance, $[K_T]$ is the thermal conduction matrices, $\{\dot{Q}_g\}$ is the total heat generated, $\{\ddot{U}\}$ is the acceleration vector, $\{U\}$ is the displacement, $\{R_{int}\}$ is the vector of internal force, whereas $\{R_{ext}\}$ is the vector of external force.

Considering the selected materials, the flow stress model for these materials may be expressed according to the Johnson-Cook constitutive equation as follows (Javidikia et al., 2020):

$$\overline{\sigma} = \left[A + B\left(\varepsilon^{n}\right)\right]\left[1 + C.\ln\left(\frac{\dot{\varepsilon}}{\varepsilon_0}\right)\right]\left[1 - \frac{\left(T - T_{room}\right)}{\left(T_{melt} - T_{room}\right)^{m}}\right] \tag{3.3}$$

Where ε is the plastic strain $\dot{\varepsilon}$ (s^{-1}) is the plastic strain rate, $\dot{\varepsilon}_0$ ($^{-1}$) is the reference plastic strain rate, T (°C) is the workpiece temperature, T_{melt} (°C) is the melt temperature, T_{room} (°C) is the room temperature, A (MPa) is the initial yield strength, and B (MPa) is the hardening modulus. C is the strain rate sensitivity coefficient, m is the thermal softening coefficient, and n is the hardening coefficient.

The numerical simulation of tool wear by 2D DEFORM is based on nodal displacement (at each node) caused by wear for a certain cutting time increment. The tool wear is expressed by its proper wear rate at every node, where the wear rate is given by the volume loss of material removed by machining per unit area and per unit time. For this study, only flank wear, which occurred on the flank area was considered (Li., 2012).

The tool wear was simulated using the Usui wear model as follows (Afrasiabi et al., 2021):

$$W = \int A.\,P.V.\,e^{-\frac{B}{T}}.\,dt \tag{3.4}$$

where W, *P, V, T* and *dt* are tool wear, interface pressure, sliding velocity, temperature and time increment, respectively. *A* and *B* are constants determined experimentally.

Boundary Conditions

The displacement and thermal boundary conditions for work piece and tool simulation are given as follows:

- The tool is fixed, and the work piece is being cut at the specified cutting speed:
  i. For heat transfer simulation, the tool-chip thermal contact is perfect with heat transfer coefficient (h_c)

ii. The boundaries of the work piece and tool are set at room temperature ($T_\infty = 25$ ºC) far from the cutting zone

iii. The convection heat transfer coefficient is $h_\infty = 20$ W/m^2 ºC

iv. The value of the convection heat transfer coefficient h_c considered for air flow was based on the velocity of the surrounding air and approximated according to the following equation:

$$h_c = 10.45 - v + 10\, v^{1/2} \tag{3.5}$$

where v is the relative velocity between object surface and air (m/s).

It should be noted that during the cutting process, heat is generated in the cutting zone. At the same time, natural cooling occurs, because of a change in temperature due to the ambient air. The cooling mechanism can be expressed according to Newton's law of cooling as follows:

$$k_i\, \Delta T = h_c\, (T_{air} - T) \tag{3.6}$$

where k_i , ΔT and T_{air} represent, respectively, the thermal conductivity of the considered material, the temperature gradient, the heat transfer coefficient for natural convection, and the ambient temperature.

3.2.2 Numerical design planning

This section is dedicated to the numerical method that was adopted in the present study. Orthogonal cutting tests were performed to study the interactive effects of different cutting nose geometries on milling process performance under different cutting conditions.

In order to study the interactive effects of different machining parameters with tool nose geometries on machining process performance, it is necessary to consider the importance of cutting conditions in identifying the main effects and the interactions of parameters. Only the round tool geometry was considered. Table 3.3 presents the design of experiments used in the numerical simulations. The clearance angle was constant at $\alpha = 15°$.

For the first set of experiments, only the nose radius and the cutting speed were varied; in the second set, the feed and the nose radius were varied; for the third set, the rake angle of the tool and the nose radius were varied, and, finally, for the fourth set of tests, only the nose radius was varied.

Table 3.3 Design for numerical simulations

	Tool Geometry and Machining Parameters			
Simulation Group ID	Nose Radius r_c (mm)	Rake Angle γ (°)	Cutting Speed V (m/min)	Feed Rate f (mm/rev)
1	0.01– 0.9	5	100, 104, 225, 250, 400, 500	0.1
2			100	0.1, 0.2, 0.3
3		− 5, 0, 5, 10		0.1
4		5		0.1

3.3 Numerical simulation results

The different machining properties were simulated numerically using the transient analysis module of DEFORM 2D software based on the two-dimensional (2D) Finite Element Method (FEM). For cutting forces, the transient proposed model enables determination of the evolution of the machining forces with time. Figure 3.4 illustrates the variation of machining force, namely the cutting force and thrust force, during the machining process for V = 400 m/min, r_c = 0.3 mm, f = 0.1 mm/rev, γ = 5°. Figures 3.5, 3.6 and 3.7 show the numerical simulation results of cutting temperature, effective stress and effective strain for nose radii (0.3, 0.5, 0.7 and 0.9 mm) at t = 0.0014 s in the workpiece, cutting tool, and at the interface. For cutting temperatures, the simulation results illustrate the distribution of temperatures in different locations in the model.

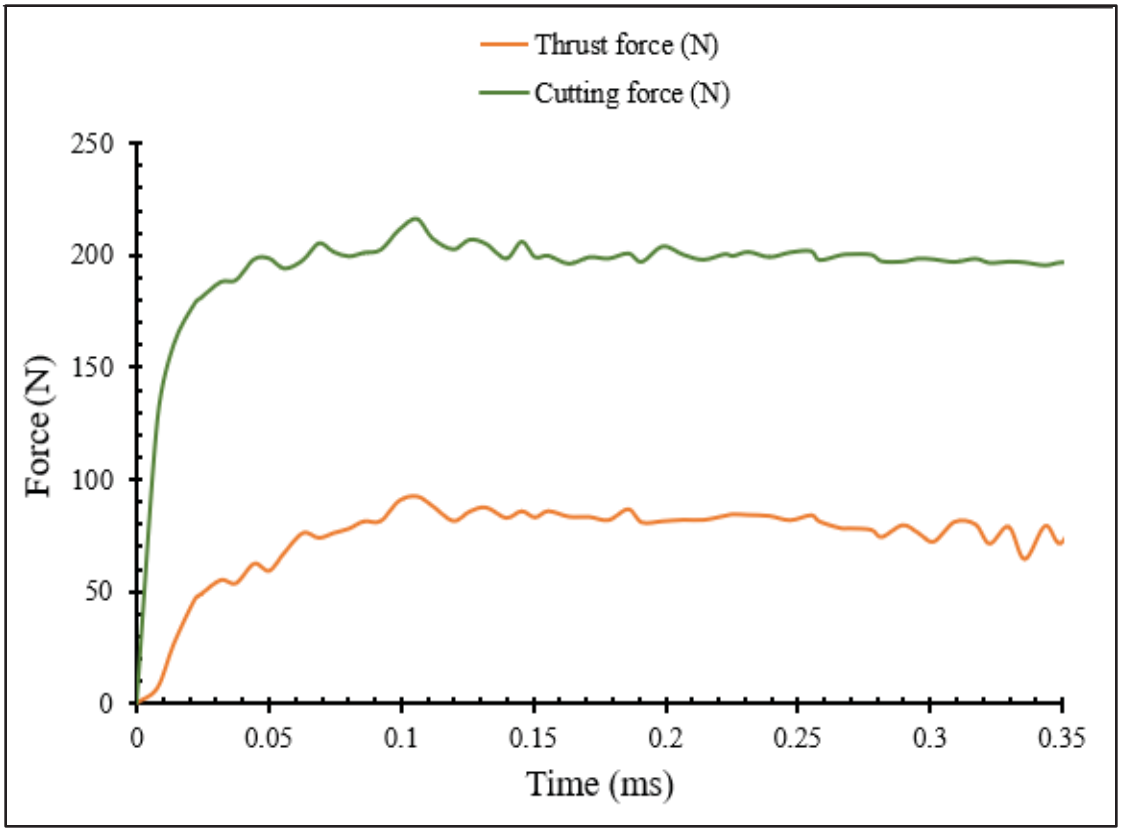

Figure 3.4 Transient force simulations during machining process
at $V = 400$ m/min, $r_c = 0.3$ mm, $f = 0.1$mm/rev, $\gamma = 5°$

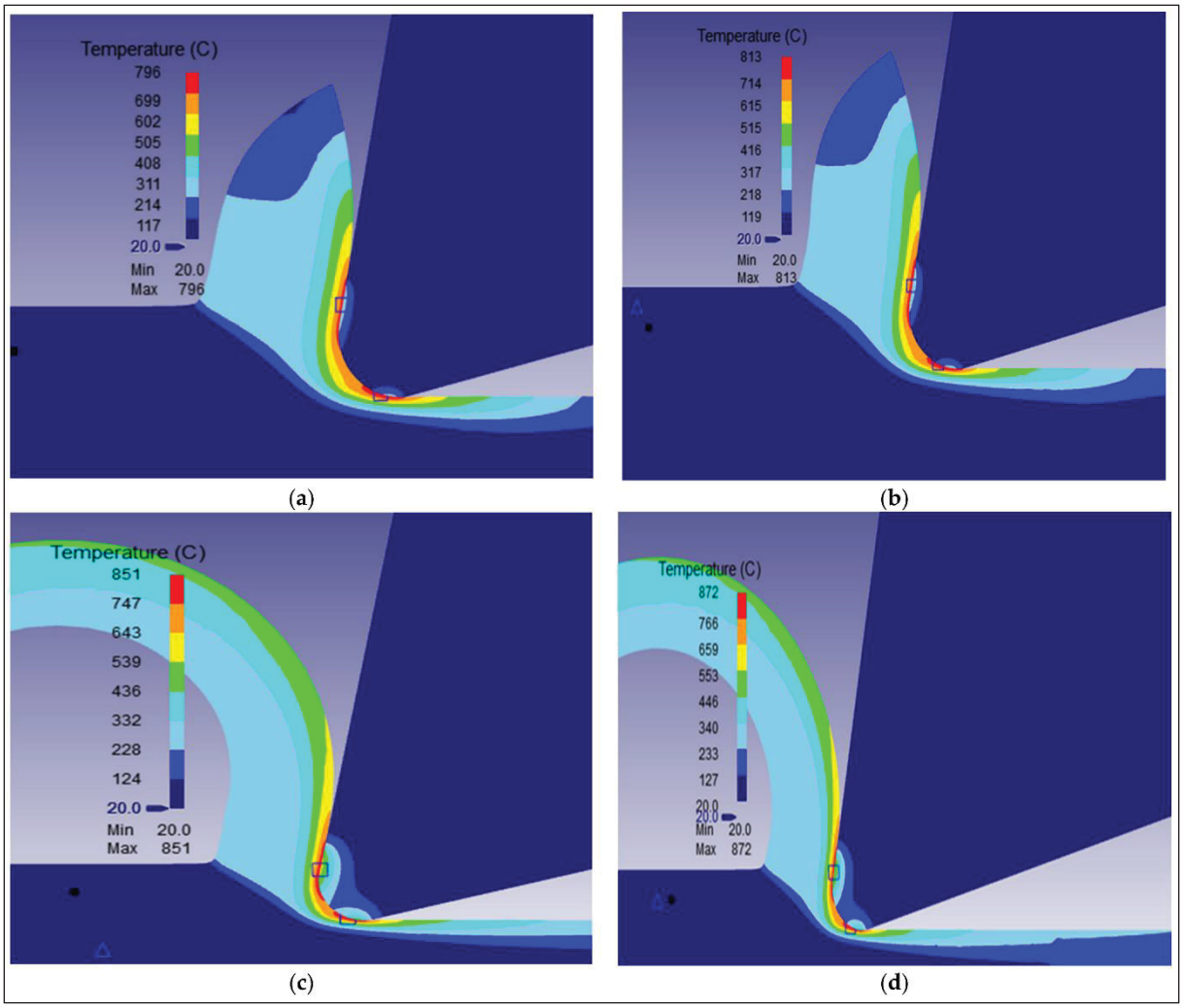

Figure 3.5 Distribution of cutting temperature in the workpiece and cutting tool at $V = 400$ m/min, $f = 0.1$mm/rev, $\gamma = 5°$ for the nose radii r_c: (**a**) 0.3 mm, (**b**) 0.5 mm (**c**) 0.7 mm and (**d**) 0.9 mm

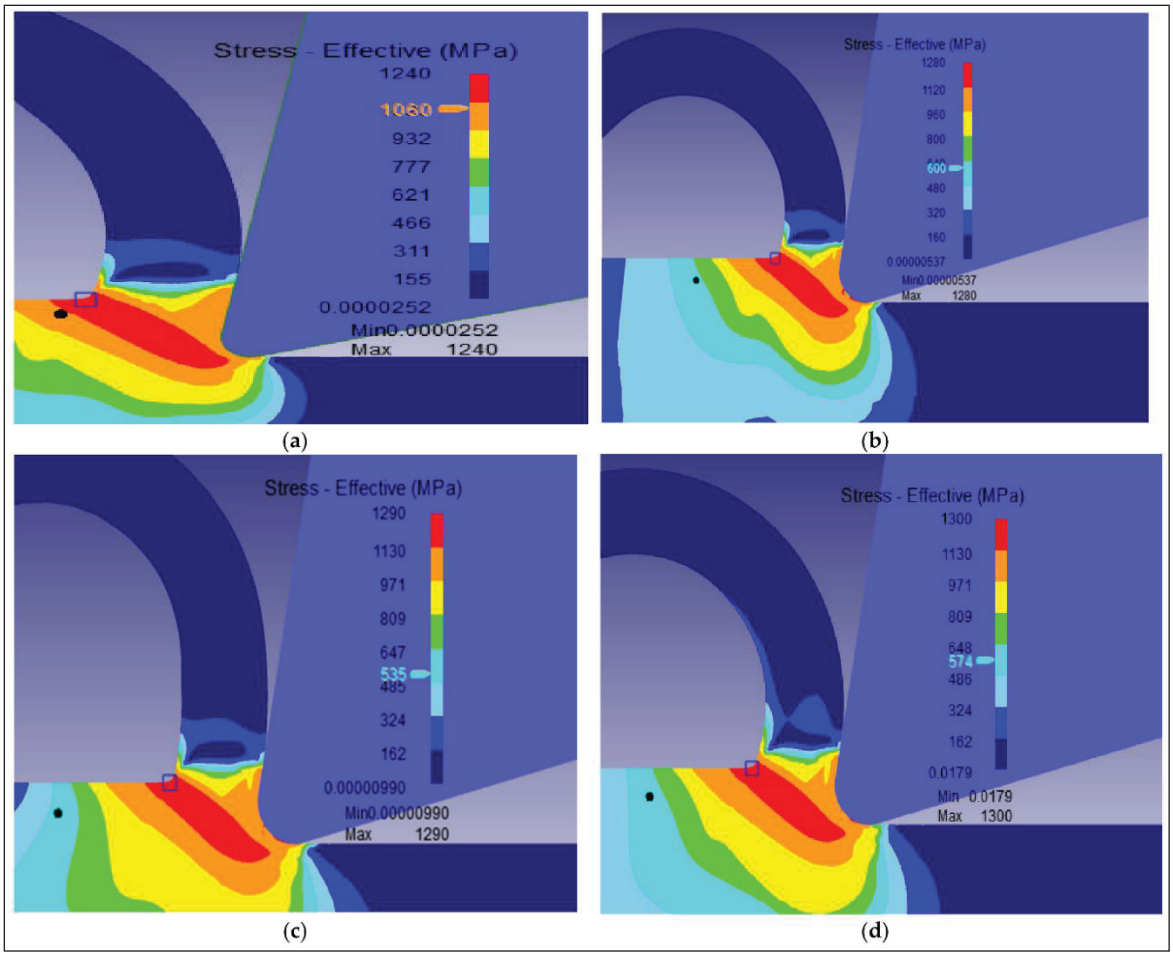

Figure 3.6 Distribution of effective stress in the workpiece and cutting tool at $V = 400$m/min, $f = 0.1$mm/rev, $\gamma = 5°$ for the nose radii r_c: (**a**) 0.3 mm, (**b**) 0.5 mm (**c**) 0.7mm and (**d**) 0.9 mm

From Figure 3.4, the cutting forces and thrust forces are extracted in the X and Y directions, respectively. For each nose radius, the numerical machining forces were obtained from the same simulation time until the steady state, when the transient variations of the cutting force are higher than those of the thrust forces.

From the distribution of cutting temperature displayed in Figure 3.5, it can be seen that the cutting temperatures were higher in the contacts areas (between the tool and in the chips, between the tool and the workpiece). Also, the higher the tool nose radius was high the higher was the maximum cutting temperature. This is a consequence of higher stresses (Figure 3.6) and strains (Figure 3.7) taking place in the workpiece in the shearing zones and frictions at

tool-chip and tool-workpiece interfaces. Figure 3.6 presents the simulation of the distribution of the stresses in the workpiece and tool. The results in Figure 3.6 reveal that cutting stresses were developed in the machining direction due to forces applied in the X direction (Figure 3.4). As expected, maximum stresses occurred in the shear plane. The higher the tool nose radius was the more maximum stress was exerted in the workpiece and the higher the shear plane. It reached 1300 MPa for a nose radius of 0.9 mm as compared to 1280 MPa for a nose radius of 0.3 mm. These high stresses, and the subsequent deformations, were responsible for the high temperatures already observed in the cutting zones.

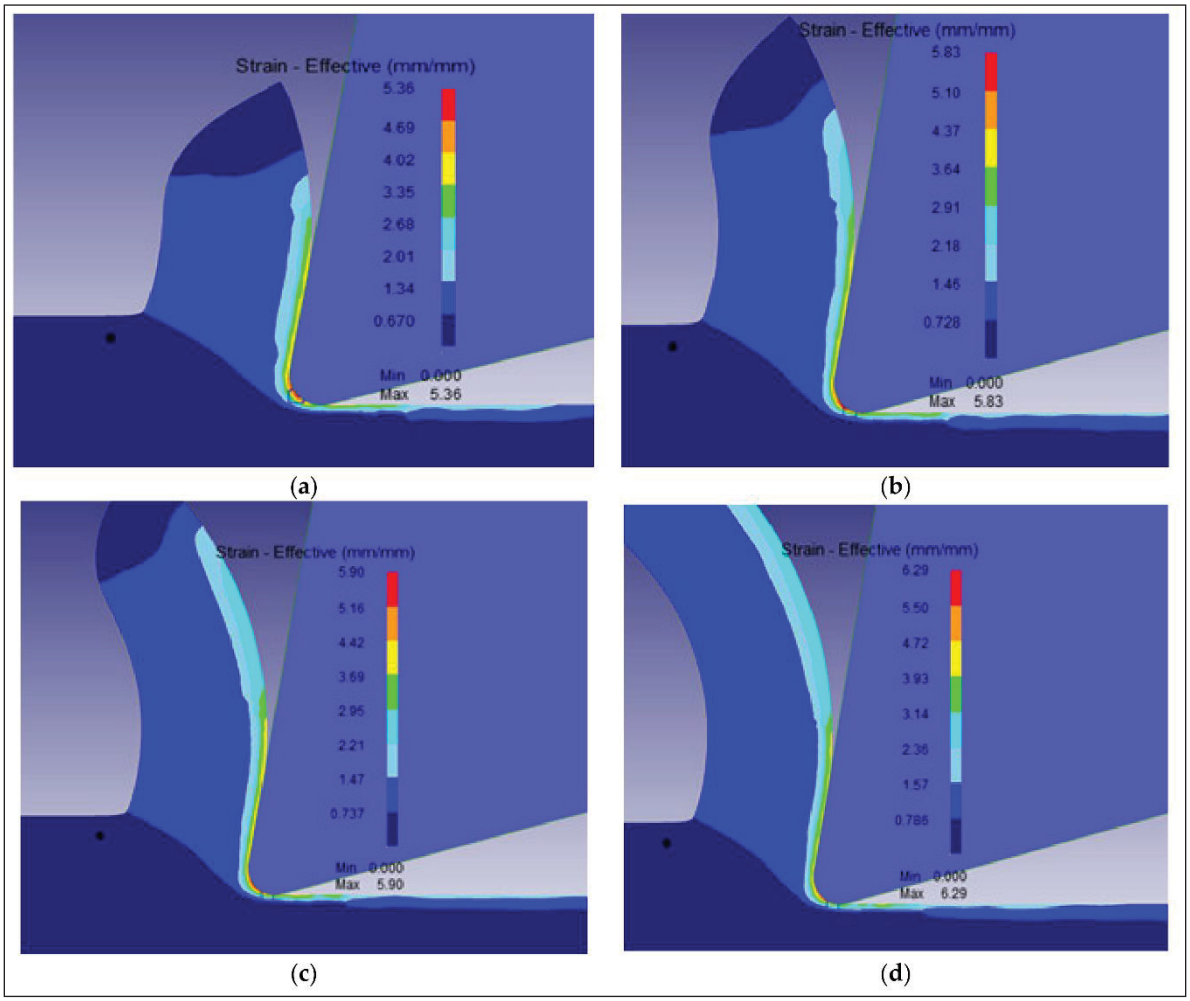

Figure 3.7 Distribution of effective strain in the workpiece and cutting tool at $V = 400$ m/min, $f = 0.1$mm/rev, $\gamma = 5°$ for the nose radii r_c:
(**a**) 0.3 mm, (**b**) 0. 5 mm (**c**) 0.7 mm and (**d**) 0.9 mm.

Figures 3.7 present the effective strain profiles predicted in the cutting zone for given tool nose radii. Maximum strain occurred at the tool tip following by the secondary deformation zone (tool-chip contact zone). As expected, these strains increased slightly with increase in the tool nose radius. For an increase of tool nose radius from 0.3, to 0.5, 0.7 and 0.9 mm, there were increases on effective strains of 9%, 10% and 17%, respectively. This is a consequence of change in flow stress and in cutting stresses when tools with large nose radii are used. Figure 3.8 displays the simulated tool wear rate distribution as a function of tool nose radii. The wear rates are higher in the rake face of the tool (middle of the tool-chip contact length) and at the tool tip interface where the effective rake angle is smallest. In fact, the more the effective tool rake angle is negative, the higher the temperature (Figure 3.5), the flow stress and strain. Consequently, the tool wears out quicker. Wear increased with tool nose radii. For example, for an increase of tool nose radius from 0.3, to 0.5, 0.7 and 0.9 mm, there were increases on effective strains of 14%, 35% and 50%, respectively.

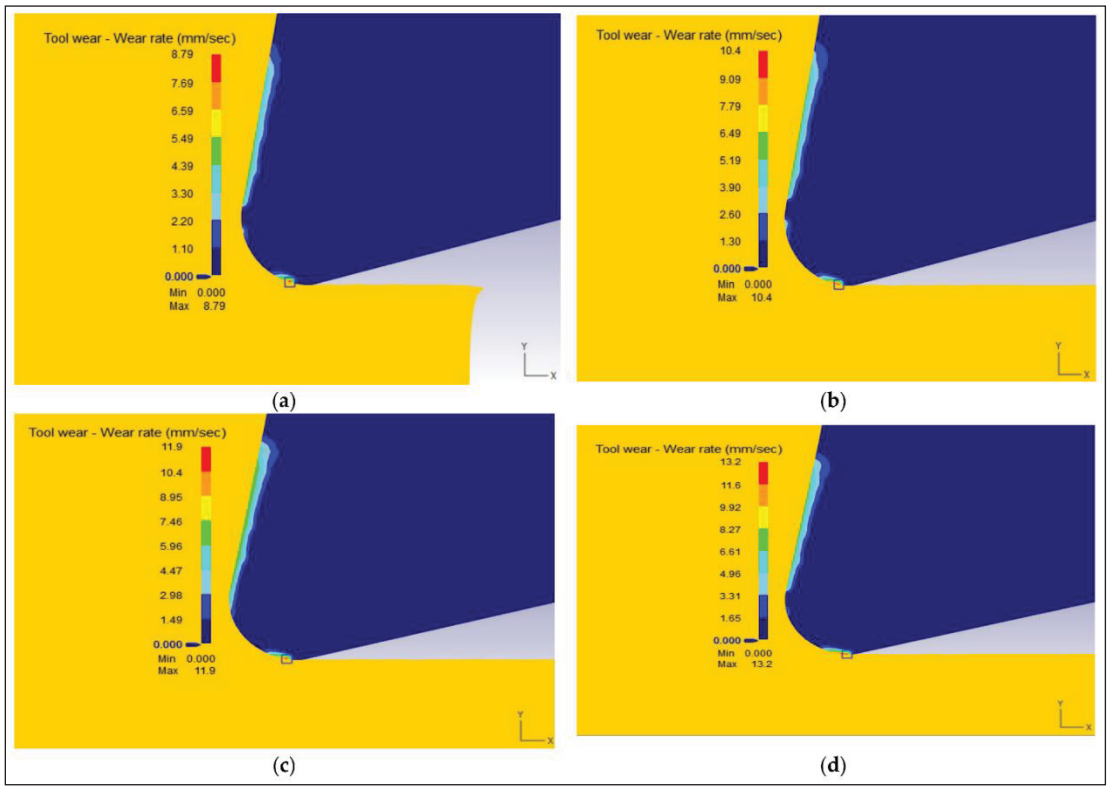

Figure 3.8 The simulation results for tool wear rate at $V = 400$ m/min, $f = 0.1$ mm/rev, $\gamma = 5°$ for the nose radii r_c: (**a**) 0.3 mm, (**b**) 0.5 mm (**c**) 0.7 mm and (**d**) 0.9 mm

Figures 3.9 and 3.10 display the evolution of cutting forces (Figure 3.9) and thrust force (Figure 3.10) when machining with tools with different nose radii. These graphs were extracted from figures, such as the one presented in Figure 3.4. As expected, cutting forces were higher than thrust forces. In general, the forces were low for small tool nose radii (0.01–0.07 mm) and high when large-nose radii were present (0.3–0.9 mm). These results are in good agreement with literature (See comparisons in Tables 3.4 and 3.5). When the tool is almost sharp (very small nose radii), the resistance to the shearing action is limited and less power and energy are required for the cutting process. On the contrary, when large nose radii are used, resistance to cutting action is high and so is the cutting force, and thus the power requirement. It should be noted that tools with high nose radii generate a better part surface finish and compressive residual stresses that could be beneficial for field performance of the machined part.

From Figures 3.9 and 3.10, it may be noted that both the cutting force and thrust force increased slightly as the nose radius increased. By increasing the edge radius 7 times (from 0.01 to 0.07 mm), the cutting force and the thrust force increased by about 15.5% and 12%, respectively. This is due to cutting nose geometry, which requires greater forces for shearing the material. As the nose radius increased, the chip thickness increased and the shear angle decreased, which led to the development of a large shear plane in the deformation area, thereby increasing cutting forces. Further increase in the nose radius from 0.3 to 0.9 mm, resulted in significant increase in the thrust and cutting forces, of about 82% and 125%, respectively.

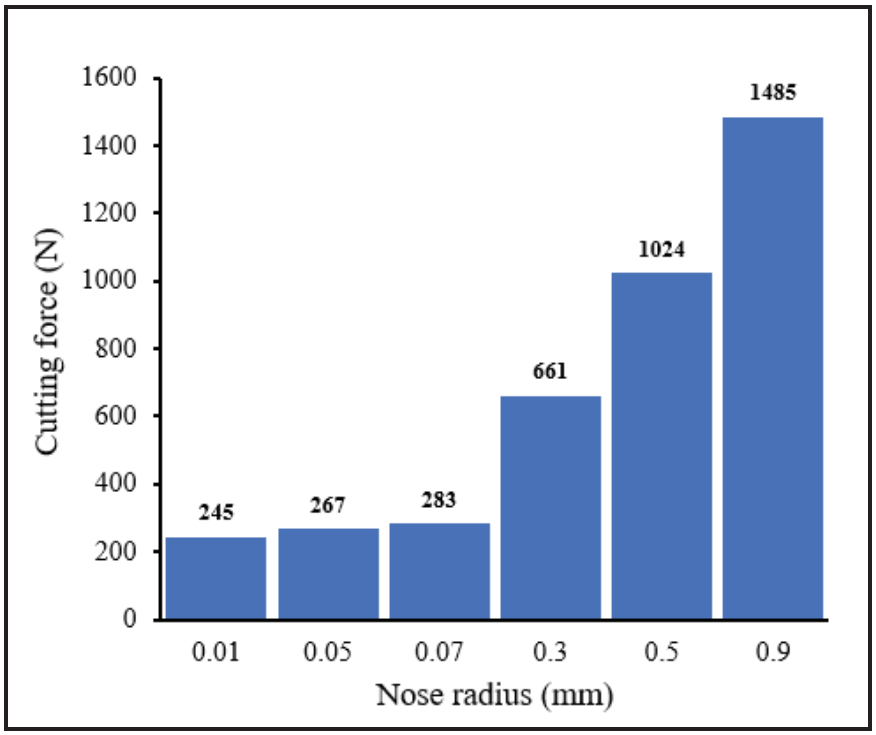

Figure 3.9 Distribution of cutting force for different tool nose radii at $V = 104$ m/min, $f = 0.1$ mm/rev, $\gamma = 15°$

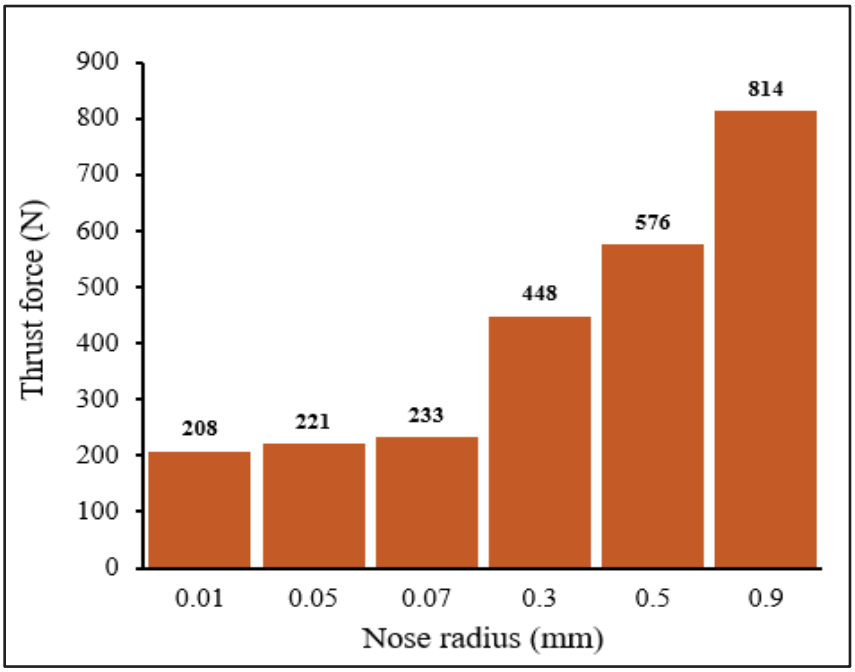

Figure 3.10 Distribution of thrust force for different tool nose radii at $V = 104$ m/min, $f = 0.1$ mm/rev, $\gamma = 15°$

The cutting forces are higher than the thrust forces, due to the fact that the cutting force is applied in the direction of primary motion. Thus, the cutting force comprises a large part of the total force (70–80%) and contributes in determining the global power necessary for the machining process to be carried out (Afrasiabi et al., 2021).

Figure 3.11 shows the distribution of tool wear for different tool nose radii for V = 100 m/min, f = 0.1mm/rev, γ = 5°. It can be noticed from Figure 3.11 that tool wear depth in the rake face of the tool does not directly depend on variation of nose radius, especially for the small tool nose radius scale. The wear width had approximately the same values for 0.03 mm and 0.07 mm radii. For 0.01 mm and 0.05 mm radii, the difference was about 7%. For large nose radius scale the tool wear width increased with increase in the nose radius. The wear widths for the large nose radius scale were higher than those obtained for the small nose radius scale. An indirect interaction between the cutting speed, or the tool rake angle, and the tool nose radius are expected on the tool wear rake as these interactions affect the cutting stress and/or the cutting temperature; these aspects are analysed later in the current article (Section 3.2 Interactive effects between cutting parameters and tool geometries).

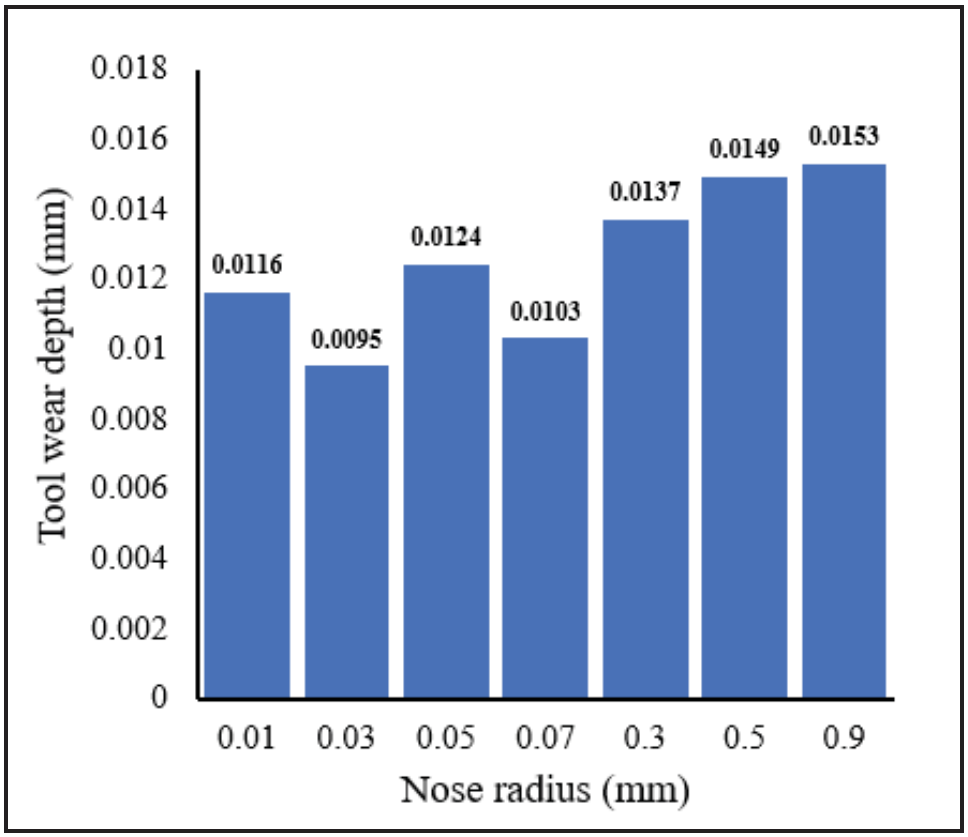

Figure 3.11 Distribution of tool wear for different tool nose radii at $V = 100$ m/min, $f = 0.1$mm/rev, $\gamma = 5°$

3.3.1 Comparison of results between numerical simulations and experimental data from literature

In order to validate the numerical simulation tests, the obtained results were compared with experimental data (Jamel, 2012; Shnfir et al., 2019). Experimental research mentioned in (Shnfir et al., 2019) investigated the effects of tool nose preparation on cutting forces, power, and tool wear in machining of AISI 1045 steel prepared with only honed nose geometry ($r_c = 0.03$ mm), by adopting the method of Taguchi. The second experimental research (Jamel, 2012) covered a study of the effects of tool edge on cutting forces, temperatures, stresses and tool wear in machining of AISI 1045 steel prepared with three honed edge geometries (0.25, 0.5, 0.75 mm). Later on, other numerical simulation tests were realised for large tool nose radii (0.2, 0.5, 0.7 mm) by considering the same machining conditions. Tables 3.4 and 3.5 present

the obtained numerical results compared to experimental results for small and large tool nose radii, respectively.

Table 3.4 Comparison of numerical and experimental results for small tool nose radius

	Numerical Results	Experimental Data Shnfir et al. (2019)	Error (%)
	Nose Radius (mm): 0.03		
Cutting temperature (ºC)	507	465	8%
Cutting stress (MPa)	1271	1318	4%
Cutting forces (N)	258	243	6%

Table 3.5 Numerical and experimental results comparison for large tool nose radius

	Numerical results			Experimental data Jamel (2012)			Error (r_c = 0.5) %
Parameter	Nose radius (mm)						
Characteristics	0.2	0.5	0.7	0.25	0.5	0.75	
Cutting temperature (ºC)	716	814	844	657	682	627	16.2
Cutting stress (MPa)	1239	1241	1237	1230	1200	1200	3.3
Cutting forces (N)	367	562	604	519.4	481	462	14.4
Tool wear width (mm)	0.012	0.0142	0.015	0.013	0.0147	0.010	3.5

The computed errors between the numerical and experimental results for the small tool nose radius varied from 4% to 8% (See Table 3.4). For large tool nose radii, the calculated errors varied from 3% to 16% only for r_c = 0.5 (see Table 3.5). These errors could be due to the combination of mesh, the model, and convergence of the process simulation. The error for cutting temperature was due to loss of heat by convection which could not be considered during the machining process.

3.3.2 Interactive effects between the cutting parameters and the tool geometries

3.3.2.1 Influence of feed rate and tool nose radius on cutting temperature and cutting stresses

Figures 3.12 and 3.13 show the variation of maximum temperature with small and large nose radii, respectively, for different feed rates. The obtained cutting temperatures and stresses can be approximated by linear equations, which can be established using appropriate statistical models (linear regression models).

From Figures 3.12 and 3.13 the cutting temperatures were observed to increase with increasing feed rate, due to increase in frictional heat resulting from an increasing tool-chip contact zone with increasing feed rate. Similarly, the cutting temperatures increased when tool nose radius increased, for all the feed rates studied. While the temperatures for the large nose radii were higher than those noted for the small nose radius range, the slopes of the temperature-nose radius lines are lower for the large nose radius scale in comparison.

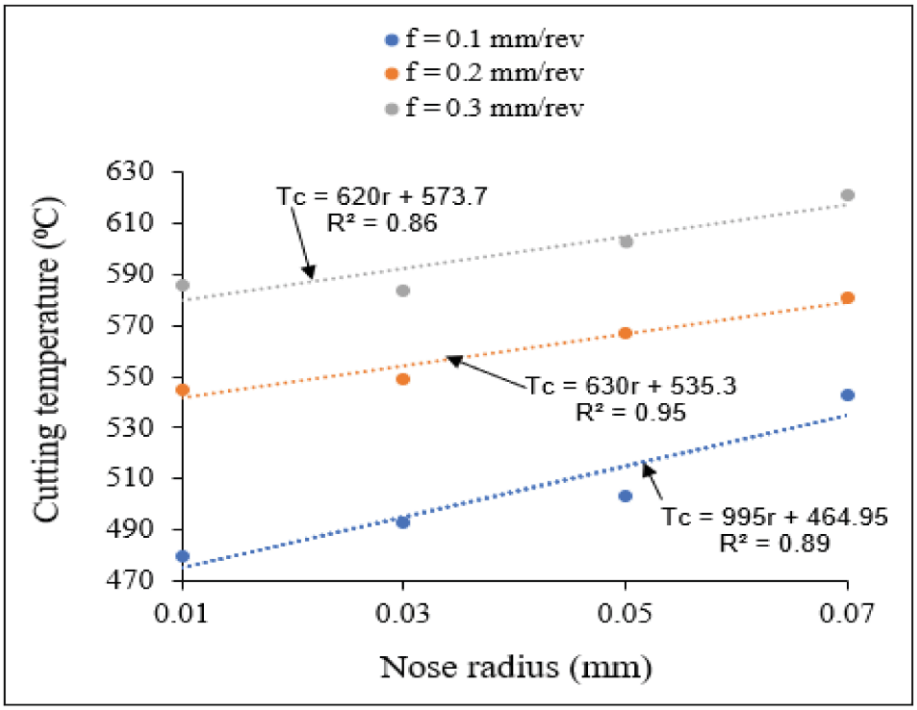

Figure 3.12 Variation of cutting temperature with small tool nose radius for different feed rates at V = 400 m/min, γ = 5º

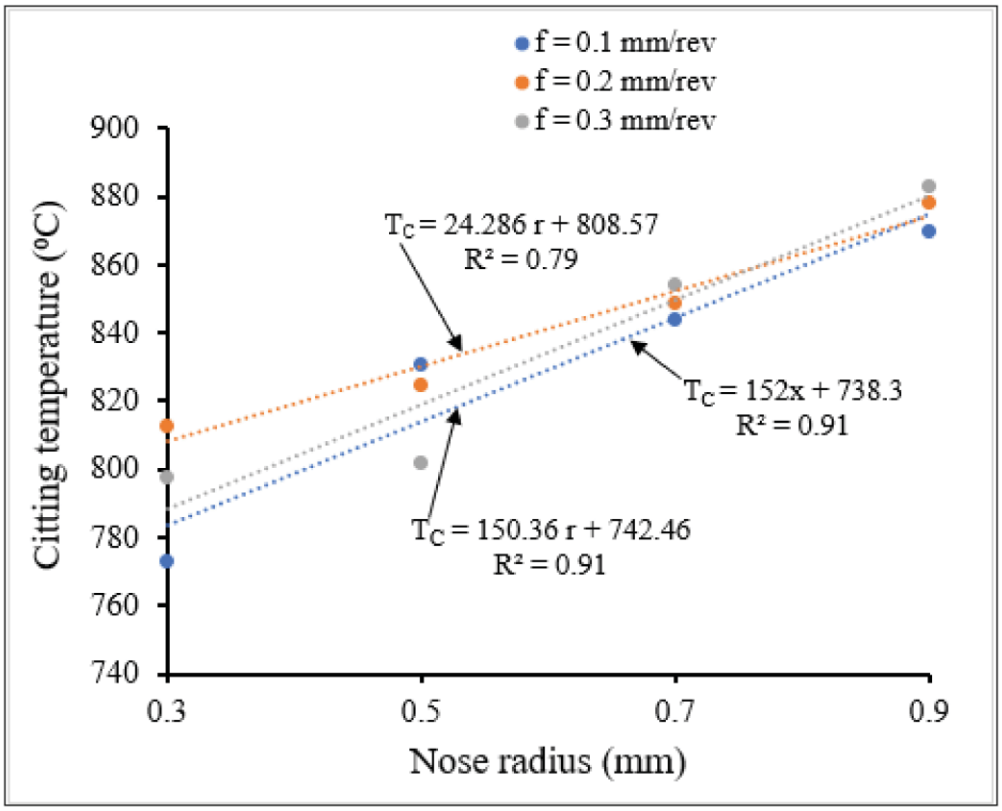

Figure 3.13 Variation of cutting temperature with large tool nose radius for different feed rates at V = 400 m/min, γ = 5°

Figures 3.14 and 3.15 show the variation in cutting stress with small and large nose radii, respectively, at different feed rates. From these figures, it is observed that for both small and large tool nose radius scales, the cutting stresses decreased with increasing feed rate for all nose radii studied, and also decreased with tool nose radius for all the considered feed rates. The slopes of cutting stress for the small nose radius scale are higher than those for the large nose radius scale.

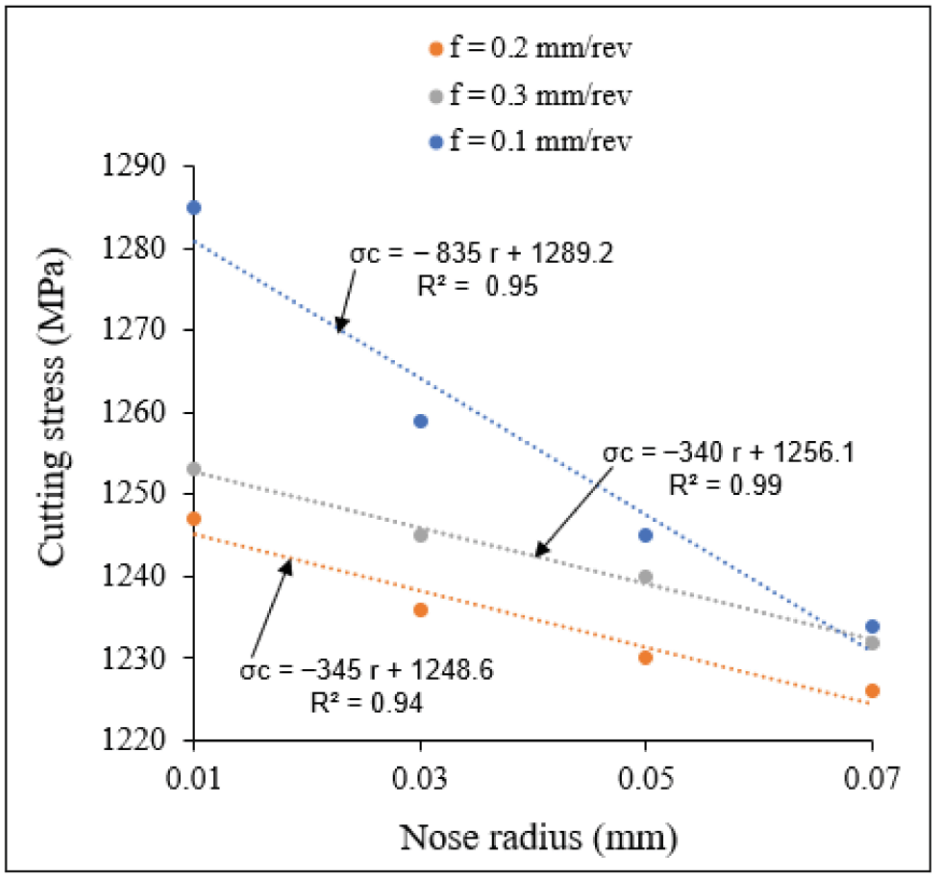

Figure 3.14 Variation of cutting stress with small tool nose radius for different feed rates at $V = 400$ m/min, $\gamma = 5^{o}$

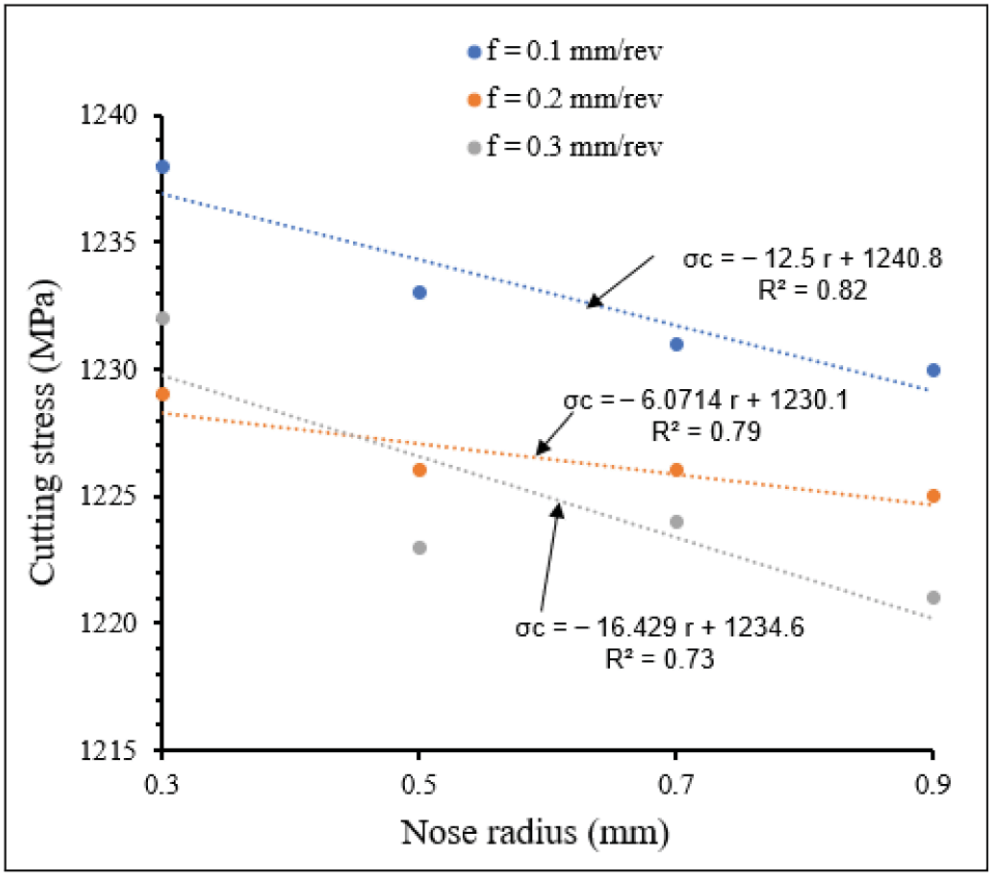

Figure 3.15 Variation of cutting stress with large tool nose radius for different feed rates at V = 400 m/min, γ = 5º

3.3.2.2 Influence of cutting speed and tool nose radius on cutting temperature and cutting stresses

Figures 3.16 and 3.17 show the effects of the combination of cutting speed and tool nose radius on cutting temperature for tools with small- and large-scale nose radii, respectively.

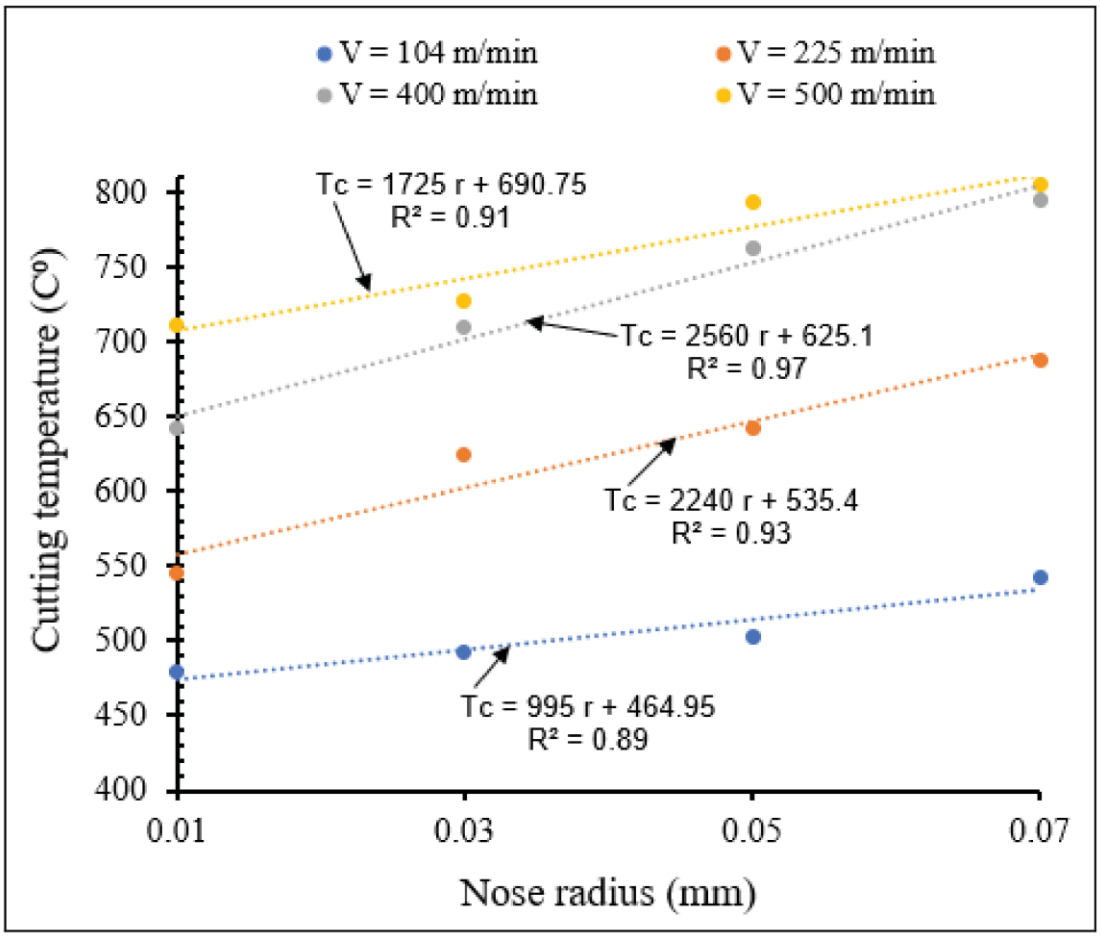

Figure 3.16 Variation of maximum temperature with small tool nose radius for different cutting speeds at f = 0.1 mm/rev, γ = 5°

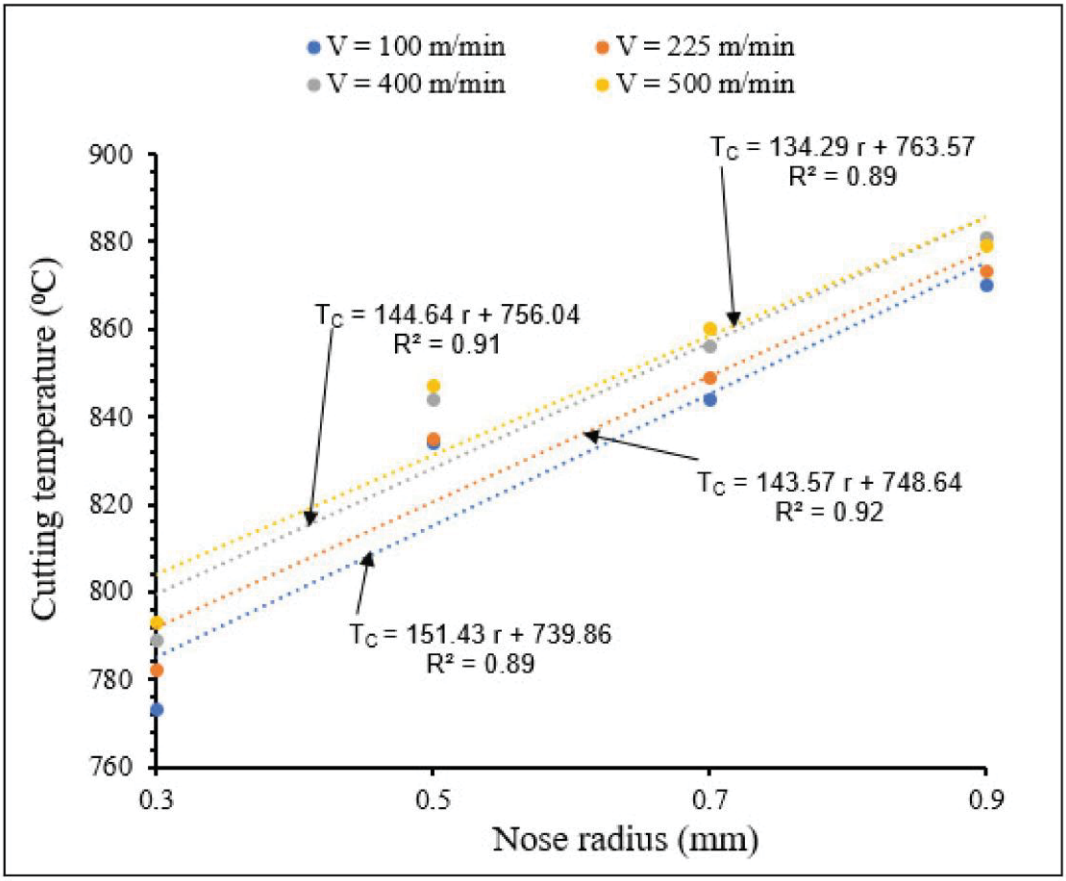

Figure 3.17 Variation of maximum temperature with large nose radius for different cutting speeds at f = 0.1 mm/rev, γ = 5º

From Figures 3.16 and 3.17 it can be seen that for all the applied cutting speeds, the cutting temperature increased when nose radius increased (small and large scale), due to large friction and plastic heat, as explained before. For the same nose radius, cutting temperature increased when cutting speed increased. There was a significant increase of cutting temperature with large nose radii tools, compared to that observed when using cutting tools with small nose radii. Figures 3.18 and 3.19 display the variation in cutting stress for different cutting speeds, using tools with small and large nose radii, respectively.

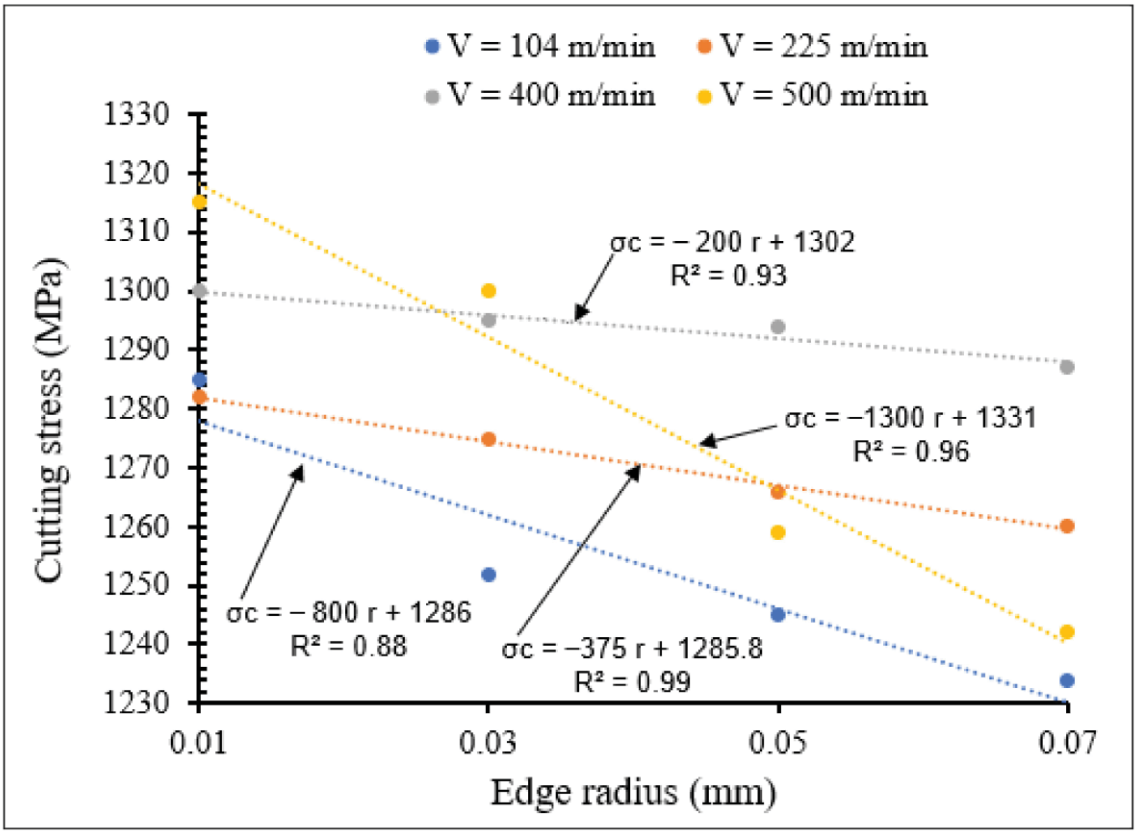

Figure 3.18 Variation of cutting stress with small tool nose radius for different cutting speeds at $f = 0.1$ mm/rev, $\gamma = 5$

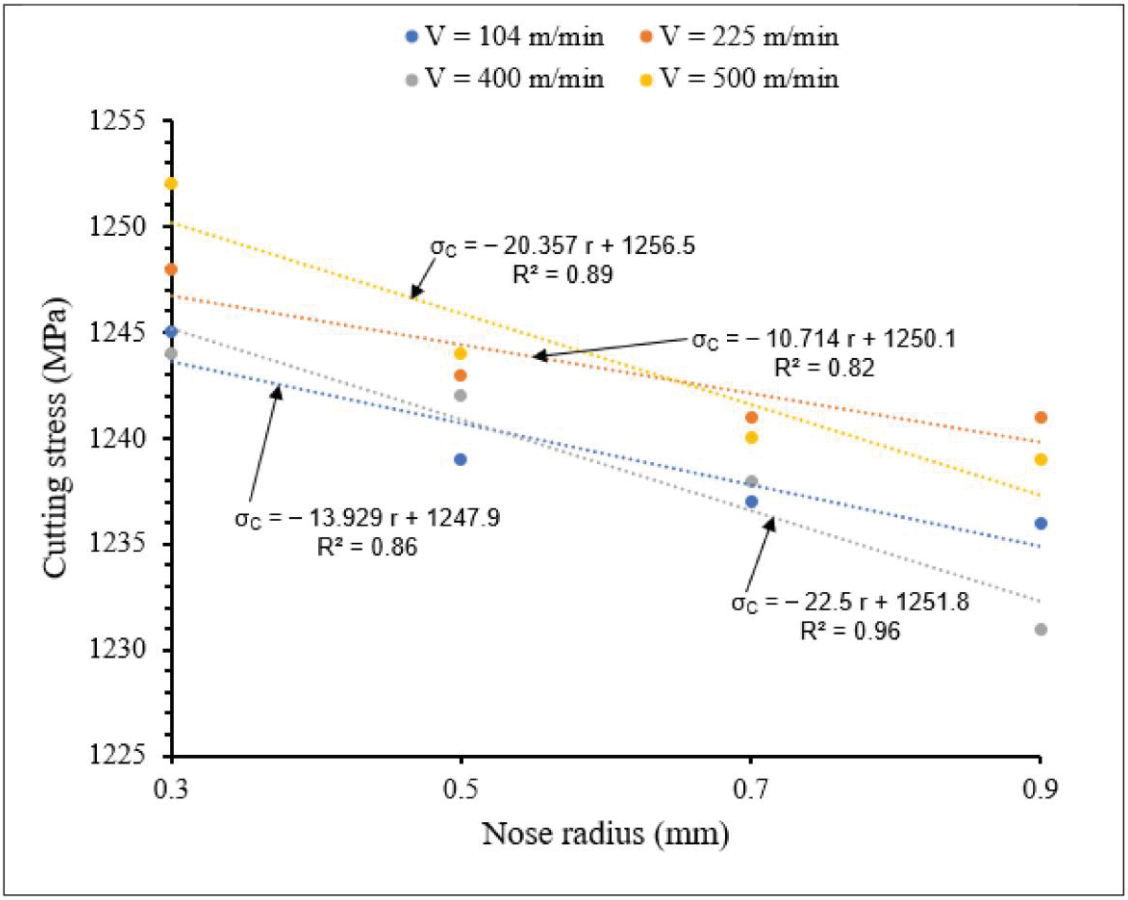

Figure 3.19 Variation of cutting stress with large tool nose radius
for different cutting speeds at f = 0.1 mm/rev, γ = 5

From Figures 3.18 and 3.19 it is noted that at all the applied cutting speeds, the cutting stresses decreased with increase in the nose radius, for both small and large nose radii scales. The sharpest decrease in cutting stress was observed at the cutting speed of 500 m/min. All these obtained results can be validated by previous data in literature during cutting comparable AISI 1045 steel materials, showing the influence of tool edge radius on machining temperature(Al-zkeri et al., 2009; Özel & Zeren, 2007). For all the nose radii the cutting stress decreased with increasing cutting speed. These decreases can be observed by the sign (–) in the established linear equations. For small tool nose radius and for higher cutting speed, especially V_c = 500 m/min, the slope of the curve is much larger due to the larger frictional and plastic heat generated during the cutting process, which results in smaller cutting forces and then in smaller cutting stresses. The cutting stresses for the small scale are higher than those for the large scale.

Therefore, the more the nose tool radius increased, the more the cutting stress variations increased. The same results were found by (Shravankumar & Kodli, 2013) who demonstrated that tool radius has inversely proportional effects on cutting stress.

3.3.2.3 Influence of rake angle and tool nose radius on cutting temperature and cutting stresses

Figures 3.20 and 3.21 show the effects of the combination of rake angle and tool nose radius on cutting temperatures for small- and large-scale tool nose radii, respectively.

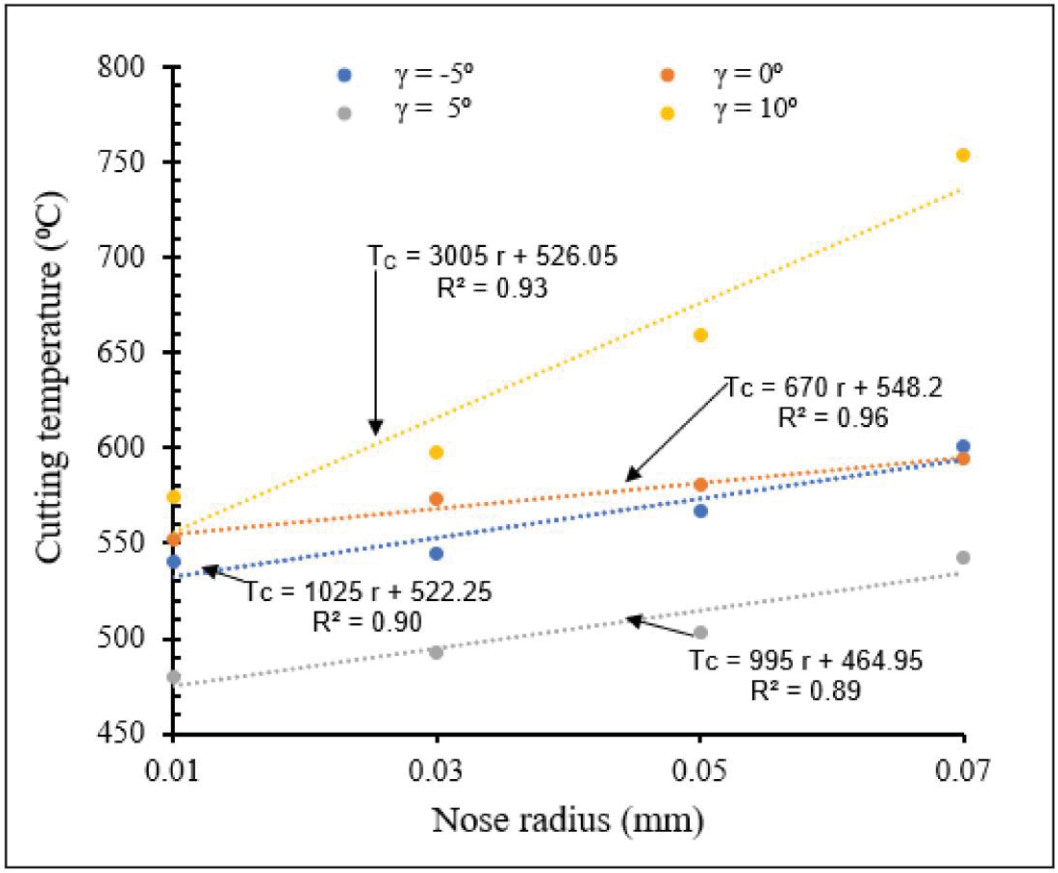

Figure 3.20 Variation of maximum temperature with small tool nose radius for different rake angles at V = 104 m/min, f = 0.1 mm/rev

From Figures 3.20 and 3.21, for both small and large nose radii, cutting temperatures increased with increasing rake angle except for the values of 5º for small scale and 0º for large scale, due

to increase of the contact force between chip and cutting tool. For all rake angles, cutting temperatures increased when tool nose radius increased. The more the nose radius increased, the more the heat volume generated in the contact area increased. The cutting temperatures for large tool nose radii were higher than those observed with small tool nose radii. However, the slopes of the Tc-r lines indicate that the cutting temperatures rise faster with increasing nose radius in the latter case than when tool nose radii are large.

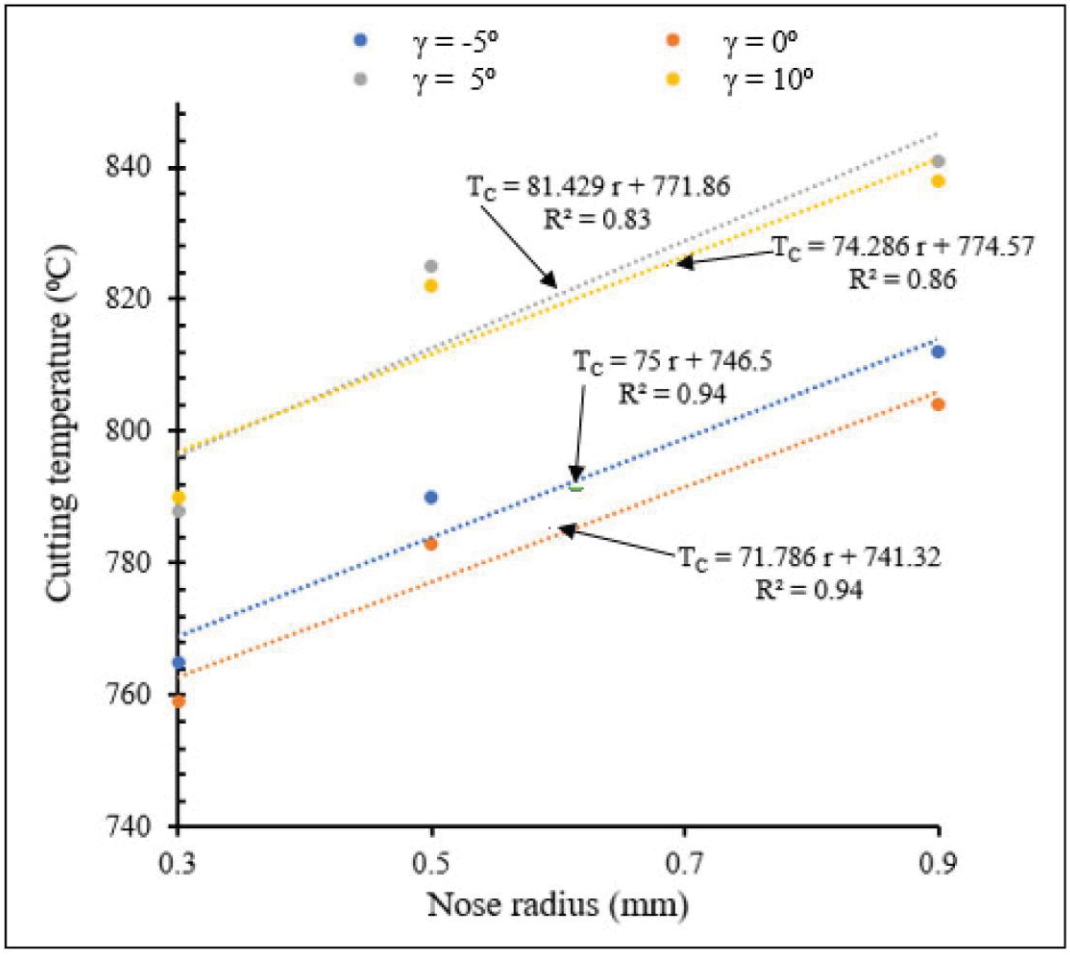

Figure 3.21 Variation of cutting temperature with large tool nose radius for different rake angles at V = 400 m/min, f = 0.1 mm/rev

Figures 3.22 and 3.23 show the influence of the combination of rake angle and tool nose radius on cutting stress for small and large tool nose radius scales, respectively.

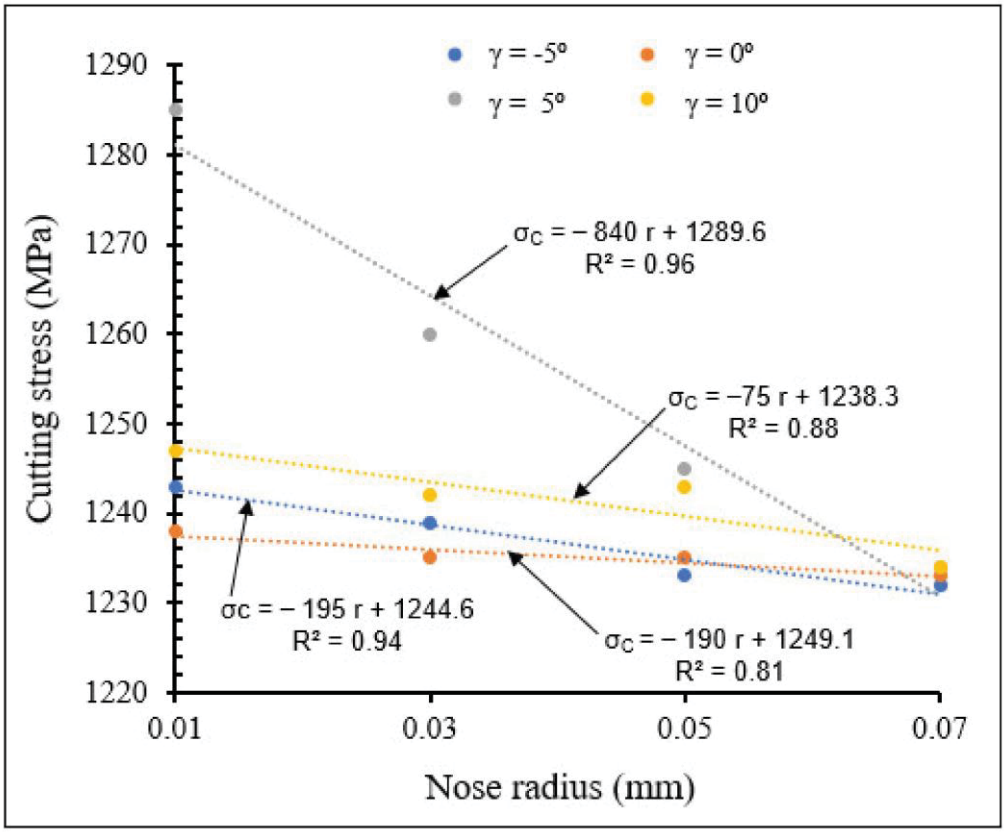

Figure 3.22 Variation of cutting stress with small tool nose radius for different rake angles at V = 104 m/min, f = 0.1 mm/rev

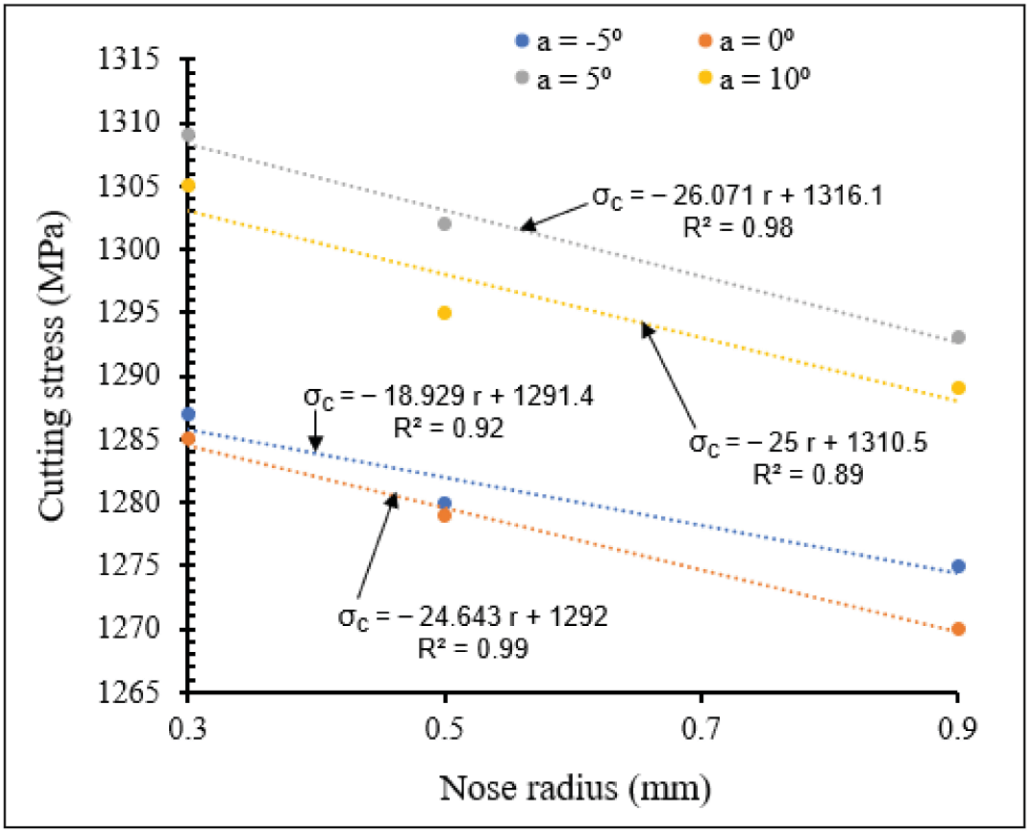

Figure 3.23 Variation of cutting stress with large tool nose radius for different rake angles at V = 104 m/min, f = 0.1 mm/rev

Taking all the tool nose radius values investigated into account, Figures 3.22 and 3.23 reveal that when rake angle increased, cutting stress decreased for both small and large tool nose radius scales, due to reduction in chip-tool contact pressure, causing decrease of cutting forces and therefore reduction in cutting stress. For all the applied rake angles, the cutting stress decreased when nose radius increased. The cutting stresses were higher for large scale than for small scale. However, large slopes are observed for small scale, especially for a rake angle of 5º.

3.3.2.4 Influence of cutting speed and tool nose radius on tool wear

Figures 3.24 and 3.25 illustrate the variations in tool wear width with nose radius for different cutting speeds, for small and large tool nose radius scales, respectively showing the interactive influence of cutting speed and tool nose radius on tool wear. Strong interaction was obtained

for small nose scale and for a cutting speed of 500 m/min where there is the sharpest slope of the linear equation of tool wear approximated by trend.

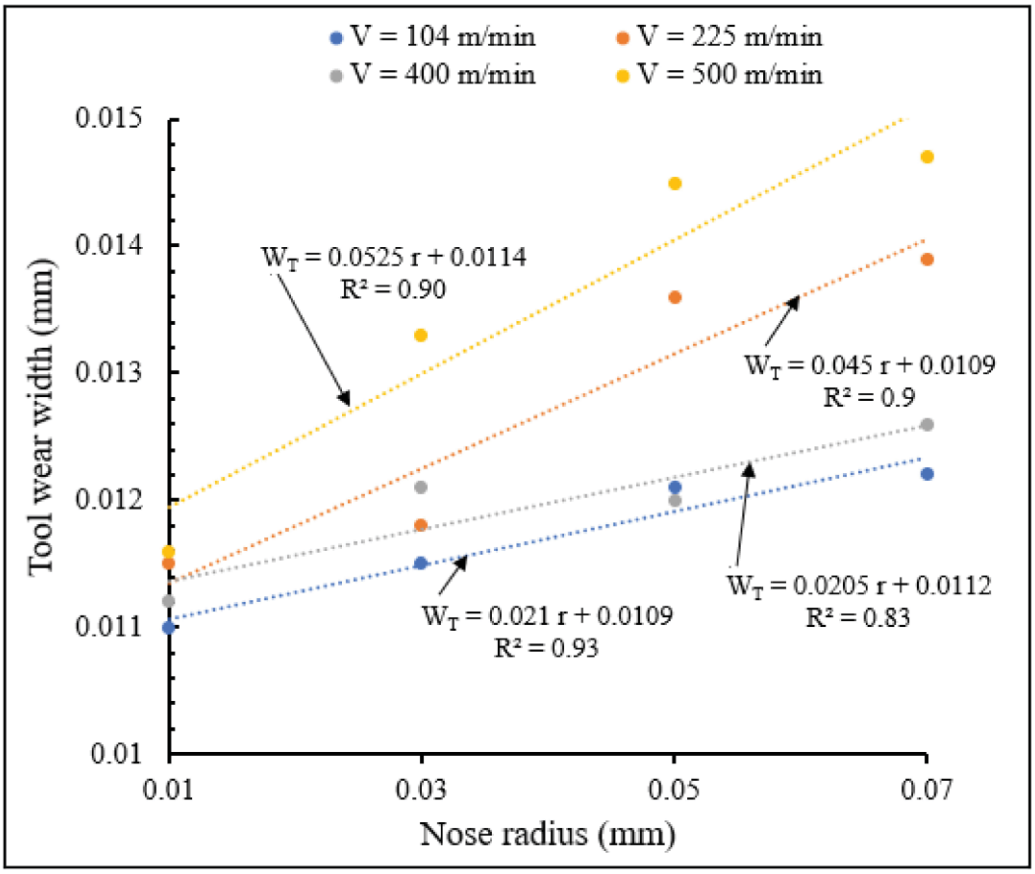

Figure 3.24 Variation of tool wear width with small nose radius for different cutting speeds at f = 0.1 mm/rev, $\gamma = 5^{o}$

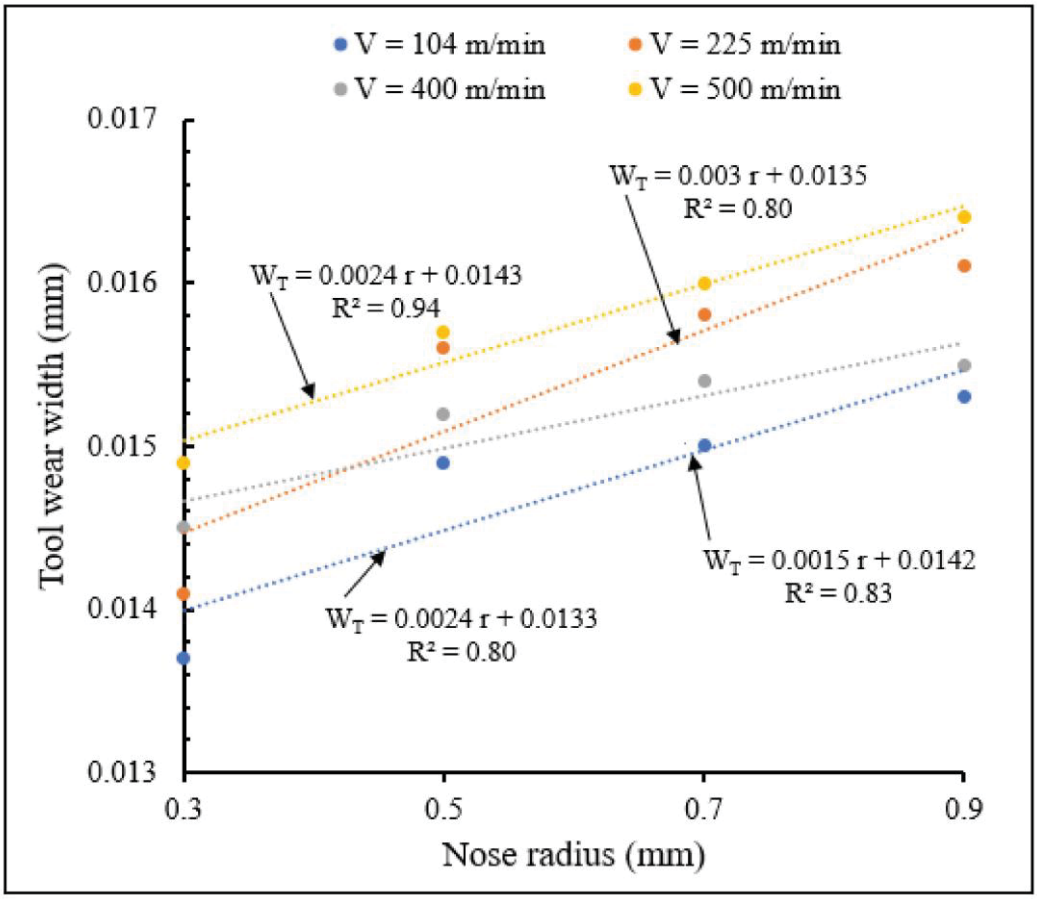

Figure 3.25 Variation of tool wear width with large nose radius for different cutting speeds at f = 0.1 mm/rev, $\gamma = 5^{o}$

It is observed from these figures that wear width increased when nose radius increased for different cutting speeds and for both small and large nose radii. Similar results were obtained in previous works conducted by(El-Hossainy et al., 2010) and (Xingzhong et al.,1999) which revealed that increasing cutting speed results in increasing temperature, leading to an increase in tool wear. For the same nose radius, wear width increases when cutting speed increases. Wear width variations for large nose radius are more important than those of small radius scale. The increase of nose radius and cutting speed increase tool wear.

3.3.2.5 Influence of rake angle and tool nose radius on tool wear

Figures 3.26 and 3.27 illustrate the variation of tool wear width with nose radius for different rake angles, for small and large nose radius ranges, respectively, showing the interactive influence between rake angle and tool nose radius on flank wear.

From Figures 3.26 and 3.27 tool wear width increased when nose radius increased for different rake angles, for both small and large nose radii. For the same small nose radius, wear width increased when rake angle increased from -5^{o} to 5, but it decreased from rake angle 5^{o} to 10^{o}. For the same large nose radius, wear width increased when rake angle increased. This is due to accumulation of chips near the tool surface, causing increase of machining force, heat generated and consequent increase in tool wear. These results can also be validated by (El-Hossainy et al., 2010; Xingzhong et al., 1999). The tool wear width comparison between small and large nose radius showed that there is no significant
difference in the results variation.

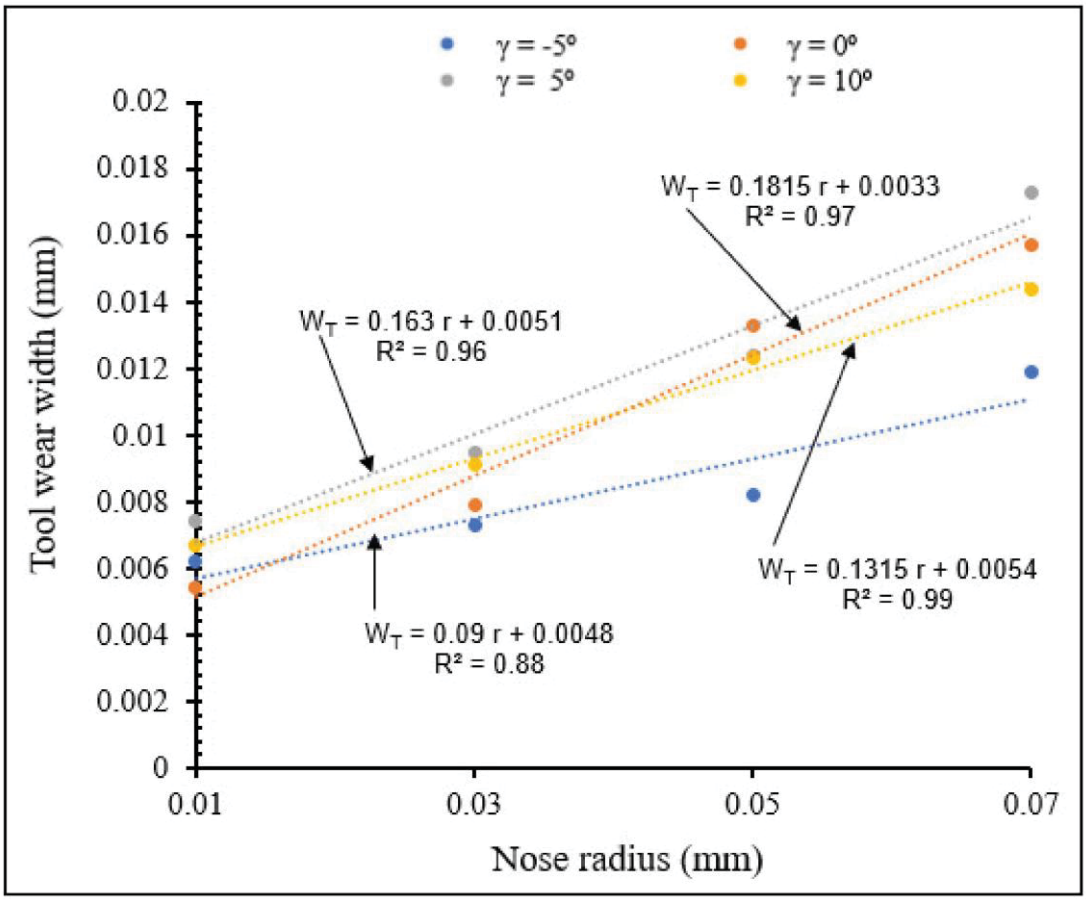

Figure 3.26 Variation of tool wear width with nose radius for different rake angles at V = 104 m/min, f = 0.1 mm/rev

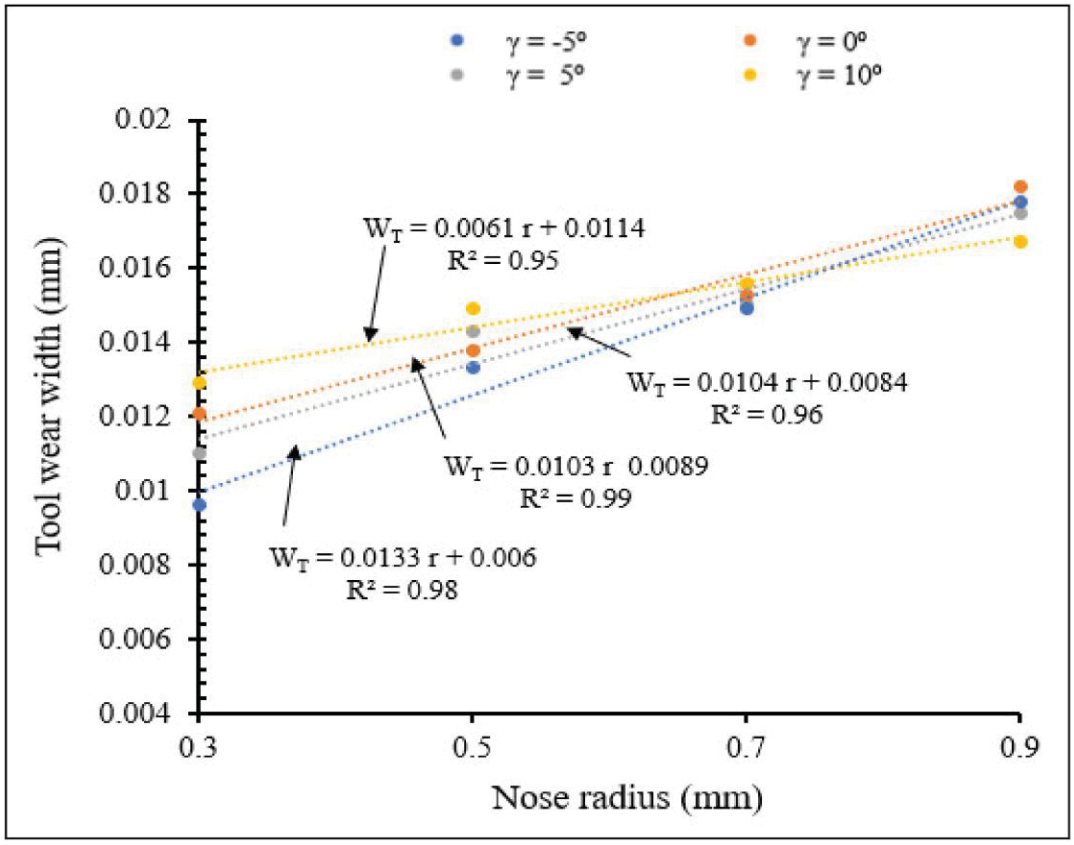

Figure 3.27 Variation of tool wear width with large tool nose radius for different rake angles at V = 104 m/min, f = 0.1 mm/rev

3.4 Conclusions

A numerical simulation model, based on the finite element method, was developed for predicting the effects of tool nose radius on cutting temperature, machining stress and tool wear in the orthogonal milling of AISI 1045 steel, using various cutting process parameters. The model was validated using data from literature. From an analysis of the results obtained, the following conclusions were drawn:

- In general, for all the tested cutting conditions and for the studied range of nose radii (From 0.01 to 0.07 mm, and from 0.3 to 0.9 mm) cutting temperature, stress and tool wear vary approximately linearly with tool nose radius.

- Tool nose radius was found to influence cutting forces, cutting stress, strain, temperature in the cutting zones and, finally, tool degradation. Tool degradation (wear rate) was high on the tool rake face and at the tool tip in the region where the effective rake angle was the smallest.

- Interactions between tool nose radius and cutting parameters (speed, feed) affected mostly cutting stress and, slightly, tool wear rate. These interactions did not much influence cutting temperature, that was found to be high when the tool nose radius and/or the cutting speed were high.

- Maximum temperature was found to take place at the middle of tool-chip contact length and at the interaction of nose radius and flank face of the tool. Except for some fluctuations, there was no significant difference in tool wear rate between small and large nose radius scales.

- The results obtained from this study and their analysis will permit future research to determine the optimal geometrical parameters for improving machining process characteristics, using appropriate optimisation methods, and to establish cutting empirical formulae that can be useful for machining industrial applications.

CHAPTER 4

NUMERICAL PREDICTION OF THE PERFORMANCE OF CHAMFERD AND SHARP CUTTING TOOLS DURING ORTHOGONAL CUTTING OF AISI 1045 STEEL

Zakaria Ahmed M. Tagiuri[1], Thien-My Dao[1], Agnes Marie Samuel[1], and Victor Songmene[1]

[1]Department of Mechanical Engineering, École de Technologie Supérieure (ÉTS)
1100 Notre-Dame Street West, Montréal, QC H3C 1K3, Canada

Paper published in Processes, October 2022, 2171; doi.org/10.3390/pr10112171

Abstract

This paper presents a numerical investigation of the effects of chamfered and sharp cemented carbide tools using finite element method-based DEFORM-2D software and cutting parameters on different machining characteristics during the orthogonal cutting of AISI 1045 steel. The objective is to study the interactions between chamfer width, chamfer angle, sharp angle and the cutting speed and feed rate on the cutting temperature, effective stress and wear depth. These effects were investigated statistically using the analysis of variance (ANOVA) test. The obtained numerical results showed that for the chamfer tool, high values of temperature, stress and wear depth were obtained for chamfer widths of 0.35 mm and 0.45 mm. In terms of combined influences, for the cutting temperature and stress, a strong interaction between the cutting speed and chamfer width was obtained. For the sharp tool design, and in terms of temperature, strong interactions are mostly observed between cutting speeds and feed rates. The ANOVA showed that for both chamfer and sharp tools, the feed rate, the cutting speed and their interactions are the most significant parameters that influence temperature and stress.

Keywords: tool edge preparation; orthogonal cutting; numerical simulation; ANOVA; temperature; stress; tool wear.

4.1 Introduction

In different machining companies, the production demands for machined metal structural components with good surface finish and close dimensional tolerances continue to increase. However, manufacturing such parts requires a good knowledge of cutting technology as, during the machining process, there is much waste of material in the form of chips, resulting in long cycle times, particularly in the case of complex parts that are difficult to cut. Such long cycle times can lead to the eventual presence of defects and irregularities due to excessive heat generation; this can lead to the breakage and damage of cutting tools, reducing the machining performance and increasing manufacturing costs. Thus, in order to circumvent these problems, realize these demands and meet the market requirements, it is necessary to develop new methods for the cutting tool edge preparation, which is one of the important aspects in the development of cutting tools and improving the machining performance. Cutting tool-manufacturing engineers use the tool edge preparation process to design the cutting-edge geometry and in order to remove edge defects and prepare the tool surface for coating, especially for the machining of difficult-to-cut materials. It has been demonstrated that cutting tool parameters, such as cutting speed, feed rate and the selection of tool edge geometry, e.g., edge radius or rake angle, have an impact on machining operations. There are several research studies in the literature, for example, the work of (Rodríguez.,2009) and the investigations of (Shnfir et al.,2019) that show the effects of cutting tool edge preparation on tool life and the thermomechanical aspects of the cutting process, such as temperature distribution, cutting forces and effective stresses, chip formation, surface roughness and tool wear resistance. (Denkena & Biermann.,2014) reviewed the development of different tool edge preparation technologies and the interactions between cutting edge microgeometry and their effects on machining processes. They concluded that cutting processes with high performance are based on the good performance of the cutting tools in order to realize good surface finish quality and thus reduce manufacturing costs. They stated that the adoption of cutting-edge preparation methods results in improving tool wear and increasing the cutting temperature and cutting forces. The majority of such research studies have been conducted on the interactive effects of cutting tool geometry and machining conditions were limited to the round tool geometry. (Yen

et al.,2004) carried out a numerical investigation of the effect of round/honed edge and T-land/chamfered edge tools on the orthogonal machining performance of AISI 1020 steels. Their results showed that there are no significant variations in terms of maximum temperature and chip thickness. (Cheng et al,2016) investigated the influence of honed tool geometry and the rake angle on the machining temperature and stress during the orthogonal machining of stainless steel using numerical methods. They showed that with increasing tool edge radius, the temperature increases slightly and the stress decreases, but increases, instead, with an increase in the rake angle.(Emamian,.2017) performed finite element analysis on the effects of tool edge radius and feed rate during orthogonal turning of AISI 1045 steel. He found that the feed rate increases the cutting force for all studied edge radii and the maximum temperature increases with increasing edge radius only for higher feed rates. (Daoud et al.,2015) studied the cutting force behavior with variation of rake angle during the orthogonal machining of Al 2024-T3 alloy. They found that cutting forces decrease with increasing rake angle. (Davoudinejad & Noordin,.2014) investigated the effects of honed and chamfered edge tools prepared with ceramic materials on the tool life, cutting forces and surface finish during the hard turning of DF-3 tool steel under various cutting experimental conditions using ANOVA. Their results showed that longer machining lengths were obtained in all cutting conditions (i.e., longer tool life), lower roughness for chamfered edge geometry and higher forces for honed tools design. (Gao et al,.2018) studied the influences of different cutting tool chamfer lengths on cutting stress, tool wear and surface roughness using a series of slot milling experiments and 3D finite element numerical simulations on aluminum alloy 7075. They found that higher chamfer lengths reduced tool wear (i.e., resulted in longer tool life) but higher flank wear width was obtained for higher stress. In addition, the contact stress with the workpiece increased with the increase of cutting-edge chamfer length.

(Wan et al., 2015) numerically analyzed the effects of chamfered geometry cutting tool on machining force in orthogonal cutting of P20 material under different cutting speeds. Their findings showed that as the chamfer angle increased the cutting and thrust forces increased but when the cutting speed increased, these forces decreased.

Despite the large volume of research realized on using the concept of cutting-edge preparation for developing different machining processes, machining problems still remain, due to a lack

of understanding of the mechanical behavior and mechanisms that occur during cutting, especially in regard to the impact of interactions between microgeometry and cutting conditions, which have not been extensively studied and analyzed thus far (Denkena & Biermann,.2014) . The topic is still of actuality. (Gregório et al., 2022) have depicted the impact on tool edge preparation (sharp-edge and rounded edge) and its interaction with tool rake angle on chip formation, friction on tool, material flow and pressure on tool. Their work clearly shows the importance that the edge preparation has on the cutting process. With the exception of some recent works, such as the experimental study realized by Javidikia et al. (2020) on the interactive impact between the cutting tool parameters of cutting-edge radius and rake angle, the machining parameters of cutting speed, feed rate and rake angle on the cutting and feed forces, chip thickness, maximum and average cutting temperature during orthogonal turning of 6061-T6 aluminum alloy, and that of (Zhuang et al.,2018) on Ti6Al4V and Inconel 718, few studies report on the interaction between the cutting speed, feed rate and cutting tool geometries (i.e., chamfer and sharp tool designs), and their effects on the machining characteristics of steel, in particular for carbon steels.

While studying the impact of tool geometry on low and high-speed turning of AA6061-T6, (Javidikia et al.,2020) found that the machining forces increased in both conventional and high-speed cutting regimes when using tool with large nose radius; additionally, the location of the maximum temperature on the tool depends on tool geometry and on cutting parameters. With high-speed machining, however, the average temperatures increased in the tool tip with increasing cutting speed.

Among the few studies on the machining process of metallic materials using chamfered and sharp tools for investigating the effects of the cutting parameters and the geometrical parameters of these tool shapes on the machining performance, there is the finite numerical model developed by (Zhuang et al,.2018) who examined the impacts of chamfer length, chamfer angle and feed rate on the cutting forces in the orthogonal cutting of Ti6Al4V and Inconel 718. They found that the cutting forces are significantly affected by chamfer length and angle. (Ren & Altintas.,2000) predicted the impacts of chamfer angle and cutting parameters on the cutting forces and temperature. The obtained results showed that with increasing chamfer angle the total forces increase and the temperatures remain nearly constant.

(Tagiuri et al.,2022) studied and numerically predicted the interactive effects between tool nose geometries (honed tools) and the cutting parameters on cutting temperature, effective stress, machining forces and tool wear during the orthogonal cutting of AISI1045 steel. The obtained results showed strong interactions between tool nose radius and cutting speed/feed rate on cutting stress and tool wear rate but not on the cutting temperature. (Chowdhury et al.,2011) investigated the impacts of chamfer tool geometries (chamfer width and chamfer angle) on machining performance in terms of cutting force, chip thickness and tool life in the turning of medium carbon low alloy steel. They observed that the cutting and feed forces increased as the chamfer width and chamfer angle increased but at large values of these parameters, the cutting forces were low. With increase in chamfer width, the chip thickness decreased but presented a non-significant variation with chamfer angle. (Khalili & Safaei.,2009) carried out a numerical study of the effects of the chamfer width and chamfer angle on cutting force, effective stress, tool temperature and tool stress during the two-dimensional (2D) orthogonal cutting of AISI 1045 steel by developing two finite element models. They found that there is almost no variation of cutting forces with increase in cutting speed, and that the thrust force is significantly influenced by the chamfer width and the chamfer angle. As cutting speed increases the maximum temperature increases at the tool tip and presents the optimum chamfer angle.

Despite the investigations presented above on the effects of tool edge geometries on machining process performance in cutting carbon steed materials, the data on different interactive configurations between tool edge geometries, such as chamfer width, chamfer angle, sharp angle and cutting parameters, e.g., cutting speed and feed rate, is still scarce. For various reasons, most of these studies were carried out for few and limited designed tests. This would imply a lack of understanding of the actual mechanisms responsible for the effects involved around the cutting edge during the cutting process, such as tribological and heat transfer aspects, for example. Thus, the ultimate goal would be to comprehend these mechanisms, rendering possible the means for the future preparations of design cutting tools.

In view of the above, the present work focuses on the influence of chamfered tool edge geometries and sharp edge on the machining performance. The objective of this article is to investigate the interactions in terms of the effects of cutting speed, feed rate, and chamfer and

sharp tool geometries on the cutting temperature, cutting stress and tool wear depth. The main cutting parameters that influence these performance characteristics will be assessed using statistical analysis employing the analysis of variance (ANOVA) technique.

4.2 Materials and methods

The numerical study consists of conducting different simulations of the two-dimensional (2D) orthogonal cutting of AISI 1045 steel using the commercial DEFORM software based on the finite element method (FEM) in order to predict the effects of the specified tool edge geometries and their interactions with machining parameters on the cutting temperature, cutting stress and tool wear. The two tool geometries examined are the chamfer and sharp tool geometry. Figures 4.1 and 4.2 show the 2D model geometry of the workpiece and the tool, respectively. These interactive effects will be evaluated based on a design plan which comprises different parameter combinations, namely cutting speed, feed rate, chamfer angle and chamfer width for the chamfer tool geometry and cutting speed, feed rate and cutting angle for the sharp tool geometry.

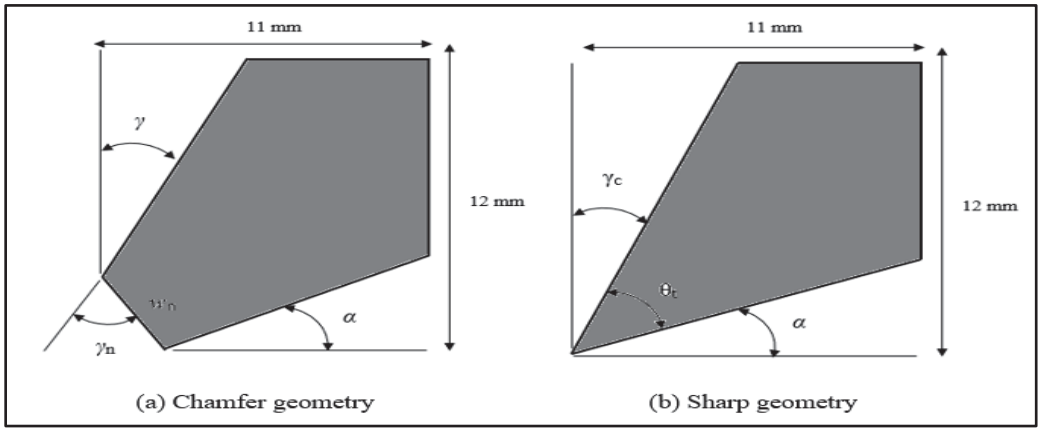

Figure 4.1 Two-dimensional (2D) models of the cutting tools studied: Chamfer tool b) Sharp tool.

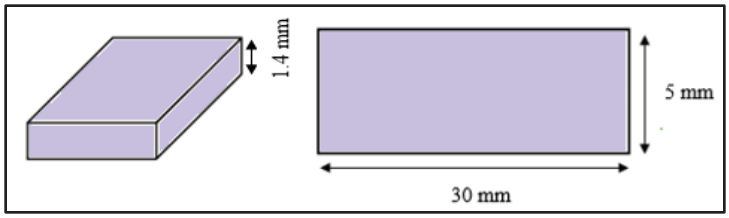

Figure 4.2 The workpiece model geometry.

4.2.1 Material and machining process characterization

The machining process specified for the present numerical simulation tests is orthogonal cutting. The studied workpiece material is high carbon steel AISI 1045, which is often selected for different product applications that necessitate higher strength and resistance than other materials of the same category. The material selected for the cutting tool was uncoated higher productivity than high-speed steel cemented carbide, which it is also widely used in many industrial applications due to its hardness, as it gives a better surface finish to the machined part and provides.

4.2.2 Finite element simulation model

In order to simulate the orthogonal milling process of high carbon steel AISI 1045, a 2D finite element model using DEFORM software was developed. The model includes the cutting tool, the workpiece and the chip. The meshing that was used in this cutting geometry model was created systematically using a default algorithm for solid modeling. The mesh consists of 2D free quadrilateral elements. The DEFORM software uses nodal finite elements for linear approximation. Each element has four nodes, and each node can have different degrees of freedom, such as temperature, force, stress, tool wear, chip thickness, etc.

Tables 4.1 and 4.2 present the thermal and mechanical properties of these materials, respectively. It is assumed that the thermal properties of the cutting tool and workpiece materials are constant by neglecting the thermal gradient. Due to the shortened time, the steady state is attained very fast (about 0.3 ms), causing little variation in thermal conductivity and specific heat with temperature. This statement has already been referred to by (Tagiuri et al.. 2022)

Table 4.1 Thermal properties of workpiece and tool materials

Properties	Tool: uncoated carbide		Workpiece : AISI 1045	
Material	used	Deform software (Default)	used	Deform Software (Default)
Density (kg/m^3)	11,900	10,850	7,870	7,850
Thermal conductivity (W/m °C)	50	59	45	55
Specific heat (J/kg °C)	375	364	590	570

Table 4.2 Mechanical properties of workpiece and tool materials

Properties	Tool: uncoated carbide		Workpiece : AISI 1045	
Material	used	Deform software (Default)	used	Deform software (Default)
Young's modulus	620 GPa	-	200 GPa	-
Poisson ratio	0.26	0.22	0.29	0. 30
Hardness	93 HRB	93 HRB	163 HB	-

During cutting simulation, the software used two numerical modules: heat transfer and motion analysis. In the DEFORM program, the transient mode was selected and the cutting temperature, force and stress were calculated by solving heat transfer and motion equations as follows (Javidikia et al., 2020):

$$[C_T]\{\dot{T}\} + [K_T]\{T\} = \{\dot{Q}g\} \quad (4.1)$$

$$[M]\{\ddot{U}\} + \{R_{int}\} = \{R_{ext}\} \quad (4.2)$$

where $[C_T]$, $[K_T]$, $\{\dot{Q}_g\}$, $\{\ddot{U}\}$, $\{U\}$, $\{R_{int}\}$ and $\{R_{ext}\}$ are the volume heat capacitance, the thermal conduction matrices, the total heat generated, the acceleration vector, the displacement, the vector of internal force and the vector of external force, respectively.

During the cutting process, two heat transfer mechanisms occur: conduction and convection. Conduction occurs between cutting tool, workpiece and chip, whereas convection occurs

between workpiece, tool surfaces and the ambient air. In order to simulate these mechanisms in 2D, the mentioned components were considered as superficial geometries in contact without internal heat generation.

For the boundary conditions, the thermal contact between cutting tool and chip is considered perfect. The initial temperature of the cutting model was set at the room temperature ($T_\infty = 20^0$C). The natural convection mode was expressed by the following equation (Zakaria, 2019):

$$k_n \Delta T = h\left(T_{air} - T\right) \tag{4.3}$$

Where T_{air} is the ambient temperature, T is the temperature, k_n is the thermal conductivity of the studied materials, h is the convection heat transfer coefficient (h = 20 W/m^2. ^{0}C), and ΔT is temperature difference between cutting tool and workpiece at the tool-chip contact.

The considered value of the convection heat transfer coefficient h for air flow was determined by approximation according to the following equation (Engineering ToolBox, 2003):

$$h = 10.45 - v + 10\, v^{1/2} \tag{4.4}$$

where v is the relative velocity between object surface and surrounding air (m/s).

The boundary conditions were stated as that (i) there was no motion for the cutting tool, and that (ii) the workpiece was cut at the specified machining speed (V).

For material modeling, the Johnson-Cook constitutive model was adopted, because it gives accurate results for machining process simulations. The flow stress model can be formulated as follows (Javidikia et al., 2020) :

$$\overline{\sigma} = \left[A + B\left(\varepsilon^n\right)\right]\left[1 + C.\ln\left(\frac{\dot{\varepsilon}}{\varepsilon_0}\right)\right]\left[1 - \frac{\left(T - T_{room}\right)}{\left(T_{melt} - T_{room}\right)^m}\right] \tag{4.5}$$

Where $\overline{\sigma}$ is the cutting stress, ε is the plastic strain, $\dot{\varepsilon}$ (s^{-1}) is the plastic strain rate, $\dot{\varepsilon}_0$ ($^{-1}$) is the reference plastic strain rate, T (°C) is the workpiece temperature, T_{melt} (°C) is the melt

temperature, T_{room} (°C) is the room temperature, and A (MPa), B (MPa), C, n and m are the initial yield strength, the hardening modulus, strain rate sensitivity coefficient, hardening coefficient and thermal softening coefficient, respectively. The constants of AISI 1045 steel that were used for Johnson–Cook model are displayed in Table 4.3.

Table 4.3 The constants of Johnson–Cook material model for AISI 1045 steel Jaspers et al (1998)

Material	A (MPa)	B (MPa)	n	C	m	T_m (°C)
AISI 1045	553.1	600.8	0.234	0.013	1	1733

For modeling tool wear, the Usui wear model was used by the DEFORM software, based on nodal displacement which is characterized by the calculated wear rate at each node. For the tool wear simulation, the Usui model was expressed as follows (Afrasiabi et al., 2021):

$$W = \int A.\,P.V.\,e^{-\frac{B}{T}}.\,dt \tag{4.6}$$

Where W is the tool wear, P is the interface pressure, V is the sliding velocity, T is the temperature and dt is the time increment. A and B are constants that are determined experimentally.

4.2.3 Design of experiments

The orthogonal cutting numerical tests were realised to investigate the interactive effects of tool chamfer angle, chamfer width and sharp cutting angle on the temperature, stress and tool wear depth under different cutting process parameters. Tables 4.4 and 4.5 respectively present the design plan for the chamfer and sharp tool geometry numerical simulations.

The first numerical simulation tests were conducted to study only the effects of chamfer and sharp tool geometry on the different machining characteristics. For chamfer tool design, the chamfer width (w_n) was varied, and the other machining and tool parameters were kept constant. Then, the chamfer angle (γ_n) was varied, with the other machining and tool parameters kept constant. For sharp tool design, the sharp angle (θ_t) was varied and the other parameters were kept constant.

Throughout the study, the clearance angle (α) was kept constant at α = 15º. For the chamfer tool, the rake angle (γ) was kept constant (γ = 10º) for different tested chamfer widths. For the sharp tool, the rake angle (γ_c) changes when the sharp angle θ_t varies.

(w_n , γ_n)

Table 4.4 Parametric design plan for the chamfer tool geometry numerical simulations

Test ID	Chamfer Angle γ_n (°)	Cutting Speed (m/min)	Feed Rate (mm/rev)	Chamfer Width w_n (mm)
1	10	150	0.2	0.1–0.75
2	10	350	0.2	0.1–0.75
3	10	500	0.2	0.1–0.75
4	10	600	0.2	0.1–0.75
5	10	150	0.1	0.1–0.75
6	10	150	0.2	0.1–0.75
7	10	150	0.3	0.1–0.75
8	15–45	150	0.1	0.1
9	15–45	150	0.2	0.1
10	15–45	150	0.3	0.1
11	15–45	150	0.2	0.1
12	15–45	350	0.2	0.1
13	15–45	500	0.2	0.1
14	15–45	600	0.2	0.1

Table 4.5 Parametric design plan for the sharp tool geometry numerical simulations

Test ID	Sharp Tool Angle θ_t (°)	Cutting Speed (m/min)	Feed Rate (mm/rev)
1	35–65	250	0.2
2	35–65	500	0.2
3	35–65	750	0.2
4	35–65	1000	0.2
5	35–65	150	0.1
6	35–65	150	0.2
7	35–65	150	0.3

In order to illustrate the influence of chamfer width, chamfer angle and sharp angle on cutting temperature, effective stress and tool wear, four tool designs were proposed. Figures 4.3, 4.4

and 4.5 display schematic representations of the cutting tool geometries with different chamfer widths, chamfer angles and sharp angles, respectively.

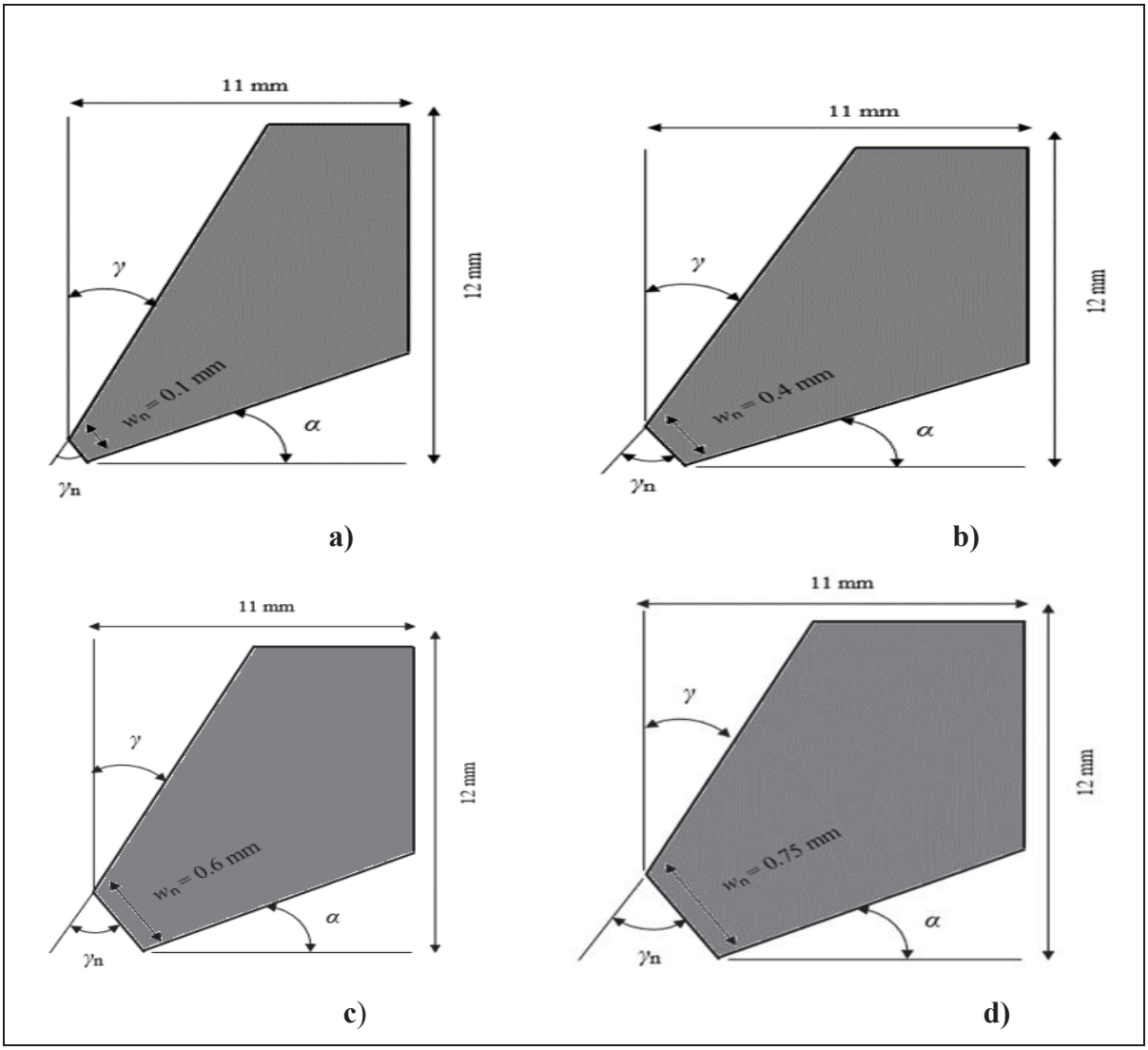

Figure 4.3 Chamfer cutting tool geometries with different chamfer widths w_n:
a) 0.1 mm **b)** 0.4 mm **c)** 0.6 mm **d)** 0.75 mm

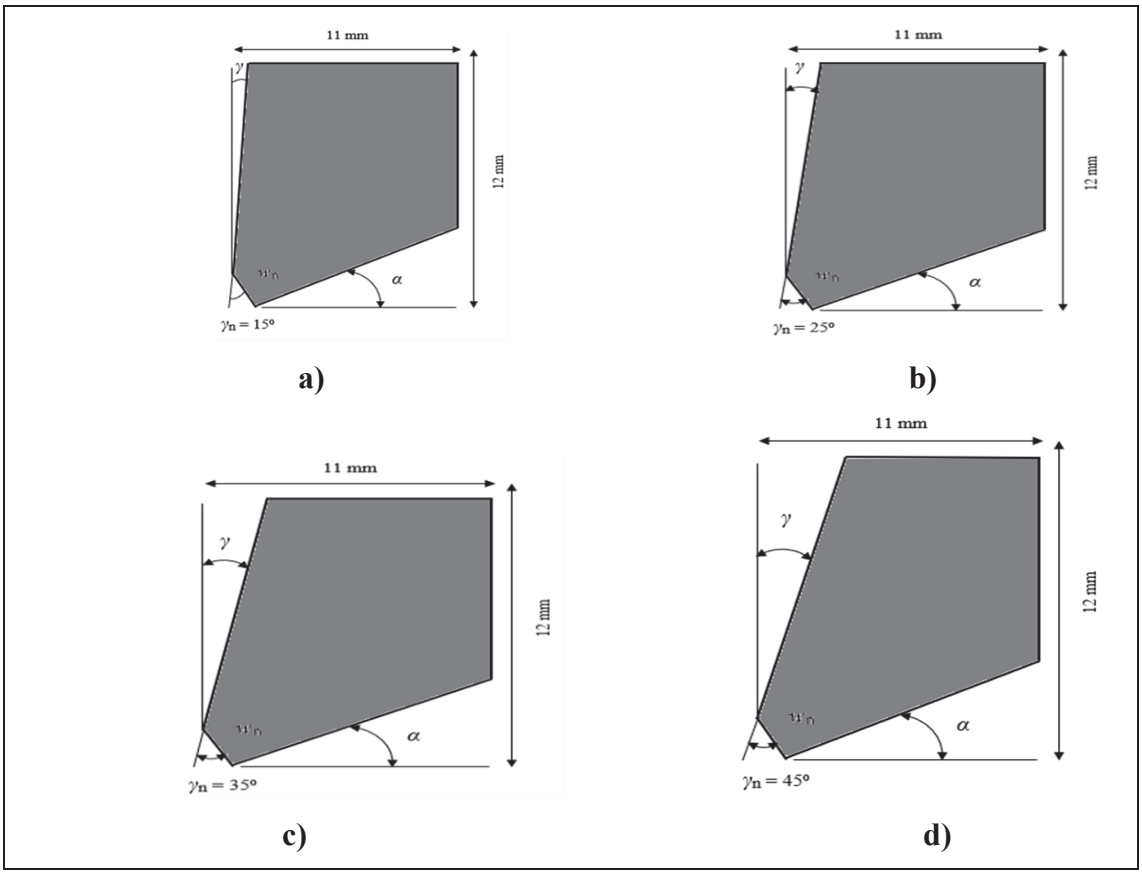

Figure 4.4 Chamfer cutting tool geometries with different chamfer angles γ_n :
a) 15º **b)** 25º **c)** 35º **d)** 45

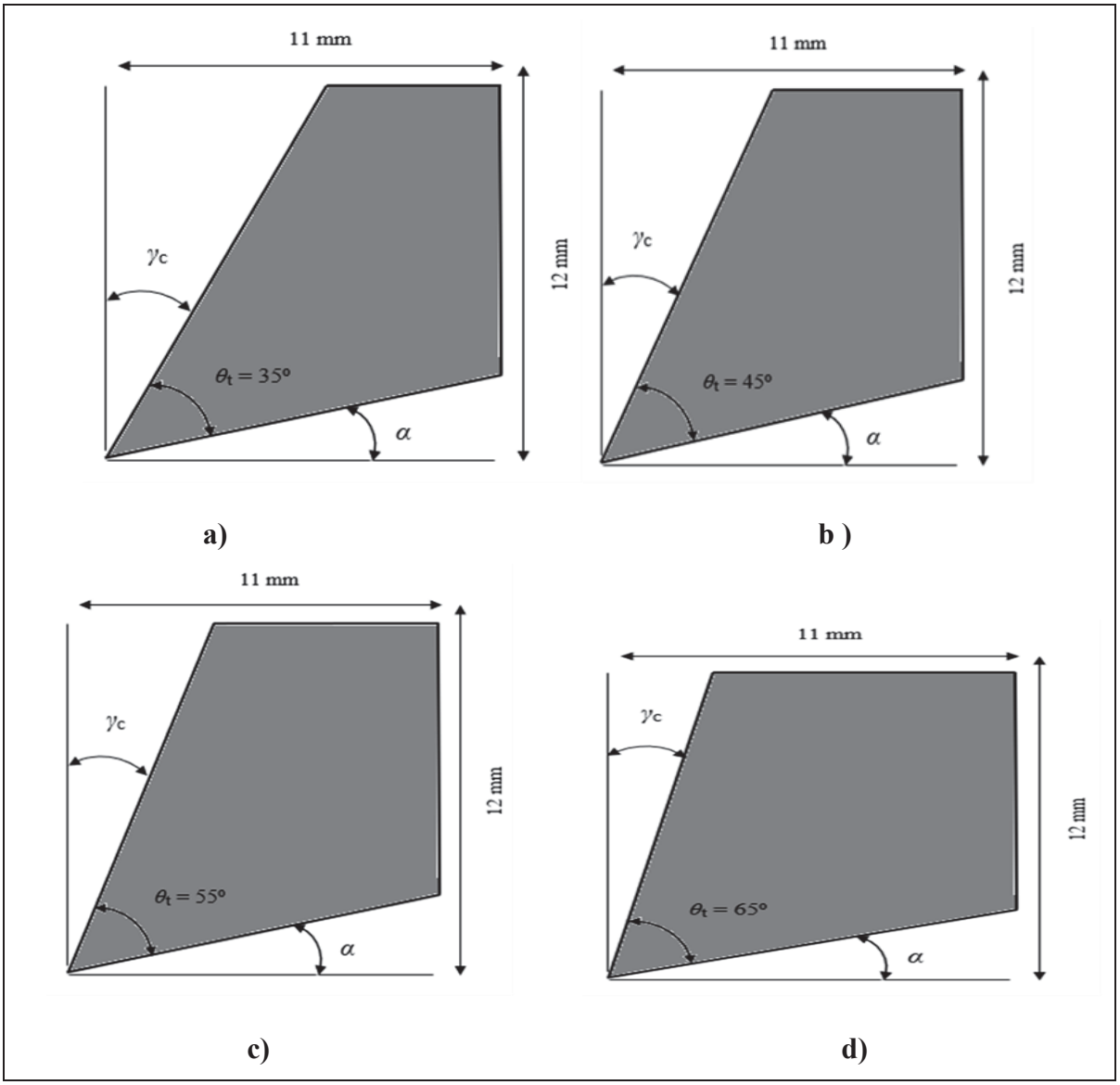

Figure 4.5 Sharp cutting tool geometries with different sharp angles θ_t :
a) 35º **b)** 45º **c)** 55º **d)** 65º

4.3 Results and discussion

4.3.1 Influence of Tool Geometry on Machining Process Performance Indicators

The simulated machining characteristics were cutting force, temperature, stress, and tool wear. The transient mode was selected in order to evaluate the evolution of forces, temperature and stress in the model with increments of time. The machining force results comprise cutting forces and thrust forces. Figure 4.6 shows the variation of these forces as a function of time for chamfer and sharp geometries, respectively, at $V = 150$ m/min, $w_n = 0.1$ mm, $f = 0.2$ mm/rev, $\gamma_n = 10^o$ and at $\theta_t = 45^o$.

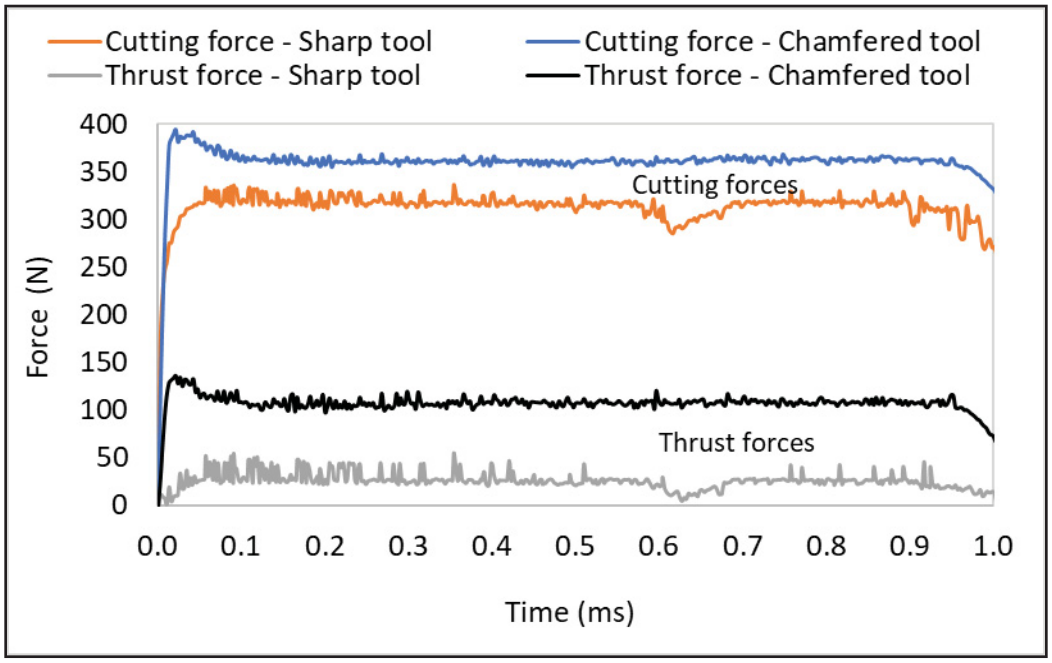

Figure 4.6 Variation in force versus time during cutting process for chamfer tool geometry at $V = 150$ m/min, $w_n = 0.1$ mm, $f = 0.2$ mm/rev, $\gamma_n = 10^o$, and sharp tool geometry at $\theta_t = 45^o$

The numerical calculation of the machining force was carried out in the plane de-fined by the cutting direction and the one perpendicular to it. Thus, the cutting and thrust forces were obtained in the cutting direction and the thrust force in the direction perpendicular to the cutting one. For every numerical test, the simulated forces reached the steady state rapidly as shown

in Figure 4.6. The total workpiece length set took about 1ms to be completed; that is why the drop of forces is noted at the end of the cutting process.

It may be seen from Figure 4.6 that for both the chamfer and sharp geometries, the cut-ting forces are higher than the thrust forces because the cutting forces are applied in the machining direction and represent 70 to 80% of the total force, which contributes to determining the global power necessary for performing the machining process (Marinov, 2018) . Additionally, the cutting and thrust forces for the chamfer tool (apparent negative rake angle) are higher than those for the sharp tool.

Figure 4.7 shows the variation of the workpiece and tool temperatures in the cutting zone as a function of the cutting time. The steady state for the temperature is reached at about 0.4 ms, depending on the cutting parameters used. That is to say, the maximum temperature is attained at about half of the sample length (30 mm) when using a sharp or chamfered edge tool. The tool temperature was higher when using a chamfered tool as compared to that obtained with a sharp tool; this can be explained by the higher forces and stresses acting on the tool when using a chamfered tool and also by the high deformation accompanying the cutting process with negative effective rake angle near the tool tip.

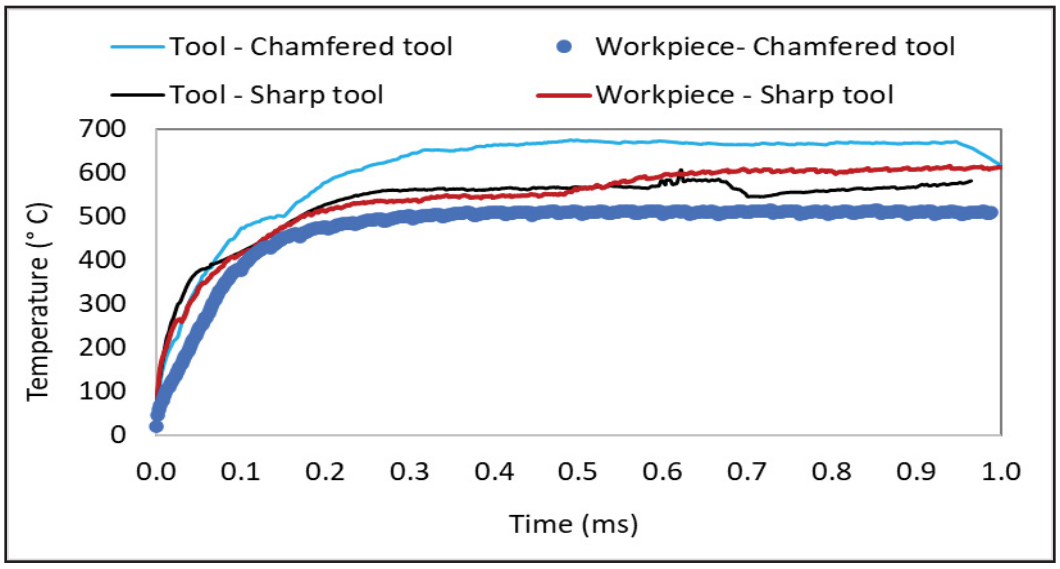

Figure 4.7 Variation in maximum temperature versus time during cutting process for chamfer tool geometry at $V = 150$ m/min, $w_n = 0.1$ mm, $f = 0.2$ mm/rev, $\gamma_n = 10$ ° and sharp tool geometry with $\theta_t = 45°$

Figure 4.8 shows the distribution of cutting temperature in the model at $V = 150$ m/min, $f = 0.2$ mm/rev, $\gamma_n = 10°$ for different chamfer widths. From Figure 4.8 it may be noted that the cutting temperature increases when the chamfer width increases. For chamfer widths from 0.1 mm to 0.75 mm, the increase in cutting temperature is around 10%. The higher temperatures were located in the chip-tool contact zone due to the higher heat generated in this area. Additionally, the more the chamfer width increased, the more the maximum temperatures were pronounced in this zone, extending to the rake face.

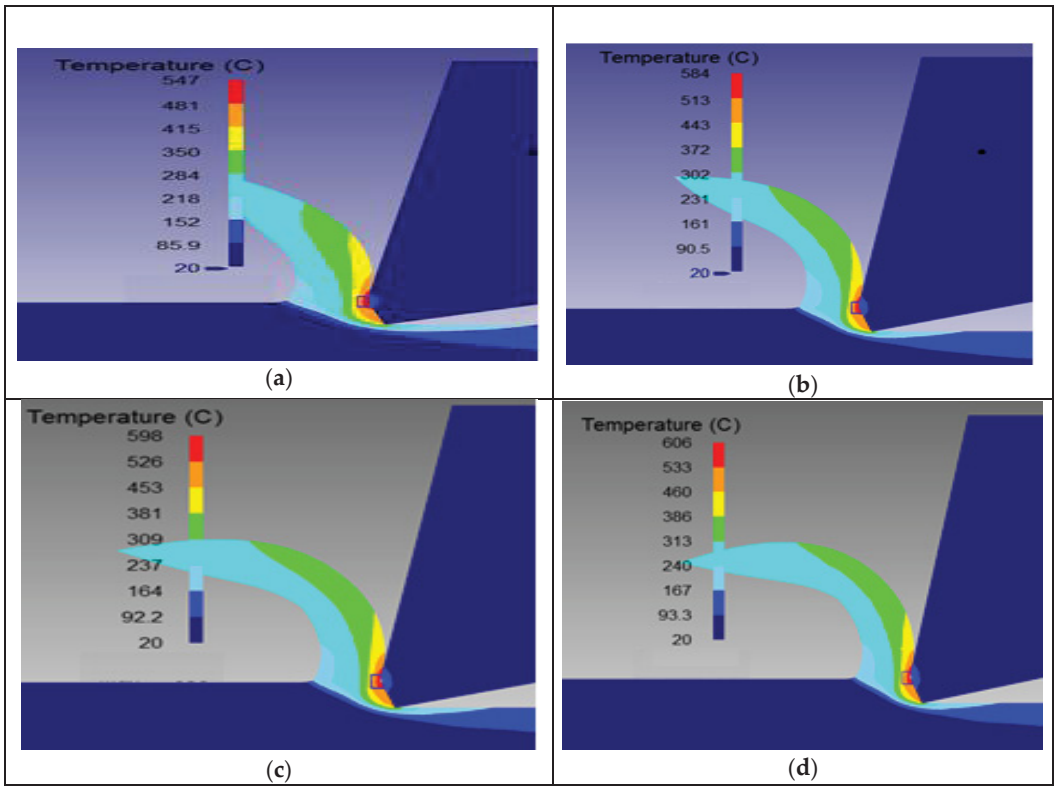

Figure 4.8 Distribution of cutting temperature in the model at $V = 150$ m/min, $f = 0.2$ mm/rev, $\gamma_n = 10°$ for the chamfer widths w_n: (**a**) 0.1 mm, (**b**) 0.4 mm, (**c**) 0.6 mm, (**d**) 0.75 mm

Figure 9 shows the distribution of effective stress in the model at $V = 150$ m/min, $f = 0.2$ mm/rev and $\gamma_n = 10°$ for different chamfer widths. It may be seen from the figure that the effective stress increases when the chamfer width increases. This result shows that a higher chamfer width produces a larger contact stress with the workpiece (Chaofeng et al., 2015).

Changing the chamfer width from 0.1 mm to 0.75 mm produced a small increase in cutting stress of about 3%. The cutting stresses were maximum in the shear plane. Tagiuri et al. (2022) also observed this result previously.

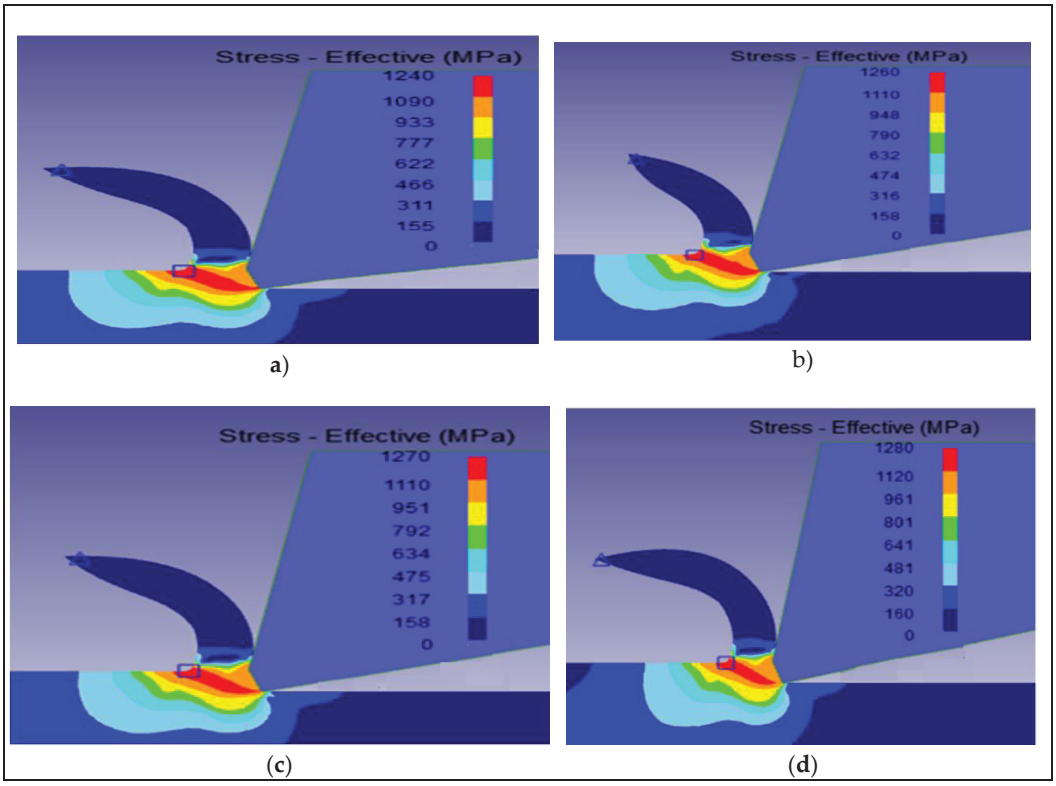

Figure 4.9 Distribution of effective stress in the model at V = 150 m/min, f = 0.2 mm/rev and γ_n =10° for the chamfer widths w_n: **(a)** 0.1 mm, **(b)** 0.4 mm, **(c)** 0.6 mm, **(d)** 0.75 mm

Figure 4.10 shows the distribution of wear depth for different chamfer widths during the cutting simulation at V = 150 m/min, f = 0.2 mm/rev and γ_n =10°. Due to the microscale nature of the obtained total wear, the images were zoomed in on the chamfer width area in order to show clearly the wear depth zone. From Figure 4.10, it is observed that the tool wear depth increases with increasing chamfer width. Increasing from a chamfer width of 0.1 mm to 0.4, 0.6 and 0.75 mm, the increases in tool wear depth were 74%, 98% and 11%, respectively. While there was a large increase from 0.1 mm to 0.6 mm, the increase noted was small from 0.6 mm to 0.75 mm. The tool wear is higher on the chamfer width of the tool at the tool–chip contact area.

These variations are due to the pressure balance applied in this area, caused by the opposing effects (Yen et al., 2004) . Otherwise, while chamfer width increases from 0.1 to 0.6 mm, the increase in pressure increases the wear depth. From 0.6 to 0.75 mm, the pressure decreases and consequently the wear depth is reduced.

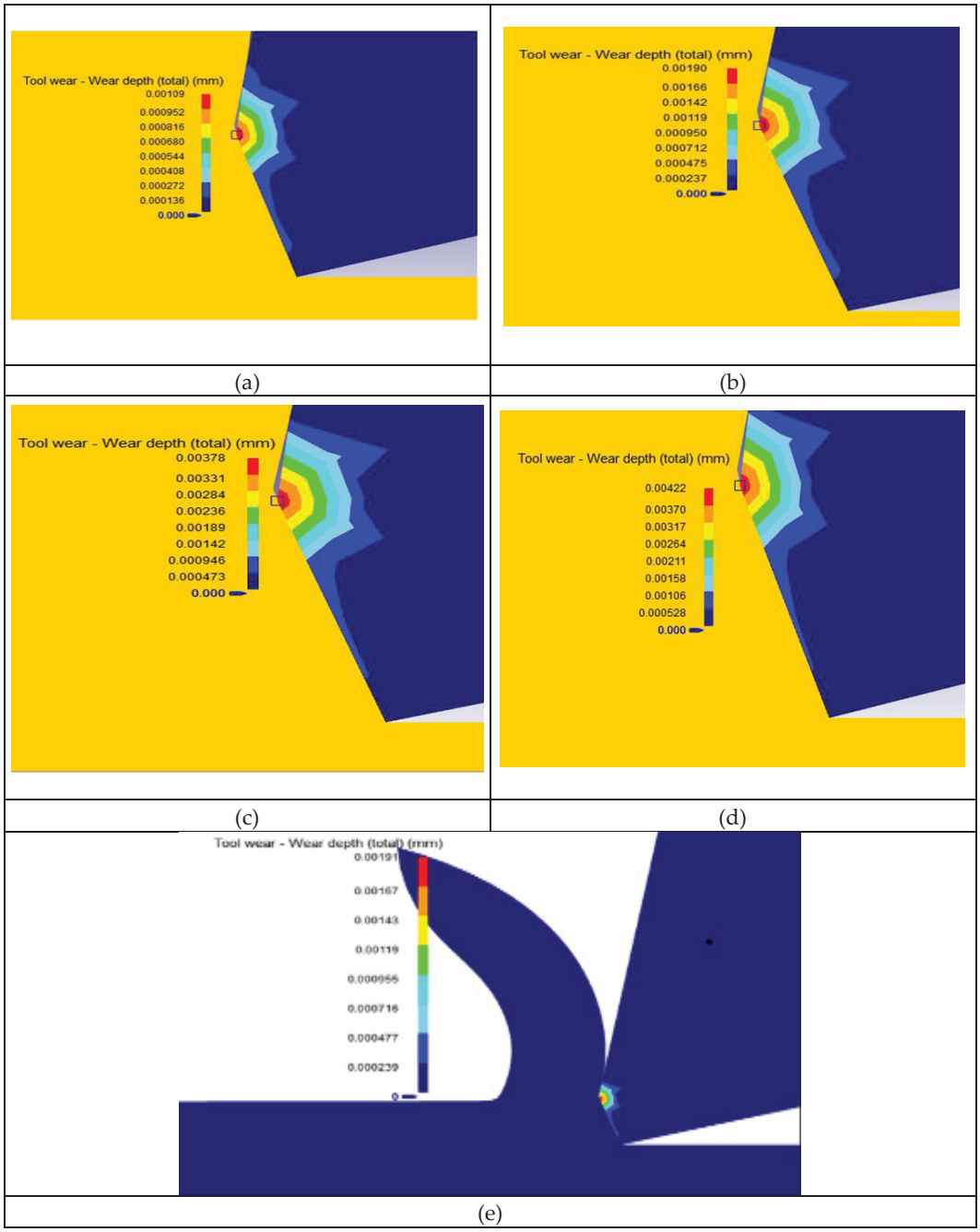

Figure 4.10 Distribution of tool wear in the model at V = 150 m/min, f = 0.2 mm/rev and γ_n =10° for the chamfer widths w_n:
(a) 0.1 mm, (b) 0.4 mm, (c) 0.6 mm, (d) 0.75 mm, (e) zoomed of (b)

Figure 4.11 shows the distribution of cutting temperature for different chamfer angles during the cutting simulation at V = 150 m/min, f = 0.3 mm/rev and w_n = 0.1 mm. From Figure 4.11, it can be noted that the cutting temperature increases with increasing chamfer angle. The increase is approximately 3% in the range of 517 ± 13 °C for the maximum temperature. From chamfer angle 25 to 35°, the cutting temperature remains nearly constant. Additionally, the more the chamfer angle increases, more the rake angle decreases. This creates longer contact between the chip and cutting tool, which produces much heat in these locations (Khalili & Safaei, 2009; Yen et al., 2004).

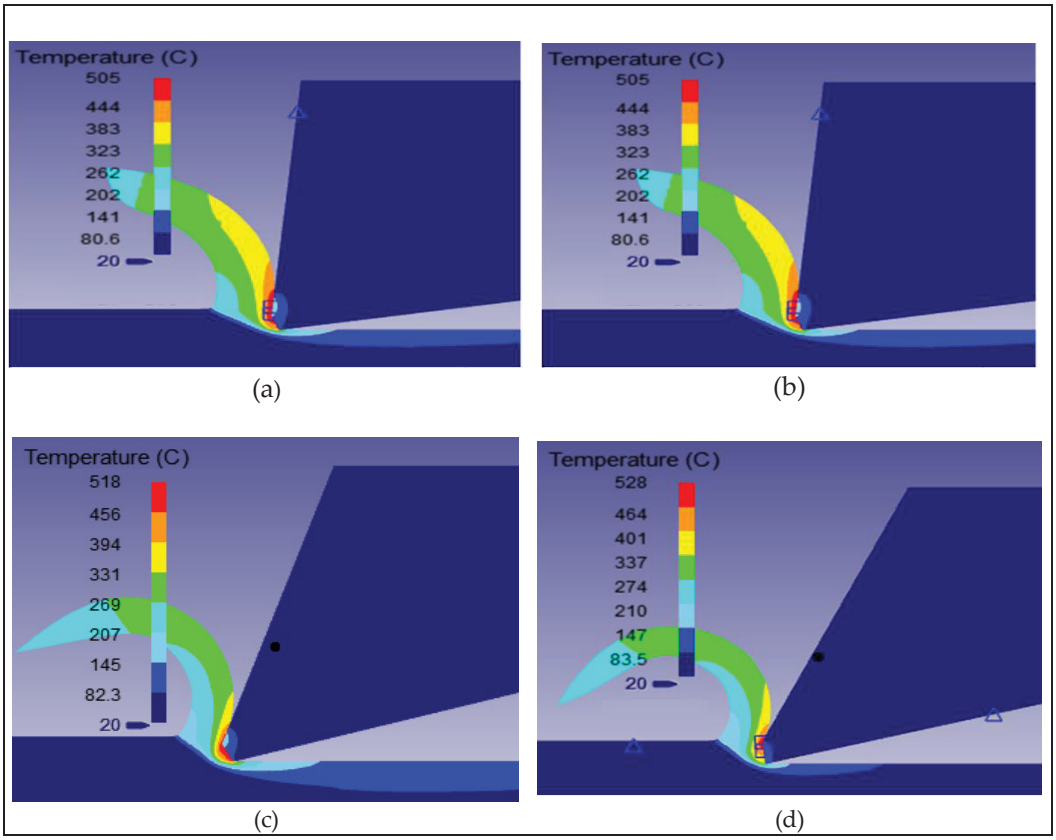

Figure 4.11 Distribution of cutting temperature in the model at V = 150 m/min, f = 0.3 mm/rev and w_n = 0.1 mm for the chamfer angles γ_n: (a) 15°, (b) 25°, (c) 35°, (d) 45°

Figure 4.12 shows the distribution of effective stress for different chamfer angles during the cutting simulation at V = 150 m/min, f = 0.3 mm/rev and w_n = 0.1 mm. An examination of the figure shows that the effective stress increases when the chamfer angle increases from 15 to

25° and from 35 to 45° but it decreases from 25 to 35° as more thrust forces are applied than cutting force in these cases (Khalili & Safaei., 2009). The variation in cutting stress is around 2%. Thus, it is reasonable to conclude that the chamfer angle does not have a significant effect on the cutting stress.

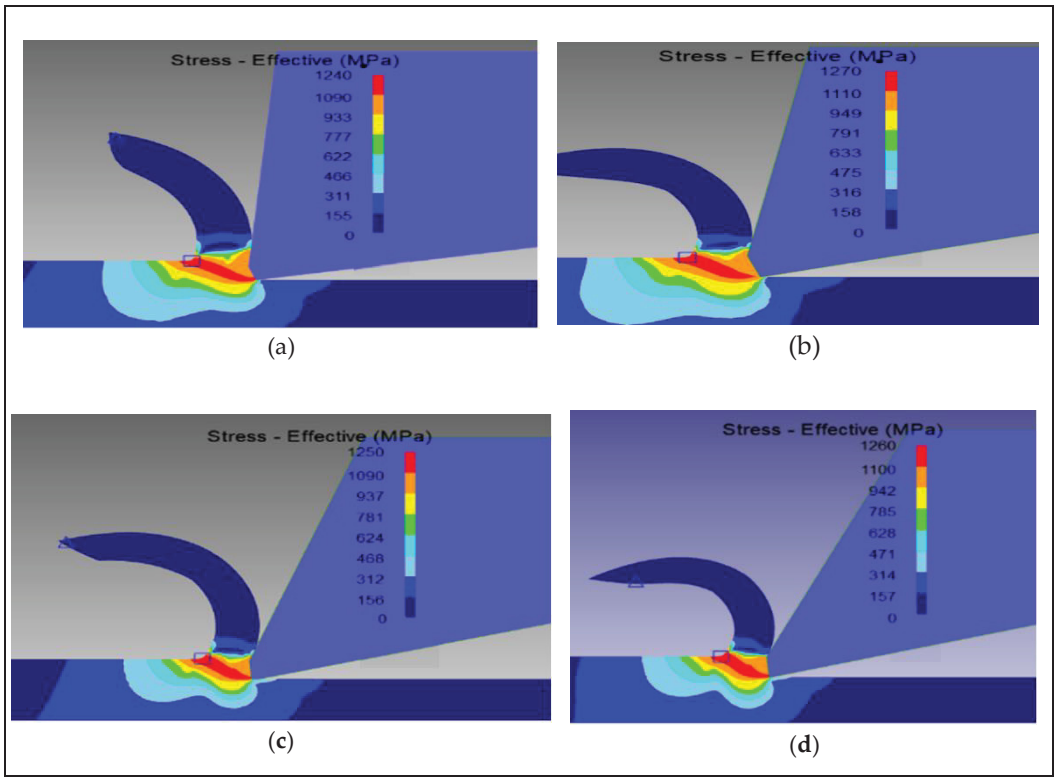

Figure 4.12 Distribution of effective stress in the model at $V = 150$ m/min, $f = 0.3$ mm/rev and $w_n = 0.1$ mm for the chamfer angles γ_n: (a) 15°, (b) 25°, (c) 35°, (d) 45°

Figure 4.13 illustrates the distribution of cutting temperature in the model at $V = 150$ m/min, $f = 0.3$ mm/rev for different sharp angles. As may be seen, the cutting temperature increases with increasing sharp angle. The rate of increase is approximately 2 to 5% in the range of 426 ± 15 °C for the maximum temperature. It is also observed that the more the sharp angle increases, the more the rake angle decreases, which creates greater contact between the chip and the cutting tool; this results in much heat in this area. The maxi-mum temperatures are located on the contact area between the chip and rake face. The more the sharp angle increases, the more the maximum temperature is pronounced in this zone, extending to the chip as well.

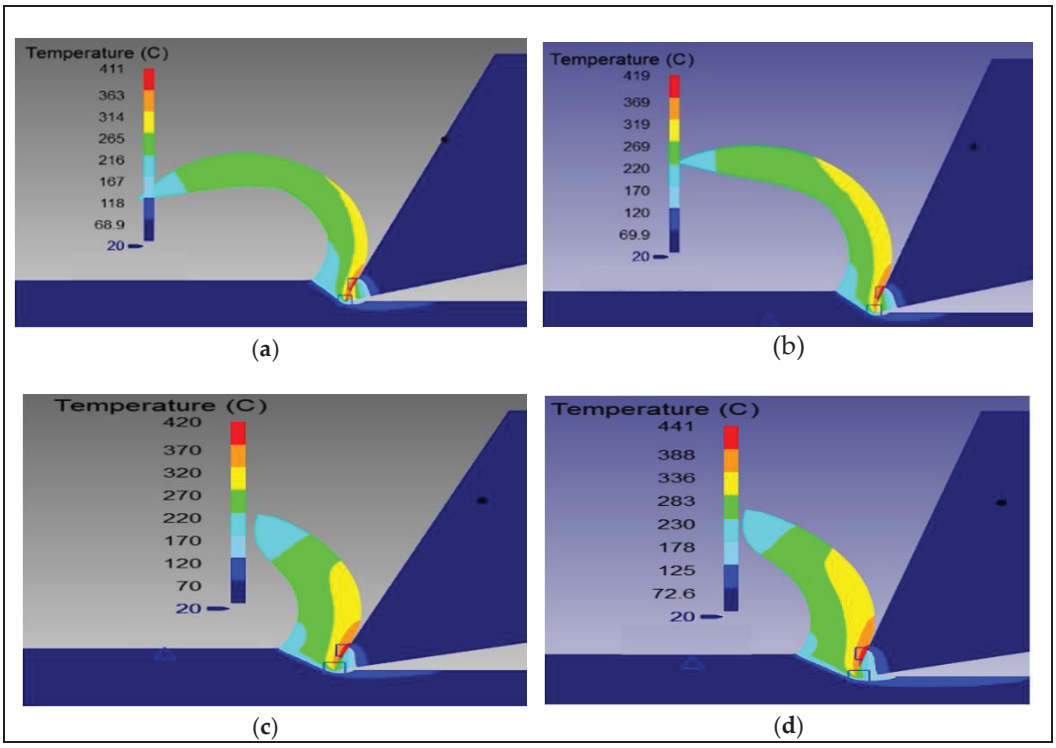

Figure 4.13 Distribution of cutting temperature at V = 150 m/min and f = 0.3 mm/rev for the sharp angles θ_t: (a) 35°, (b) 45°, (c) 55°, (d) 65°

Figure 4.14 shows the distribution of effective stress for different sharp tool angles during the cutting simulation at V = 150 m/min and f = 0.3 mm/rev. From Figure 4.14, it is noted that there is a slight increase in cutting stress when moving from a sharp angle of 45° to 65°. The increase is around 1% for maximum stress. For the values from 35° to 45°, how-ever, the cutting stress variation is about 4%.

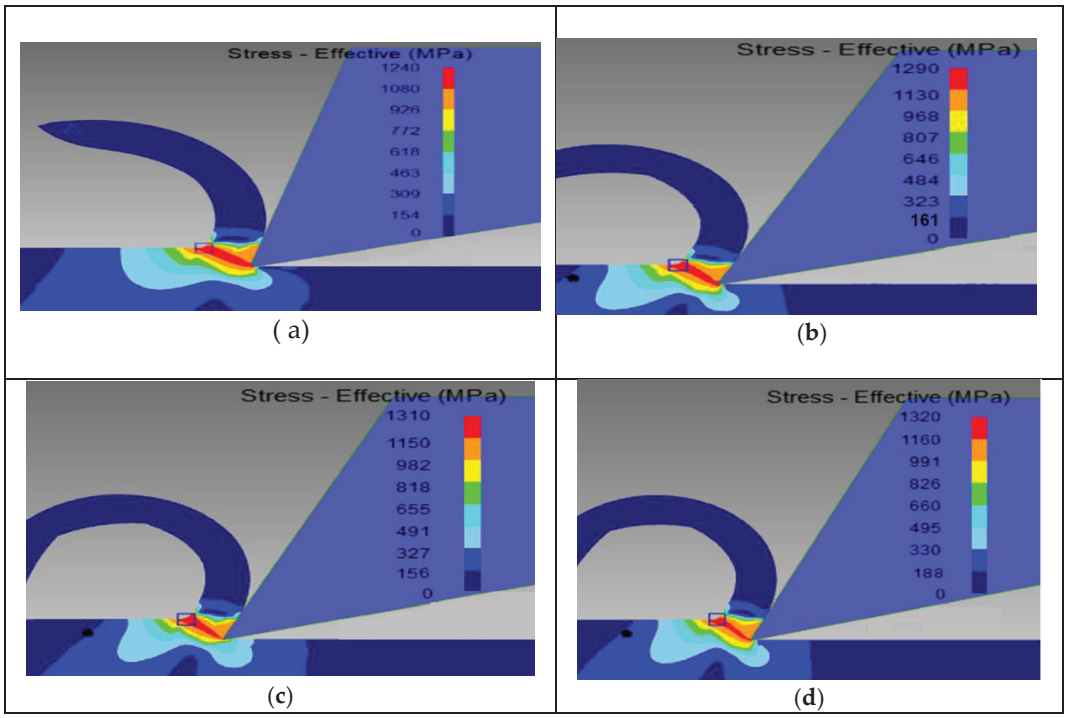

Figure 4.14 Distribution of effective stress in the model at V = 150 m/min and f = 0.3 mm/rev for the sharp angles θ_t: (a) 35°, (b) 45°, (c) 55°, (d) 65°

Figure 4.15 illustrates the distribution of tool wear depth for different tool sharp angles during the cutting simulation at V = 150 m/min and f = 0.3 mm/rev. From Figure 4.15 it is observed that wear depth increases with increasing sharp angle and chamfer angle. For the sharp tool, the tool wear occurred on the rake face, whereas it occurs on the chamfer width for the chamfer tool. As discussed earlier, the more the tool angle (sharp or chamfer angle) increases, the more the rake angle decreases, which creates longer contact between chip and cutting tool which presses the chips against the cutting tool in the contact area (Javidikia et al., 2020). Hence, both the rake face of the sharp tool and the corner at the chamfer width become more stressed, which causes significant wear at these respective locations. Furthermore, tool wear depths for the sharp tool were observed to be higher than those for the chamfer tool, due to the lower rake angles created.

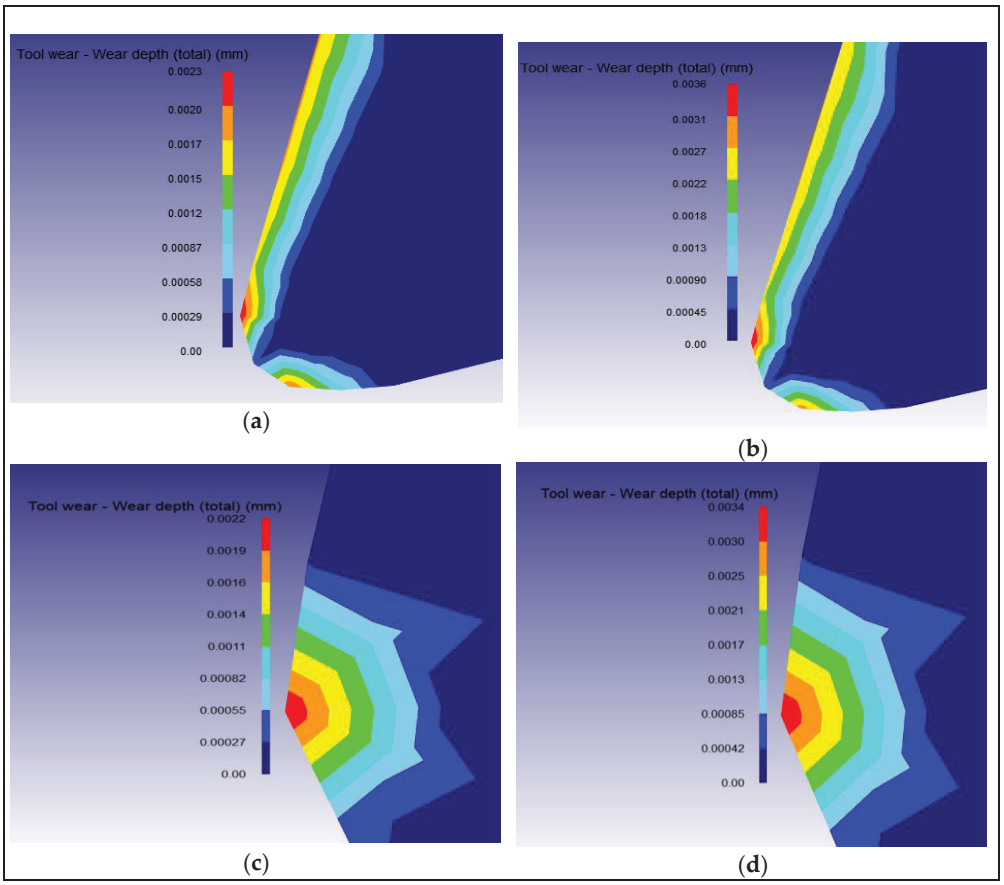

Figure 4.15 Distribution of tool wear depth in the model at $V = 150$ m/min and $f = 0.3$ mm/rev, for the cutting tool angles: (**a**) sharp edge; $\theta_t = 45°$, (**b**) sharp edge; $\theta_t = 55°$, (**c**) chamfered edge; $\gamma_n = 25°$, (**d**) chamfered edge; $\gamma_n = 35°$

4.3.2 Analysis of variance (ANOVA)

In order to identify the main parameters that influence the different machining performance characteristics, such as temperature, effective stress, chip thickness and tool wear, it is necessary to study statistically the above-investigated interactive effects. This statistical study consists of performing an analysis of variance (ANOVA) test based on the Taguchi design method, using the Statgraphics Centurion software in our case. The design of experiments (DOE) developed consisted in selecting four factors with different levels. Two types of DOEs were designed for the chamfer tool geometry and the sharp tool geometry, respectively. Tables

4.6 and 4.7 present the two designs of experiments for the two tool-type geometries, respectively.

Table 4.6 Design of experiments for the chamfer tool

Factors	Level 1	Level 2	Level 3	Level 4
V: Cutting speed (m/min)	250	350	500	600
f: Feed rate (mm/rev)	0.1	0.2	0.3	-
w_n: Chamfer width (mm)	0.15	0.25	0.35	0.45
γ_n: Chamfer angle (°)	15	25	35	45

Table 4.7 Design of experiments for the sharp tool

Factors	Level 1	Level 2	Level 3	Level 4
V: Cutting speed (m/min)	250	350	500	600
f: Feed rate (mm/rev)	0.1	0.2	0.3	-
θ_t: Sharp angle (°)	35	45	55	65

Accordingly, two ANOVA analyses were carried out, one for the chamfer tool and the other for the sharp tool to obtain the response parameters of temperature and stress. The significant parameters were identified using the condition that the p-values must be less than 0.05 at the 95.0% confidence level. Several models were analyzed and only those statistically valid at the 95% confidence level were retained.

4.3.2.1 ANOVA for chamfer tool

The obtained results showed that the feed rate, the cutting speed and their interactions were the most significant parameters affecting temperature, stress and wear depth. In addition, it can be noted that the interactions between the cutting speed and chamfer width and that between the cutting speed and chamfer angle are also most significant for temperature.

A first general linear model was analysed, and the non-statistically significant terms or interactions were removed for the analysis. Table 4.8 summarizes the final ANOVA parameters retained for the temperature when using a chamfered tool. The cutting speed was the most influential factor (F-value = 80.74), followed by the chamfer width (F-value = 42.03).

The cutting speed × feed rate interaction exhibits the most important term with an F-value of 18.81.

Table 4.8 Analysis of variance for temperature as a function of cutting speed (V), feed rate (f) and tool geometry (γ_n and w_n) when using a chamfered tool

Source	Df	Sum of Square	Mean Square	F-Value	p-Value
Model	7	2.974248×10^7	4.24891×10^6	833.85	0.0000
V: Cutting speed	1	411,429	411,429	80.74	0.0000
f: Feed rate	1	57,900.1	57,900.1	11.36	0.0016
w_n: Chamfer width	1	50,961.4	50,961.4	10.00	0.0029
γ_n: Chamfer angle	1	214,141	214,141	42.03	0.0000
$V \times f$	1	95,862.4	95,862.4	18.81	0.0001
$V \times \gamma_n$	1	74,028.0	74,028.0	14.53	0.0005
$w_n \times \gamma_n$	1	56,705.8	56,705.8	11.13	0.0018
Residual Error	41	208,918.0	5095.56		
Total	48	2.99513×10^7			

Table 4.9 summarizes the ANOVA results of the stress on the tool when machining with a chamfered tool. The tool chamfer angle did not show a statistically significant influence on the result (for the 95 % confidence interval considered). This was also the case for the interactions between the chamfer angle and the other factors: cutting speed, feed rate and tool chamfer width. Therefore, this factor and its interactions were removed from the analysis. It can thus be seen from Table 4.9 that the stress on the cutting tool is influenced mainly by the cutting speed, the chamfer width and feed rate, plus their interactions.

Table 4.9 Analysis of variance for stress as a function of cutting speed (V), feed rate (f) and tool edge chamfer with (w_n)

Source	Df	Sum of Square	Mean Square	F-Value	p-Value
Model	6	8.34658×10^7	1.3911×10^7	1401.19	0.0000
V: Cutting speed	1	1.0384×10^6	1.0384×10^6	104.59	0.0000
f: Feed rate	1	495,304	495,304	49.89	0.0000
w_n: Chamfer width	1	674,986	674,986	67.99	0.0000
$V \times f$	1	170,323	170,323	17.16	0.0002
$V \times w_n$	1	252,041	252,041	25.39	0.0000
$f \times w_n$	1	107,954	107,954	10.87	0.0020
Residual Error	42	416,974	9927.94		
Total	48	8.38828×10^7			

4.3.2.2 ANOVA for sharp tool

The performance of the sharp tool was analyzed as a function of the cutting parameters (cutting speed and feed rate) and tool angle (θ_t). Table 4.10 summarizes the results of analysis of variance obtained for the temperature, considering a general linear model and before removing non-statistically significant factors and terms. The tool angle and its interactions with cutting and feed rate were not statistically significant at the 95% confidence interval, and hence these terms were removed from the final model.

Table 4.10 Analysis of variance for temperature as a function of cutting speed (V), feed rate (f) and sharp tool angle (θ_t)—Original model before suppression of factors

Source	Df	Sum of Square	Mean Square	F-Value	p-Value
Model	6	722,164	120,361.0	52.94	0.0000
V: Cutting speed	3	22,731.0	22731	10	0.0029
f: Feed rate	2	36,024.6	36,024.6	15.84	0.0003
θ_t: Sharp tool angle	3	1331.57	1331.57	0.59	0.4485
$V \times f$	6	9055.13	9055.13	3.98	0.0526
$V \times \theta_t$	9	1564.35	1564.35	0.69	0.4116
$f \times \theta_t$	6	0.00110	0.00110	0	0.9994
Residual Error	41	93,221.5	2273.7		
Total	47	815,385.0	-		

The cutting speed, the feed rate and the cutting speed x feed rate interaction were the most significant terms. This was confirmed by Ucun et al. (2011) during the turning of AISI 1045 steel using carbide cutting sharp tools. They reported that the cutting speed and the feed rate are the most significant factors for cutting temperature and cutting force, respectively.

For the stress on the cutting tool, the results of the analysis of variance are presented in Table 4.11. Once again, the tool angle and its interactions with cutting speed and feed rates were found to be not statistically significant when using a general linear model with a constant. Some effects were found, however, when considering a general linear model without a constant, as will be seen in the equations and response surface analysis presented in the next section.

Table 4.11 Analysis of variance for stress as a function of cutting speed (V), feed rate (f) and sharp tool angle (θ_t)

Source	Df	Sum of Square	Mean Square	F-Value	p-Value
Model	6	7.55473×10^7	1.2591×10^7	3392.62	0.0000
V: Cutting speed	1	329,927	329,927	88.9	0.0001
f: Feed rate	1	167,344	167,344	45.09	0.0001
θ_t: Sharp tool angle	1	604,873	604,873	162.98	0.00001
$V\times f$	1	42,829.7	42,829.7	11.54	0.0015
$V\times \theta_t$	1	129,005	129,005	34.76	0.00001
$f\times \theta_t$	1	50,784.1	50,784.1	13.68	0.0006
Residual Error	42	155,877	2273.7		
Total	48	7.57×10^7	-		

In order to show the most influencing parameters that affect the cutting temperature and the effective stress during orthogonal cutting, the above results can be explicitly given in terms of the effect order. Table 4.12 summarizes the influential parameters in terms of importance with 1 being most influential and 4 being the least. It may be seen that the cutting speed and feed rate are the most influential parameters affecting the different machining characteristics studied.

Table 4.12 Summary of most influential parameters in terms of importance (1 = most, 4 = least)

Parameters	Chamfer Tool		Sharp Tool	
	Temperature	**Stress**	**Temperature**	**Stress**
V: Cutting speed	1	1	2	2
f: Feed rate	-	3	1	3
T:* Tool geometry	2	2	-	1
$V \times f$: Interaction Speed × Feed rate	3	3	3	4
$V \times T$: Interaction speed ×Tool geometry	4	4	-	
$f \times T$: Interaction feed × Tool geometry		-		

*T**: Tool geometry: Chamfer width (w_n) or chamfer angle (γ_n); sharp tool angle for sharp tool (θ_t)

4.3.3 Response surface analysis

The results obtained from the ANOVA tests may be expressed through mathematical and statistical equations using regression models to establish response functions fitting the available data. The following empirical models were obtained from statistical analysis:

For the chamfer cutting tool, the regression equations for temperature and stress are presented in Equations (4.7) and (4.8):

$$\text{Temperature} = 1.467\,V + 1172\,f + 719.78\,w_n + 16.463\,\gamma_n - 3.490\,V f - 0.0208\,V\gamma_n - 23.635\,w_n\gamma_n \quad (4.7)$$

$$R^2 = 97.5\%$$

$$\text{Stress} = 2.21154\,V + 3565.15\,f + 2713.88\,w_n - 4.53194\,V f - 3.84915\,V w_n - 4596.42\,f w_n \quad (4.8)$$

$$R^2 = 99.5\%$$

For the sharp cutting tool, the regression equations of temperature and stress predicted from statistical analysis are given in Equations (4.9) and (4.10). The analysis of the wear did not show statistical significance at the 95% confidence interval.

$$\text{Temperature} = 229 + 0.650\,V + 1867\,f - 1.25\,V\,\text{f} \quad (4.9)$$

$$R^2 = 88\%$$

$$\text{Stress} = 1.902\,V + 2993.72\,f + 17.763\,\theta_t - 2.5146\,Vf - 0.02486\,V\theta_t - 30.06\,f\theta_t \qquad (4.10)$$

$$R^2 = 99\%$$

The general linear model for the estimation of the stress for the sharp tool gave a coefficient of correlation that was not acceptable (68%). For this reason, a model with no constant was preferred. The predicted results shown in Equations (4.7) and (4.10) fitted well with the results obtained by simulation as displayed in Figures 4.16 and 4.17.

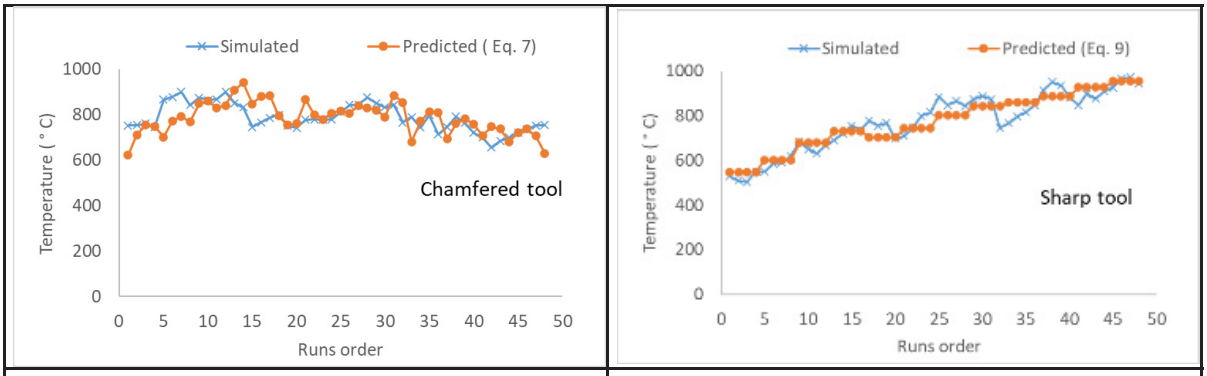

(a) Chamfered tool | **(b)** Sharp tool

Figure 4.16 Comparison of predicted and simulated temperatures:
(**a**) chambered tool and (**b**) sharp tool

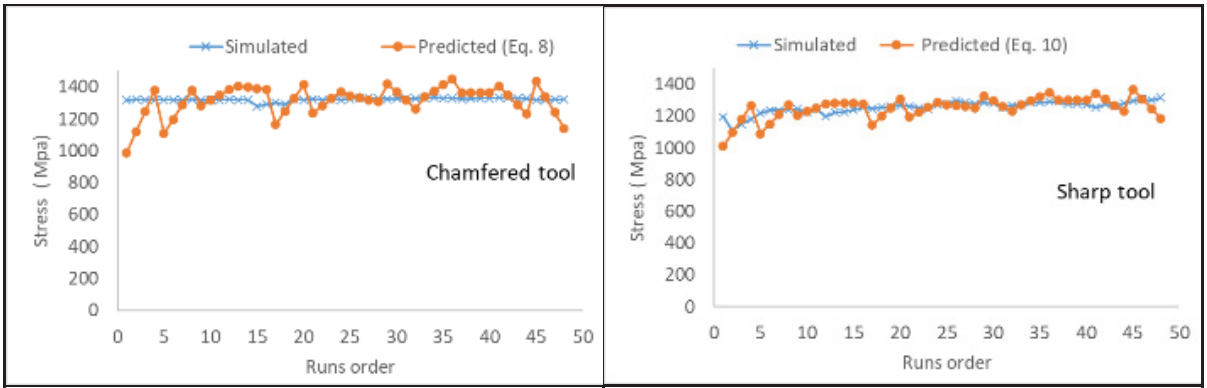

(a) Chamfered tool | **(b)** Sharp tool

Figure 4.17 Comparison of predicted and simulated stress:
(a) chambered tool and **(b)** sharp too

In order to predict the unknown response values and the corresponding cutting conditions, 3D statistical graphs or 3D surface plots were produced to interpret the effects of the continuous parameters on the response values based on the fitted model. Figure 4.18 shows the surface plots of the parametric effects on temperature for the chamfered cutting tool. This figure shows the interaction between the chamfered tool geometry and the machining parameters (cutting speed and feed rate) on the cutting temperature. For low chamfer angles (15° and 20°; Figure 4.18a, b), the maximum temperature occurs at a higher cutting speed and low feed rate setting (at speed about 650 m/min and a feed rate of about 0.1 mm/rev). At a higher value of chamfer angle (40°; Figure 4.18d), the maximum values of cutting temperatures occurred in irregular settings of cutting speed and feed rates as depicted in Figure 4.18d. This is due to the interactive effects between the tool edge preparation and the cutting parameters, as also noted in Equation (4.8). As both the chamfered tool width (w_n) and the chamfered angle (γ_n) influenced the temperature (Equation (4.8)), a 3D effect of cutting speed, feed rate and chamfer width (w_n) on the cutting temperature was also analyzed and is presented in Figure 4.19. It is seen from Figure 4.19 that the effect of chamfer width (w_n) on temperature is moderate, as compared to those of the cutting speed and feed rate.

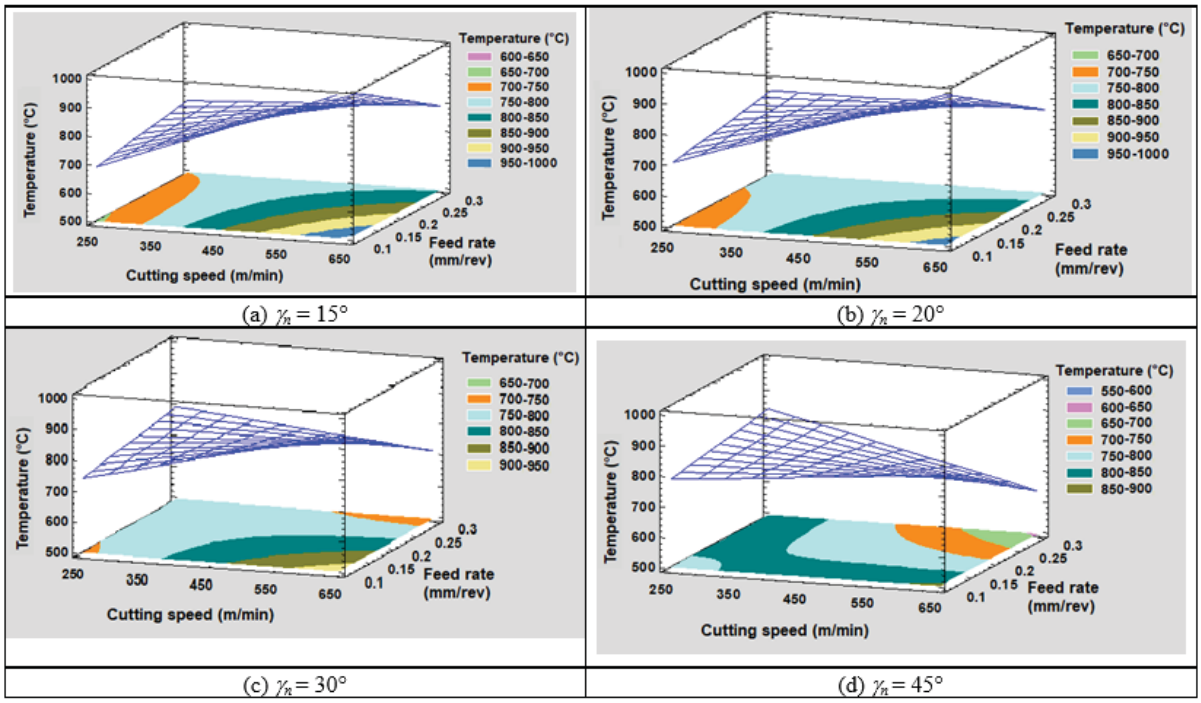

Figure 4.18 3D Surface plots of parametric effects of cutting speed, feed rate and chamfered tool angle (γ_n) on temperature (°C) when using a chamfered tool (w_n = 0.34 mm)

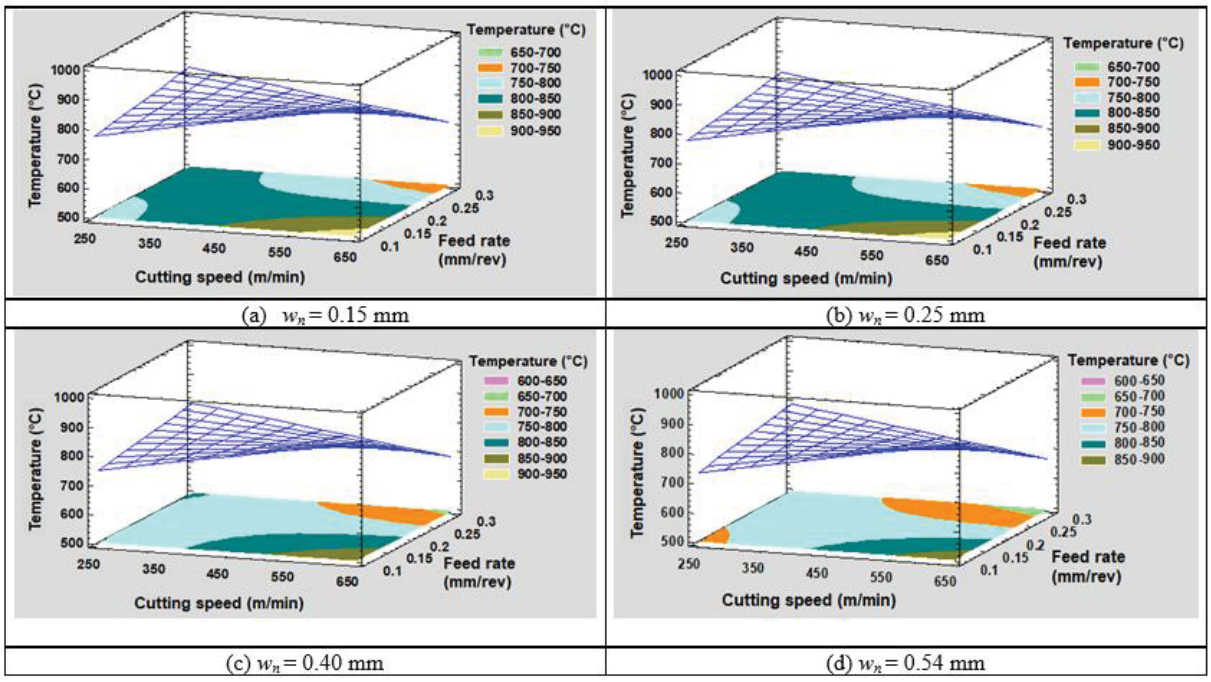

Figure 4.19 3D Surface plots of parametric effects of cutting speed, feed rate and chamfered tool length (w_n) on temperature (°C) when using a chamfered tool ($\gamma_n = 35°$)

A 3D surface plot of cutting speed and feed rate on the cutting stress on chamfered tool is presented in Figure 4.20. This stress is mostly influenced by the cutting speed and the feed rate and, in second order, by the chamfer width and its interactions with cutting speed and feed rate (see Equation (4.9)). For chamfer width below 0.25 mm, the maximum stress takes place at high cutting and low feed rate (Figure 4.20a, b), while for higher values of chamfer width (0.35 mm and 0.50 mm), the maximum stress occurs at high feed rate and low cutting speed but also at high cutting speed and low feed rate settings. The stresses are higher for the large feed rate, as the chip section is thicker and the forces high.

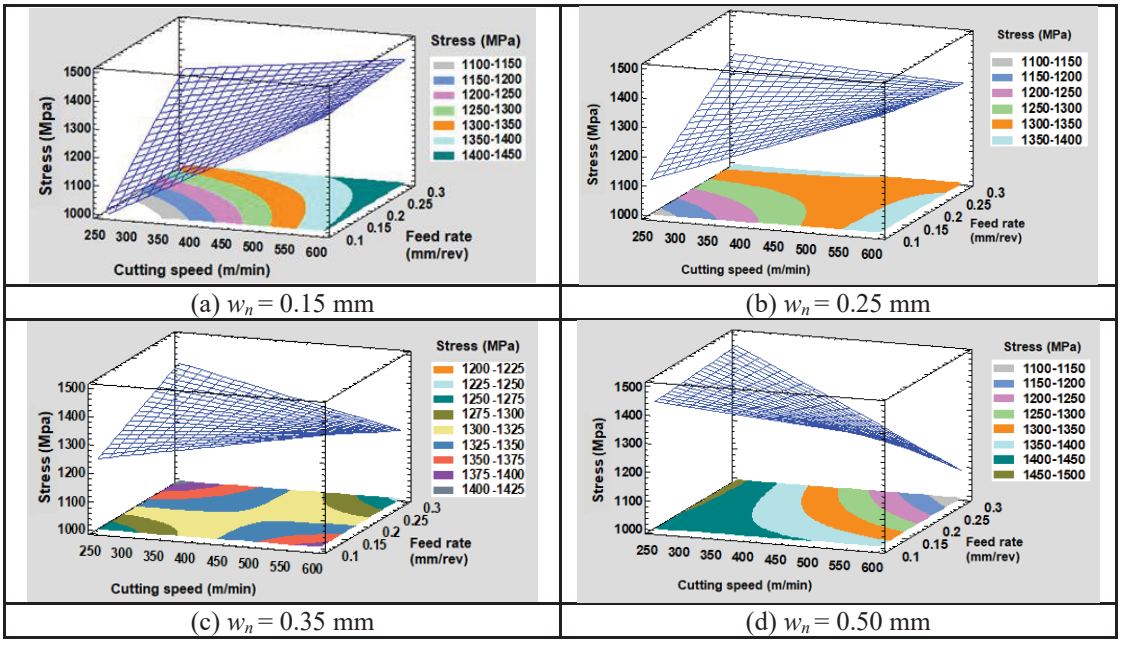

(a) $w_n = 0.15$ mm (b) $w_n = 0.25$ mm

(c) $w_n = 0.35$ mm (d) $w_n = 0.50$ mm

Figure 4.20 3D Surface plots of parametric effects of cutting speed, feed rate and chamfered tool length (w_n) on the stress when using a chamfered tool ($\gamma_n = 35°$)

For a sharp tool, the maximum temperature occurred when using a high feed rate and a high cutting speed (Figure 4.21a, b) independently of the sharp tool angle used. At this setting, the stress on the cutting tool is high (Figure 4.22a, b).

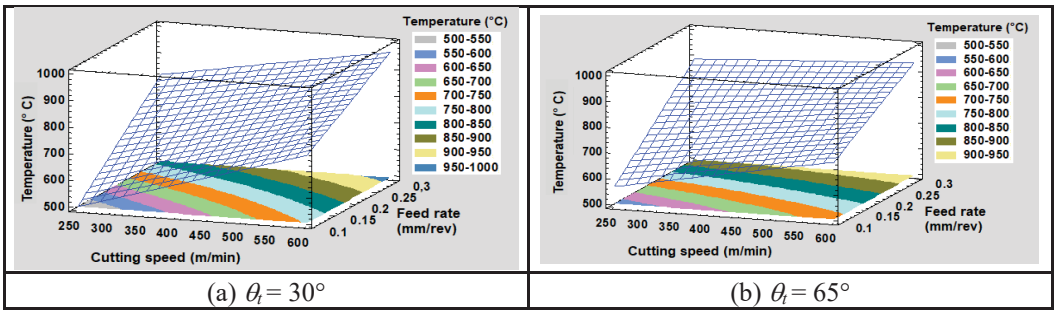

(a) $\theta_t = 30°$ (b) $\theta_t = 65°$

Figure 4.21 3D Surface plots of parametric effects of cutting speed, feed rate and sharp tool angle (θ_t) on the temperature (°C) when using a sharp tool ($\gamma_n = 35°$)

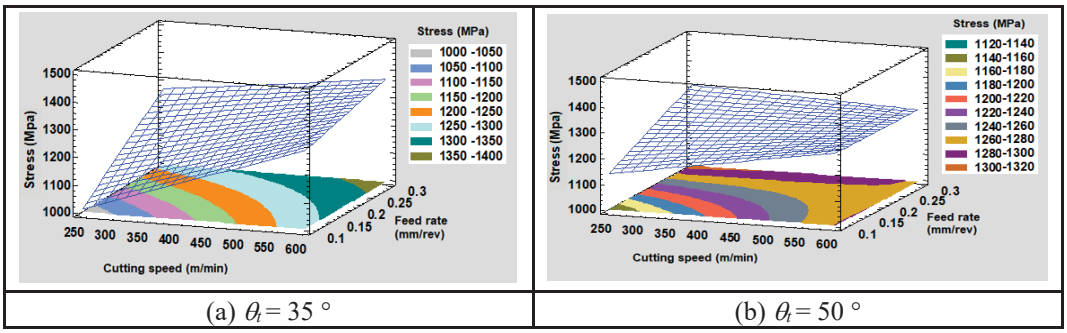

(a) $\theta_t = 35°$ (b) $\theta_t = 50°$

Figure 4.22 3D Surface plots of parametric effects of cutting speed, feed rate and sharp tool angle (θ_t) on the stress (MPa) when using a sharp tool ($\gamma_n = 35°$)

4.3.4 Validation of Results

The obtained numerical results for chamfered tools were validated using the experimental data obtained (see Table 4.13) by Khalili & Safaei (2009) who conducted a study on the effect of tool edge preparation on 1045 steel for a feed rate of 0.20 mm/rev and using chamfered carbide tools with different chamfer widths. The results of effective stress are very comparable (errors of about 4.7 to 6.9 %), while those of the temperature are slightly more different (errors varying from 10 –15%).

Table 4.13 Comparison of numerical and experimental results for chamfer tool

	Numerical Results (V = 250 m/min)			Experimental Data (Khalili & Safaei, 2009) (V = 100–200 m/min)			Errors (%)		
Parameter	Chamfer width w_n (mm)						Chamfer width w_n		
Characteristics	0.1	0.2	0.3	0.1	0.2	0.3	0.1	0.2	0.3
Temperature (°C)	741.23	750.32	799.35	637	675	680	14.1	10.0	14.9
Cutting stress (MPa)	1320.87	1325.48	1290.75	1230	1225	1230	6.9	7.6	4.7

The obtained numerical and statistical analysis results obtained with chamfered tools are also in good agreement with the study by Ucun et al. Ucun et al. (2011), who conducted a similar numerical study on AISI 1045 steel with similar properties using ceramic tools and cutting speeds ranging from 100 m/min to 400 m/min and feed rates from 0.1 – 0.5 mm/rev and with a depth cut of 1 mm. The numerical results of Ucun et al. (2011) were validated by experimental data from the literature Yen et al. (2004) . The experimental conditions have been described in this study (Yen et al., 2004). Ucun et al. (2011) obtained a cutting temperature of about 800 °C and they found that the tool chamfer lengths (0.1 mm – 0.3 mm) and chamfer angle (5°C – 20°C) do not have a significant effect on the cutting temperature but may increase the machining forces. Although a straight comparison cannot be made since ceramic tool has different heat transfer properties, it remains that the effect of the tool geometry (chamfer parameters) in similar machining conditions can be compared, as it follows the same trend and leads to the same conclusion as in the present study.

For orthogonal cutting of AISI 1045 with sharp carbide tool, the closest comparison we found was that of the work by Qasim et al. (2015) . They compared the process performance for a large range of cutting speeds (200–630 m/min) and cutting feed rates (0.1 to 0.2 mm/rev). The results obtained in the present study are close those of Qasim et al. (2015), as shown in Table 4.14, in which the tool angle is ignored as it did not affect our results. The differences observed could be explained by the small variations in the materials data used in the two cases.

Table 4.14 Comparison of numerical and experimental results for sharp tool

	Temperature	Temperature (Qasim et al., 2015)	Error
Variable feed rates (cutting speeds ranging from 200 m/min to 630 m/min)			
0.1 mm /rev	629	700	10%
0.2 mm /rev	793	765	−4%
Variable cutting speeds (feed rates ranging from 0.1to 0.2 m/rev)			
200 m/min	677.5	600	−13%
600 m/min	830	800	−4%

4.4 Conclusions

In the present research study, the interactive effects between chamfer width, chamfer angle, sharp angle, and cutting speed and feed rate on cutting temperature and effective stress were investigated during the milling of AISI 1045 steel using the finite element method and employing DEFORM-2D software. The statistical analysis of numerical simulation results using ANOVA was carried out in order to determine significant parameters. From the results obtained, the following points may be summarized:

- Statistical analysis showed that the effective stress and cutting temperature are mainly influenced by the cutting speed, the feed rate and their interaction for the chamfer tool and by the feed rate for the sharp tool. For the chamfer tool, the interactions between cutting speed and chamfer width and between cutting speed and chamfer angle have a significant influence on the cutting temperature. Whereas for the sharp tool, the cutting speed and the interaction between the sharp tool angle and feed rate are important. Therefore, for a given tool edge geometry, the cutting speed and the feed rate should be chosen wisely.

- The main effects of the tool edge preparation parameters tested did not show significant influence on the tested machining process performance (temperature, stress), especially for chamfered tools. The performance of these tools is mainly influenced by the cutting speed, the feed rate and their interactions. In contrast, the tool with cham-fer edge led to high temperature and high effective stress as compared to the sharp edge tool.

- For the chamfer tool, the cutting speed and the tool chamfer width were found to be the most influential factors, followed by the interaction between the cutting speed and the feed rate and then by the interaction between the cutting speed and the tool chamfer width. The maximum temperature obtained on chamfered tools ranged from 700 °C to 900 °C, while the minimum was about 550 °C, depending on the feed rates and speeds used. The effective stress varied less and was about 1320 MPa.
- For the sharp tool, the tool angle has a slight influence on temperature and stress. The values of tool angle affected the 3D surface responses of maximum temperature and effective stress when both the cutting speed and the feed rates were varied. The maximum temperature reached was 970 °C while the minimum was about 550 °C, depending on the feed rate and speeds used. The effective stress varied less and was about 1250 MPa.

CHAPTER 5

COMPARATIVE EVALUATION OF THE PERFORMANCES OF HONED, CHAMFERED AND SHARP TOOLS IN ORTHOGONAL CUTTING OF AISI 1045 STEEL

Zakaria Ahmed M. Tagiuri[1], Thien-My Dao[1], Agnes Marie Samuel[1], and Victor Songmene[1]

[1]Department of Mechanical Engineering, École de Technologie Supérieure (ÉTS)
1100 Notre-Dame Street West, Montréal, QC H3C 1K3, Canada

Paper submitted to Manufacturing and Materials. June,16th 2024

Abstract

The present paper investigates the effects of machining conditions on cutting temperature, effective stress, chip thickness, tool wear and residual stress during orthogonal cutting of AISI 1045 steel. The investigation aimed at finding the cutting-edge tool preparation in relation to the machining process parameters that would determine the best possible cutting tool performance using numerical comparison. A numerical simulation study based on 2D finite element method was conducted to predict the data for analysis. Using design of experiments based on factorial design, the analysis of variance (ANOVA) was performed in order to determine the most significant parameters during the cutting process. The design of experiments was set for three cutting tool geometries (round, chamfer and sharp). The results showed that for all the three cutting tools studied, the cutting speed square term had the greatest influence influencing on the different machining characteristics, except the chip thickness. Only the significant terms were selected to establish the empirical model. For the optimal cutting conditions, the sharp cutting tool minimizes tool wear, effective stress and residual stress. Whereas the chamfer and round cutting tools are recommended for reducing cutting temperature and chip thickness respectively.

Key words: Machining, tool edge preparation, numerical modeling

5.1 Introduction

During the past decades, the historical data collected from the literature review has shown that the machining industry knew the important evolutions required for the goal to increase the productivity of specified components with high quality, low cost in short production times. In order to realise this goal, it was necessary to develop different and new technologies such as in the area of the cutting-edge preparation method which was widely used by cutting tool manufacturing engineers for several machining applications, due to its great importance in reducing tool wear and increasing tool life, so as to influence the cutting forces, the temperature distribution, to affect the surface integrity of the workpiece, and give a good geometrical accuracy. In several research works, the authors adopted the cutting tool preparation technology for improving machining performance during cutting processes. Some of them studied the effects of machining parameters and tool edge geometries on cutting temperature, effective stress, chip thickness, tool wear and roughness. Whereas other researchers worked on the optimization of the cutting process using statistical analysis to identify the influencing machining parameters or cutting tool geometrical properties. However, in terms of machining optimization. On one hand, little work was done on optimization of cutting-edge geometries using Finite Element Method (FEM) the studies being limited to some specified materials and machining processes. The previous research results showed that from the optimization analysis of cutting-edge parameters during machining of Fe-Cr-Ni stainless steel, the round cutting tool edge preparation is realizable for small edge radius (Cheng et al., 2016; Liao et al., 2017) but is difficult for large edge radius in a rough machining process (Cheng et al., 2017). On the other hand, most of the studies were realized only on roughness, temperature and specially on the tool wear, but stress and chip thickness were ignored. They showed that a round cutting edge geometry can improve the tool life of cutting tools (Bouzakisa et al., 2002; E D'Errico et al., 1998; Yen et al., 2004). They considered that tool life is one of the most important output variables influencing the manufacturing process and takes a large part of the total cost. (El-Hossainy et al,. 2010) proposed an experimental optimization model based on time as variable for maximizing tool life and minimizing production time. The obtained results using the

analysis of variance (ANOVA) showed that the tool wear, force and roughness can be expressed as a function of different variables such as cutting speed, feed rate, depth of cut, approach angle, rake angle and time. (Makadia et Nanavati,.2014) developed also an experimental model to predict the surface roughness during turning of AISI 1040 steel using round cutting edge geometry. They optimized the response using statistical analysis and investigated the effects of tool nose radius and cutting speed, feed rate, and depth of cut. The results showed that low feed rate, high cutting speed and tool nose radius are the important factors for minimizing the surface roughness and the obtained optimal values for cutting speed, feed rate, depth of cut and nose radius are 270.303 m/min, 0.1 mm/rev, 0.3 mm and 0.91 mm, respectively.

(Aouici et al,. 2011) studied the effects of three cutting parameters (cutting speed, feed rate and cutting time) on flank wear and surface roughness in hard turning of AISI H11. The objective of this study is to optimize the response of these machining characteristics using ANOVA and response surface methodology (RSM). The results show that the feed rate is the most influencing parameter on surface roughness and the flank wear is strongly affected by cutting time, followed by the cutting speed, and then by the interaction between cutting time and cutting speed.

(Elgnemi et al,.2021) realized an optimization experimental study of force, specific cutting energy, temperature, tool wear, and fine dust emission in milling of carbon fiber reinforced polymer under dry machining conditions. This study evaluated the influence of the spindle speed and feed rate on these different machining properties, and determined the optimal parameter values using statistical analysis. It was concluded that the feed rate is the most significant parameter influencing the cutting force and tool wear. In terms of cutting temperature and fine particle emission, the spindle speed had a the greater effect than the feed rate. The optimal values for cutting force and tool wear were also obtained for the spindle speed of 10,000 rpm and feed rate of 2 μm/tooth. The results for cutting temperature, specific cutting energy and total number of particles were obtained for the spindle speed of 10,000 rpm and feed rate of 2 μm/tooth.

The present paper aims to investigate numerically the combinate effects of the cutting parameters (cutting speed, feed rate) and the cutting tool geometries (edge radius, chamfer

width, chamfer angle and sharp angle) on temperature, force, stress, chip thickness and wear depth during machining of AISI 1045 steel. The statistical analysis of these effects will be conducted using analysis of variance (ANOVA) with the goal of comparing the different mentioned parameters. A surface response approach will be adopted to establish the response variables as mathematical formulations using the regression model.

5.2 Materials and Methods

5.2.1 Cutting tool and workpiece materials

The materials used were high carbon steel AISI 1045 and uncoated cemented carbide for the workpiece and cutting tool, respectively. These two materials were widely used in several manufacturing industries especially in machining due to different advantages. Table 5.1 presents the physical, mechanical and thermal properties of workpiece and tool materials.

Table 5.1 Thermal and mechanical properties of workpiece and tool materials Adapted to (Yen et al. 2004; Zakaria et al., 2022)

Item	Workpiece	Tool
Properties	High carbon AISI 1045	Uncoated cemented carbide
Density (kg/m^3)	7870	11900
Young's modulus (GPa)	200	620
Poisson ratio	0.29	0.26
Thermal conductivity (W/m°C)	45	50
Specific heat (J/kg°C)	590	375

5.2.2 Cutting tool and workpiece designs

For machining process design, three geometry types for cutting tool were selected: round, chamfer and sharp tool geometry. Whereas a parallelepiped design was proposed for the workpiece. Figure 5.1 shows the 2D design of the cutting tools and Figure 5.2 shows the chamfer cutting tool geometries compromising different chamfer widths and angles.

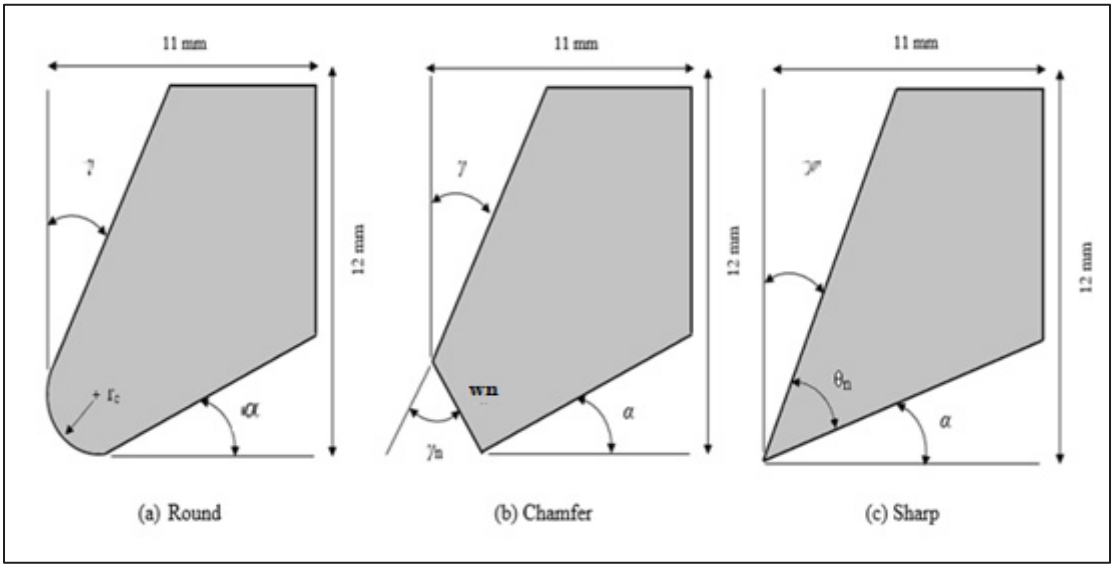

Figure 5.1 The 2D model design of cutting tool: (a) round (b) chamfer (c) sharp.

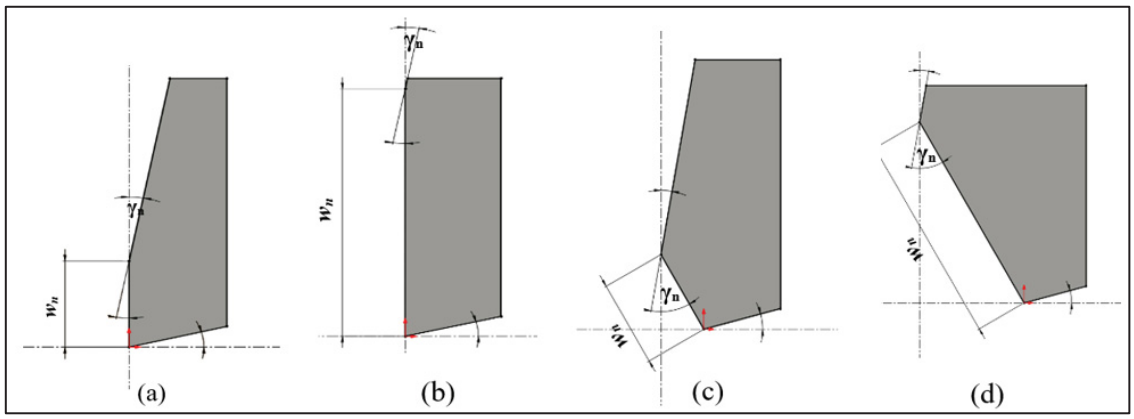

Figure 5.2 Chamfer cutting tool geometries with different chamfer width and angles (a) $\gamma_n = 10^\circ$; $w_n = 0.15$mm (b) $\gamma_n = 10^\circ$; $w_n = 0.45$mm (c) $\gamma_n = 40^\circ$; $w_n = 0.15$mm (d) $\gamma_n = 40^\circ$; $w_n = 0.45$mm

5.2.3 Numerical simulation tests characterization

The numerical simulation tests carried out consisted in performing the orthogonal cutting simulation of AISI 1045 steel using DEFORM software based on a 2D finite element method. The mesh finite element which was created automatically by default is 2D free quadrilateral element. It is used to calculate the cutting temperature, cutting force, effective stress, chip thickness and tool wear depth during the time in the whole model using transient heat transfer and motion equations integrated in the DEFORM software. In order to obtain the numerical test results, the cutting tool edge geometry and the process cutting parameters were specified. For the tool edge geometrical properties, the edge radius, chamfer width and chamfer angle and sharp angle were selected for round, chamfer and sharp tools, respectively. For the process cutting parameters, the cutting speed and feed rate were proposed.

It was assumed that the cutting process took place in an ambient environment in such way that cutting tool was fixed, and the workpiece was moved in the y-axis direction using the designated machining parameters.

The optimization of different machining characteristics such as temperature, effective stress, residual stress and tool wear depth will be done using analysis of variance (ANOVA) in order to identify the main parameters for obtaining the optimal results.

Figure 5.3 shows the distributions of the machining forces at V = 200 m/min, f = 0.2 mm/rev, $\alpha = 15°$ for different cutting tool geometries: (a) round (b) chamfer (c) sharp.
The mean values of stresses obtained were plotted in the form of residual stress graphs for the round tool, expressed in terms of the variations with workpiece depth for different rake angles (r_c = 30 μm) (see Figure 5.4).

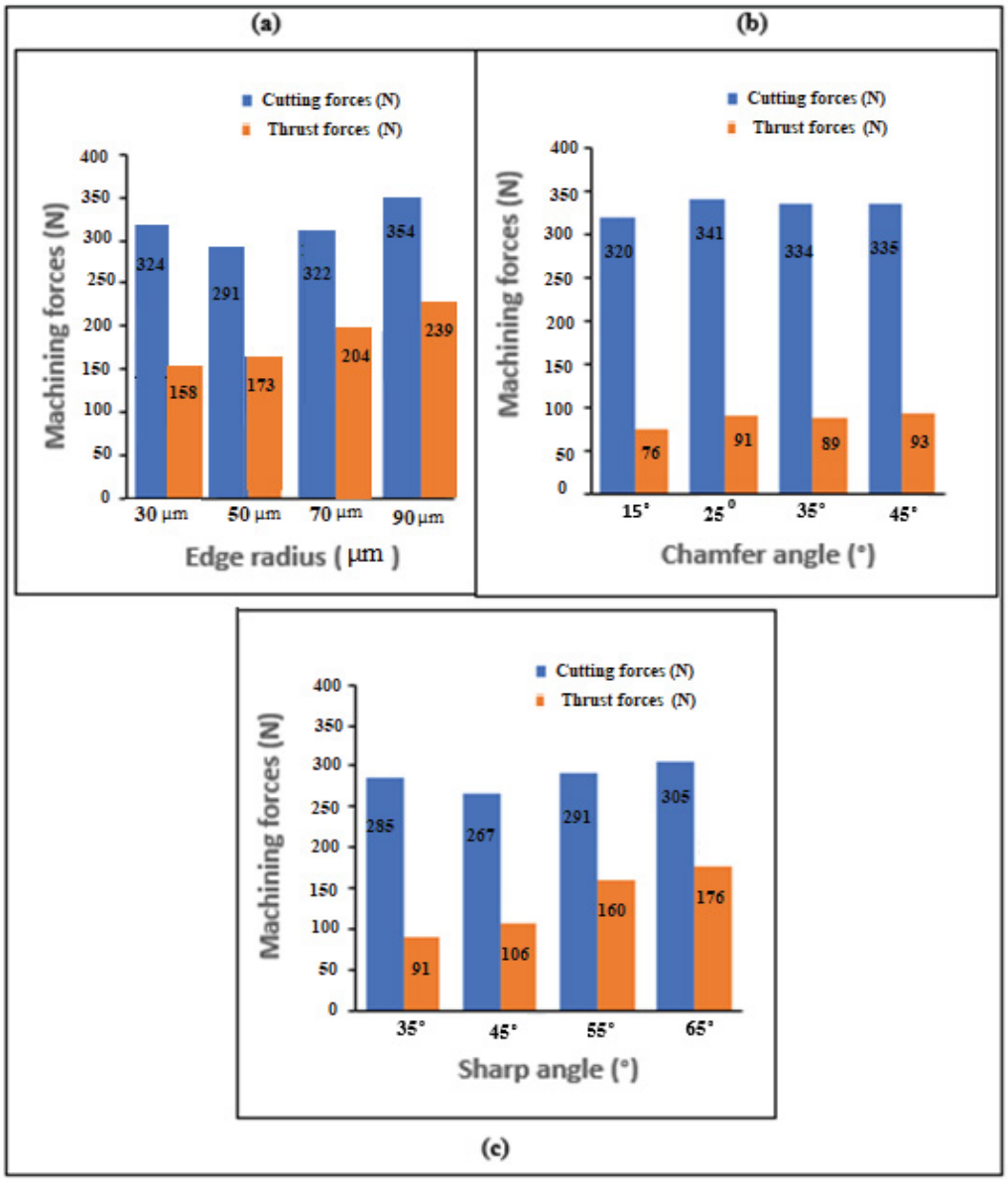

Figure 5.3 Distributions of machining forces at V = 200/min, f = 0.2 mm/rev, α = 15° for different cutting tool geometries: (a) Round (b) Chamfer (c) Sharp

From Figure 5.3 it may be seen that for all the cutting tool geometries, there are no significant variations in cutting forces with edge radius, and chamfer or sharp angles. The cutting forces are higher than the thrust forces. This is due to the global machining forces which are almost represented by the cutting forces, as they are applied in the cutting direction. This analysis was

already realized by (Zakaria et al.,2022). Furthermore, the cutting forces of the chamfer tool are higher than those of sharp and round tools. For the thrust forces, there is a little variation with the chamfer angle, but the forces increase with edge radius and chamfer angle (i.e., with decrease of rake angle).

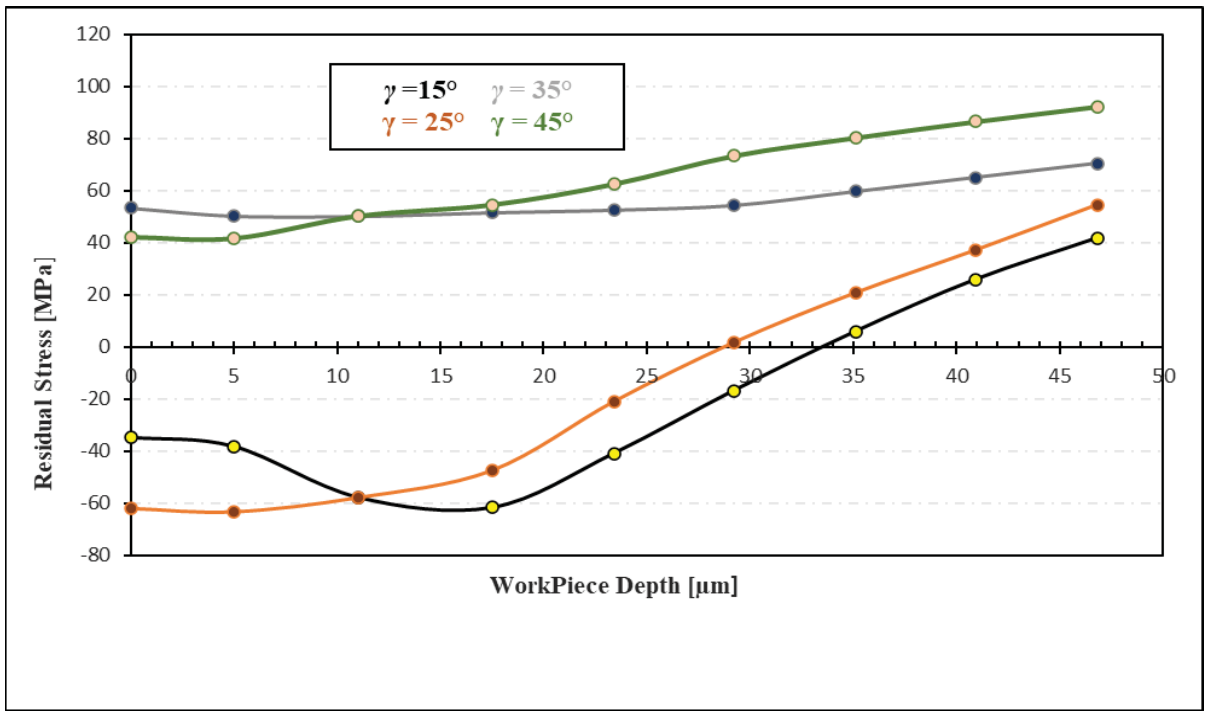

Figure 5.4 Variation of residual stresses with workpiece depth for different rake angles γ (15°, 25°, 35°, 45°); (Edge radius r_c = 0.03 mm)

It is observed from Figure 5.4 that for the rake angles 15° and 25°, the behavior of the residual stresses changes from compressive to tensile in character at the depths of approximately of 34 µm and 29 µm, respectively and reach maximum values of 41.87 MPa and 54.55 MPa at workpiece depth of 47 µm. However, the tensile nature of the residual stress is maintained for the rake angles 35° and 45°. From workpiece depths greater than 16 µm, the residual stresses continue to increase with increasing depth.

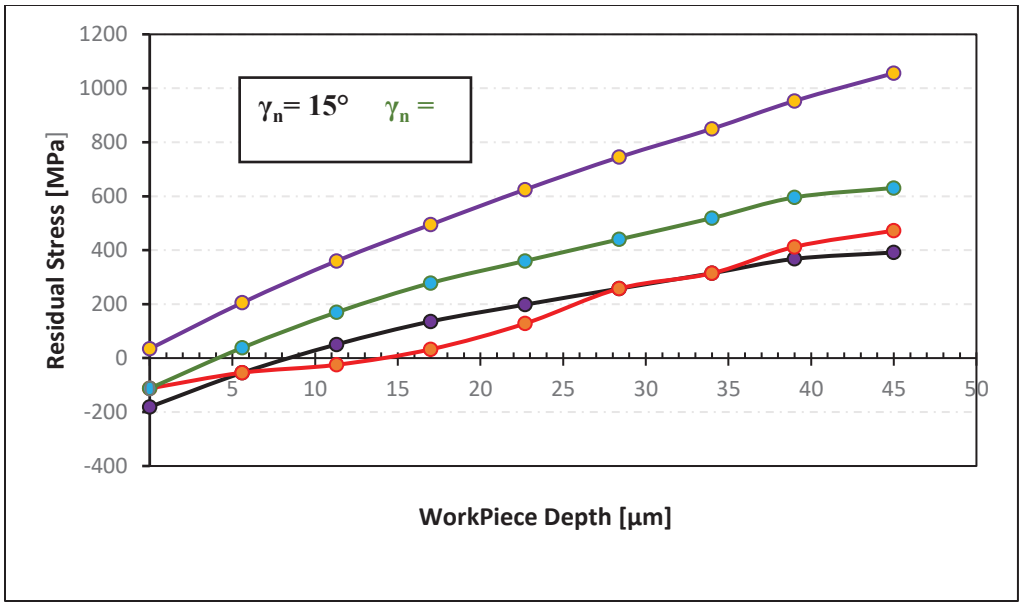

Figure 5.5 Variation of residual stresses with workpiece depth for different chamfer angles γ_n (15°, 25°, 35°, 45°)

Figure 5.5 shows the variation of the residual stresses with workpiece depth for different chamfer angles γ_n (15°, 25°, 35°, 45°) at V = 200 m/min, f = 0.2 mm/rev, α = 15°. From Figure 5.5 it may be seen that, for the chamfer angles γ_n = 15˚, γ_n = 25˚, and γ_n = 35˚, the residual stresses change from compressive to tensile in nature at the depths of 9 µm, 15 µm and 4 µm respectively and maintain approximately constant values beyond 40 µm depth. For the chamfer angle γ_n = 45˚ the residual stress maintains its tensile behaviour. Moreover, it was also noted that the higher chamfer angle the greater the residual stresses that remained in the workpiece material after the machining operation was completed.

Figure 5.6 displays the variations in the residual stress with workpiece depth for the sharp angles at θ_n = 10°, 15°, 20°, and 25°, V = 200 m/min, f = 0.2 mm/rev, α = 15°. It can be seen that the residual stress changes from compressive to tensile character only for the sharp angle of 10° at the depth of 4 µm, maintaining tensile character thereafter. For the other sharp angles; the residual stresses were always tensile and increased and reached their maximum values at depths between 10 and 18 µm.

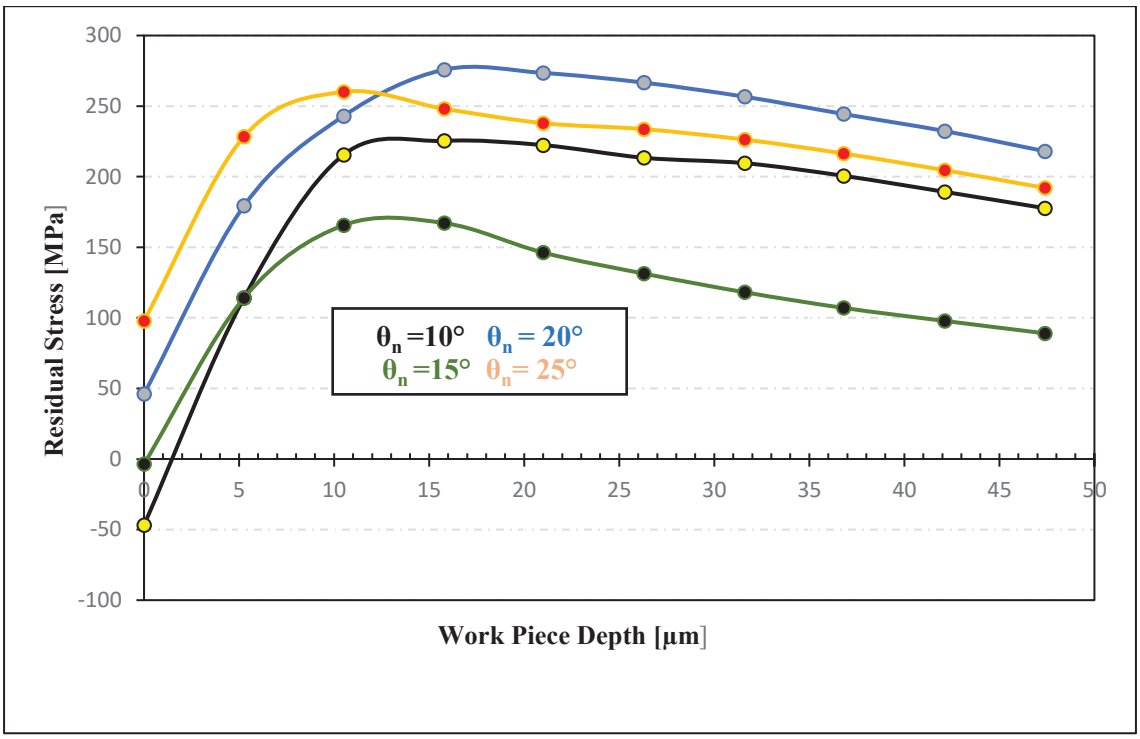

Figure 5.6 Variation of residual stresses with workpiece depth for different sharp angles θ_n (10°, 15°, 20°, 25°)

Figure 5.7 demonstrates the distribution of the residual stress as a function of the various tool edge radii selected, at $V = 200$ m/min, $f = 0.2$ mm/rev, $\alpha = 15°$. It may be seen that the residual stress increases with the increase in the tool edge radius. It should be noted that the residual stresses were generated under the machined surface and were developed in the cutting direction. The greater the edge radius, the more the maximum residual stress created in the workpiece, due to the higher cutting forces and larger area of contact between the tool and the workpiece. The residual stress attained was 881 MPa for an edge radius of 0.09 mm and only 816 MPa for an edge radius of 0.01 mm. These numerical results were validated experimentally using data from (Nasr et al. 2007) and (Jacobus et al., 2000), who found that larger tool edge radii produce higher residual stresses beneath the surface of the workpiece during orthogonal cutting of AISI steel material.

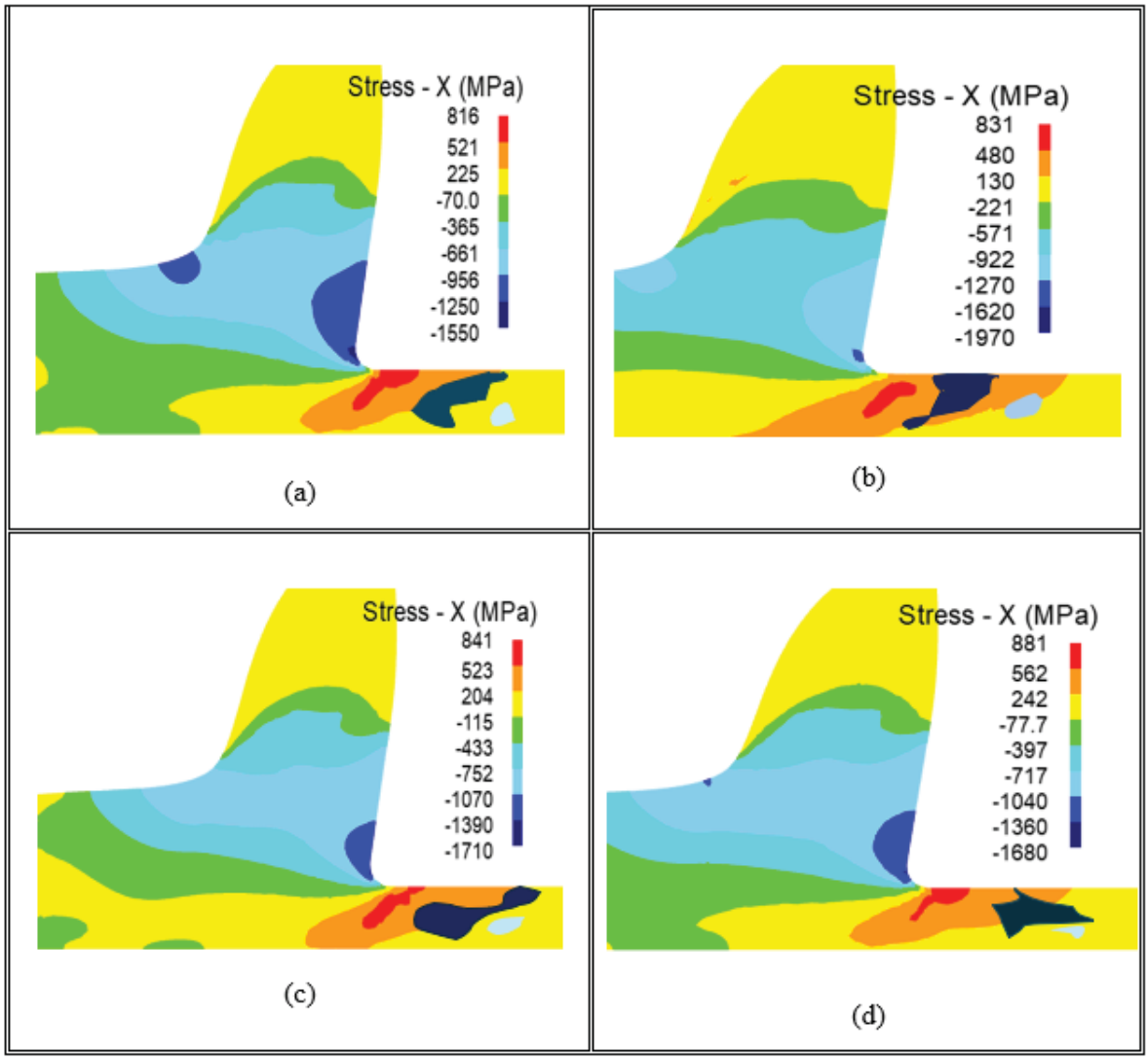

Figure 5.7 Distributions of residual stresses for various tool edge radii r_c: (a) = 0.01 mm, (b) = 0.03 mm, (c) = 0.05 mm , (d) = 0.09 mm

Figure 5.8 shows the distribution of the residual stress with chamfer angles of 15˚, 25˚, 35˚, and 45˚ for machining parameters V = 200 m/min, f = 0.2 mm/rev, α = 15°. It can be observed that the residual stress increases with increase in the chamfer angle. These results have been presented earlier in Figure 5.5 and are supported by the experimental work of (Altintas, 2000) who reported the increase in the cutting forces with increasing chamfer angle, and consequently the increasing residual stress in the cutting of AISI 1045 steel, with properties similar to the material used in the present study. The residual stress attained the maximum value of 1680 MPa for the chamfer angle of 45° and only 1350 MPa for an angle of 15°. The

compressive stresses were developed in the cutting direction parallel to the rake face whereas the tensile stresses were observed in the other areas of the workpiece.

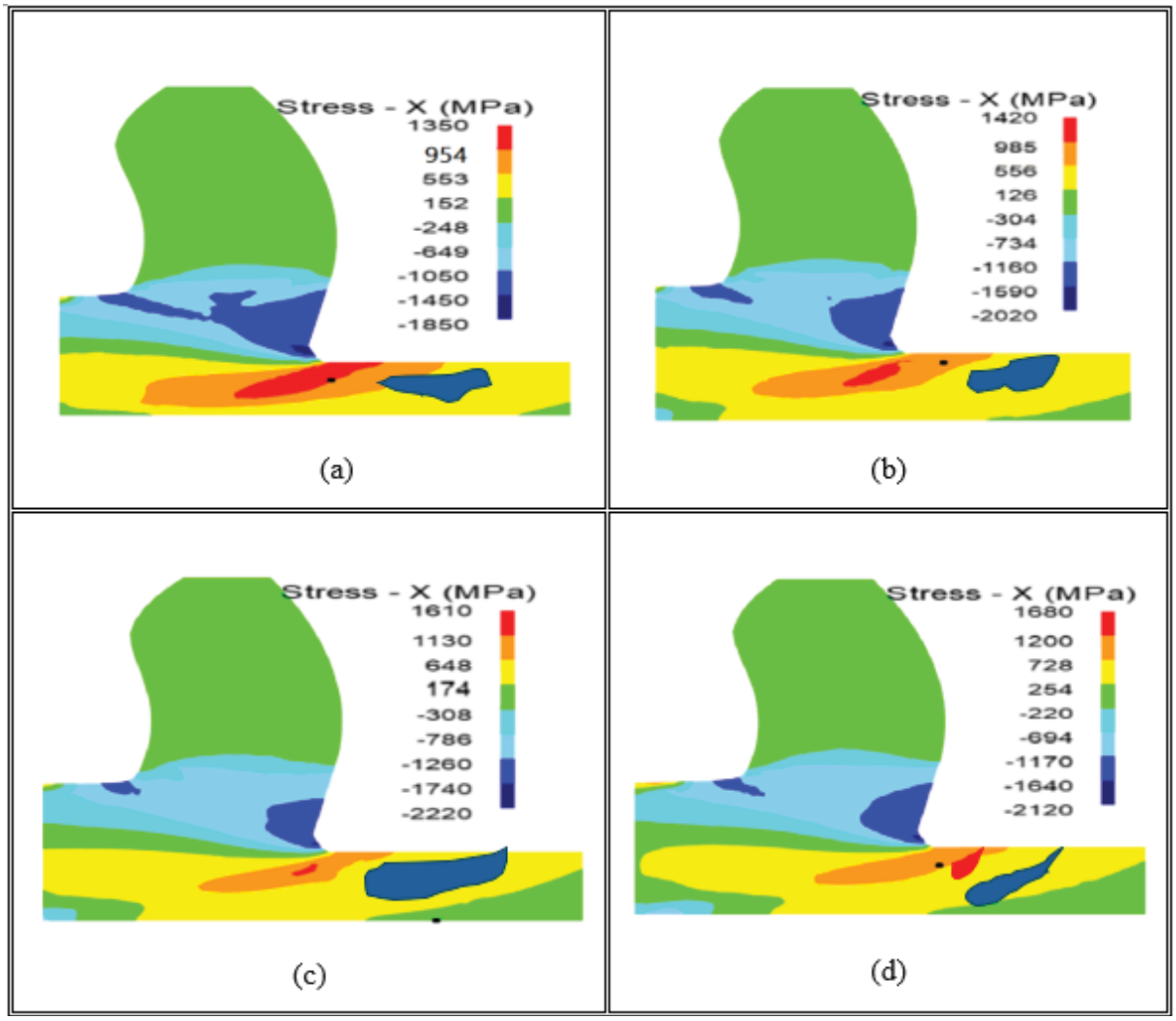

Figure 5.8 Distributions of residual stresses for different chamfer angles γ_n : a) 15˚, (b) 25˚, (c) 35˚, (d) 45˚

Figure 5.9 shows the distribution of the residual stresses obtained with different sharp angles at the same machining parameters of V = 200 m/min, f = 0.2 mm/rev, α = 15°. From Figure 5.9 It can been noted that the greater the sharp angle, the greater the residual stress generated. The maximum compressive stresses were developed in the rake face region, but the maximum tensile stresses were generated in the rankle areas.

No experimental data on residual stress was found in the literature for sharp edge tools. However, the response surface analysis that was performed later showed the increasing effects of the continuous parameter (sharp angle) on the residual stress values based on the fitted model.

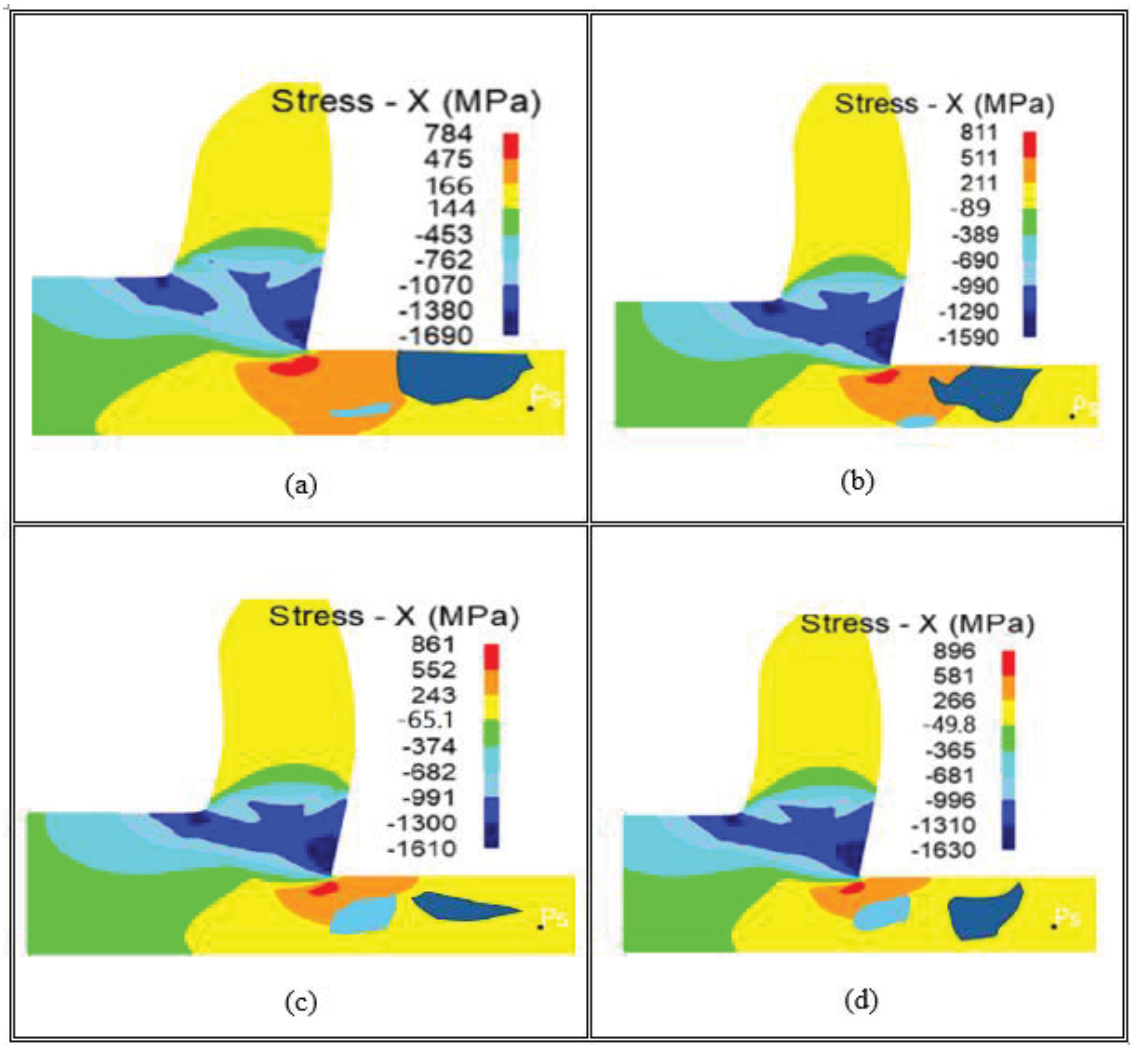

Figure 5.9 Distributions of residual stresses for different sharp angles γ_n : (a) 10°, (b) 15°, (c) 20°, (d) 25°

Figures 5.10, 5.11 and 5.12 show the distributions of cutting temperature for different edge radii, chamfer angles and sharp angles respectively at V = 200 m/min, f = 0.2 mm/rev and α =

15°. It can be observed from these figures that the cutting temperatures increase when the tool geometrical parameters (edge radius r_c, chamfer angle γ_n and sharp angle θ_t) respectively increase. These increases are approximately 2% in the range of 723 ± 13°C for the different tested parameter values. Moreover, the maximum temperatures were obtained in the rake face areas for all the studied cutting tool forms. The present results were discussed previously in other studies by the same authors (Zakaria et al., 2022). The numerical results of these works were validated experimentally in literature (Shnfir et al.,2019). For the residual stresses, the numerical results were validated by the experimental data.

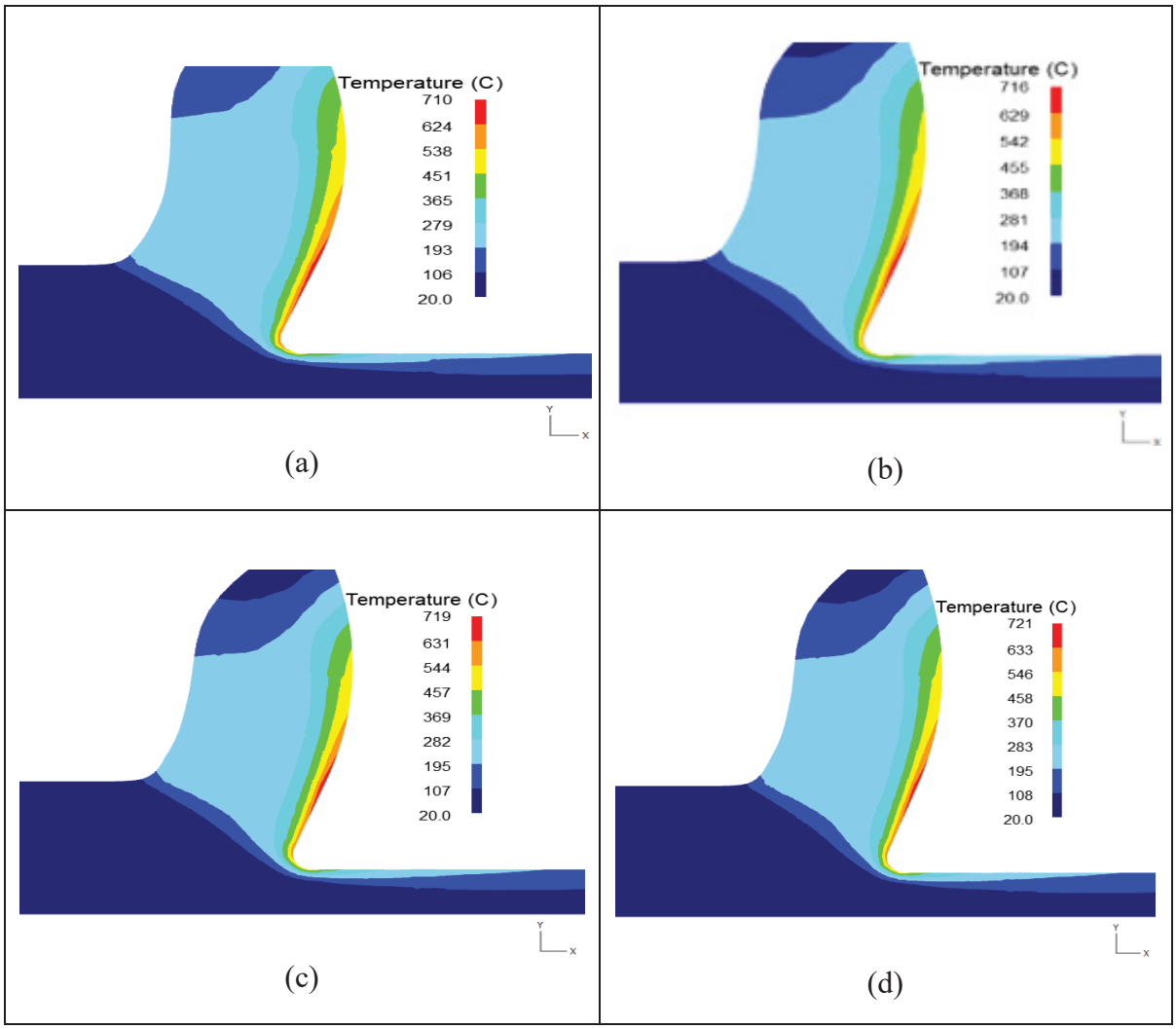

Figure 5.10 Distribution of cutting temperature for different tool edge radii:
(a) = 0.01 mm, (b) = 0.03 mm, (c) = 0.05 mm, (d) = 0.09

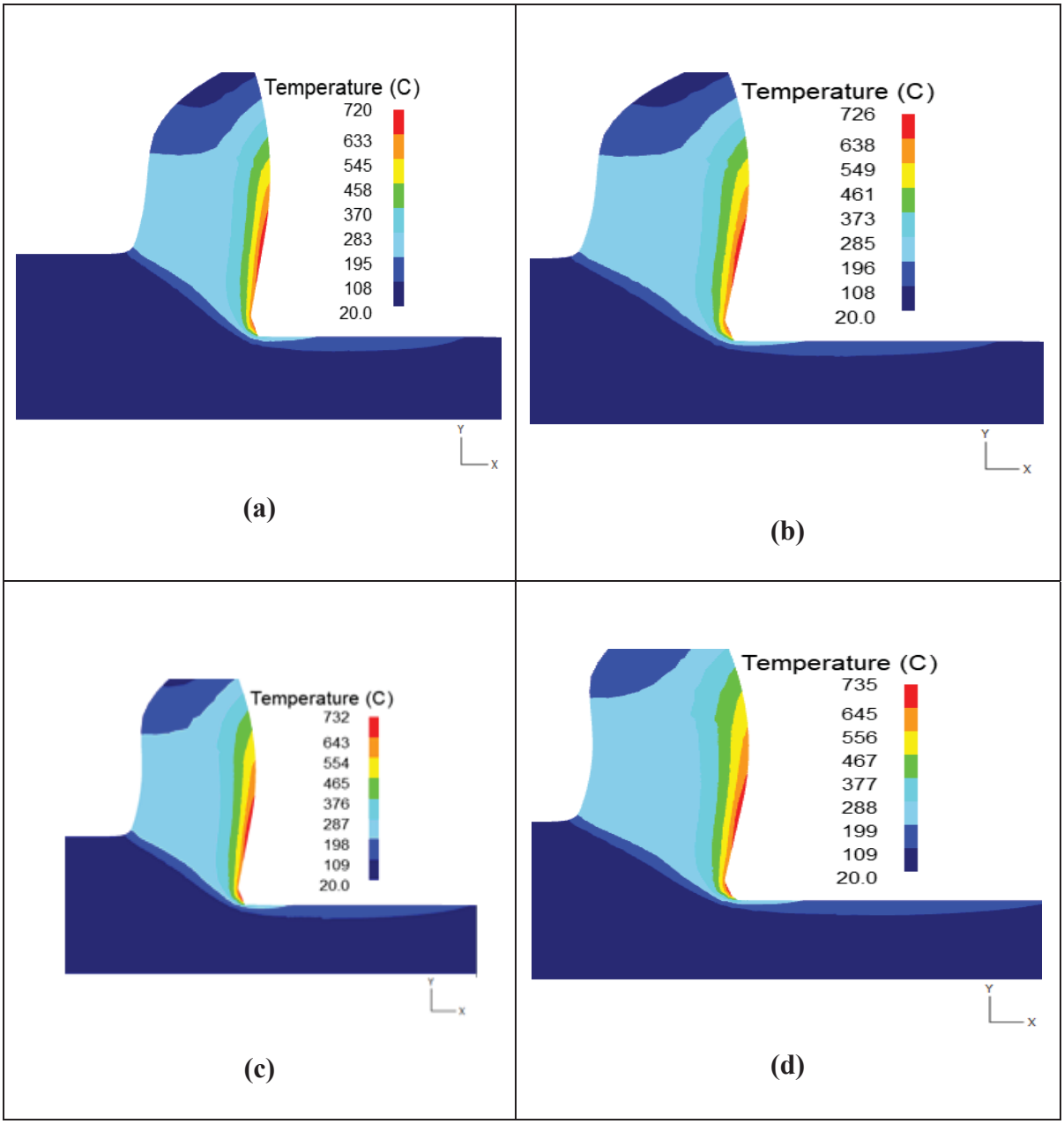

Figure 5.11 Distribution of cutting temperature for different chamfer angles γ_n: (a) 15˚, (b) 25˚, (c) 35˚, (d) 45˚

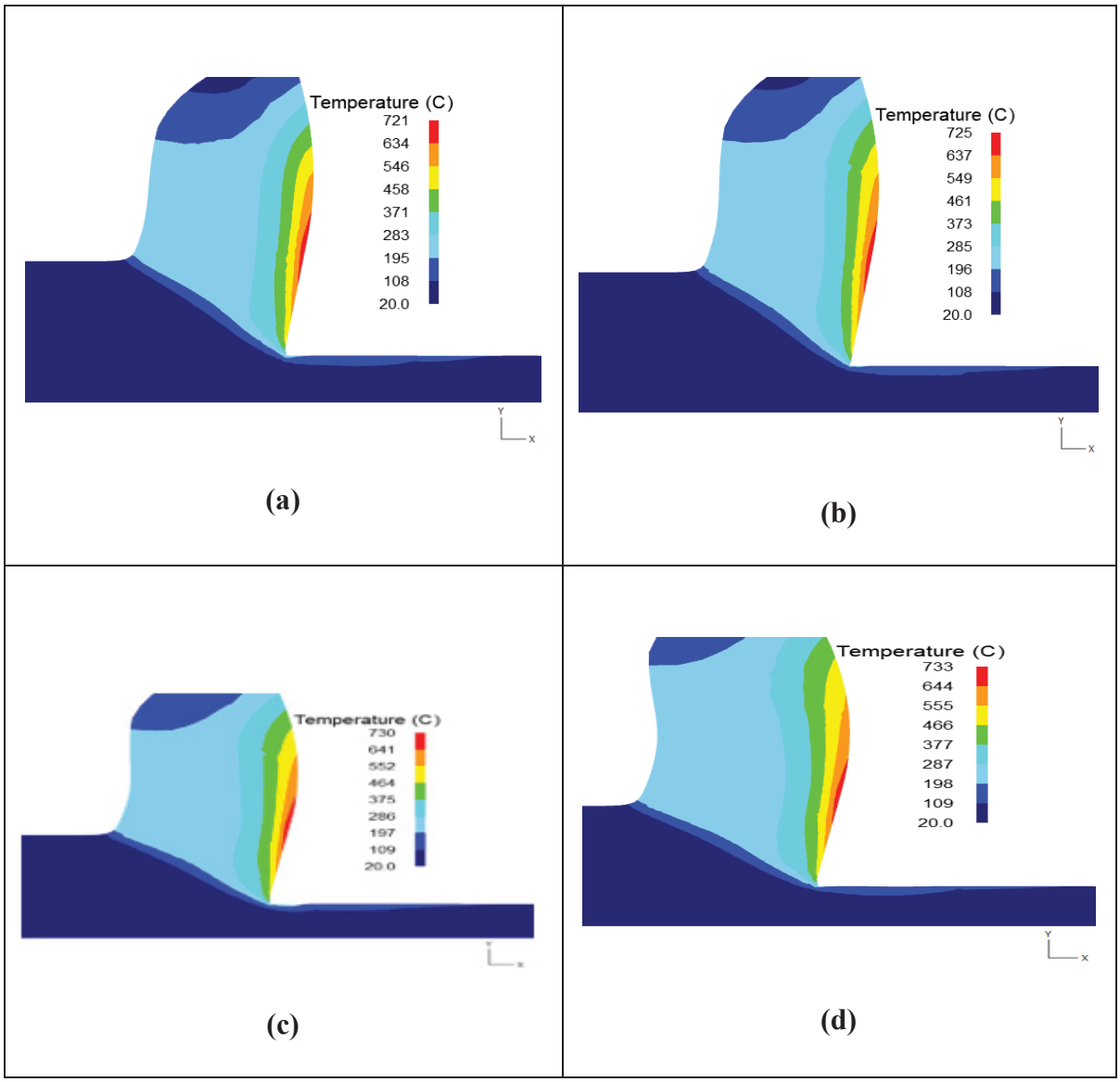

Figure 5.12 Distribution of cutting temperature for various sharp angles θ_t : (a) 35°, (b) 45°, (c) 55°, (d) 65°

5.2.4 Validation results

The obtained numerical results for round, chamfered and sharped tools were validated using the experimental data from literature (see Table 5.2). With respect to the properties obtained for orthogonal cutting of AISI 1045 steel, acceptable errors were found in terms of edge radius (r_c = 0.03mm), chamfer angle (γ_n = 35°) and sharp angle (θ_t = 25°) for cutting temperature, cutting stress, tool wear and residual stress. These errors approximately ranged between 5 to

8%, 2 to 8%, 6 to 16%, and 4 to 7%, for these four properties, respectively. The 16% error in tool wear width can be due to combination of mesh, the model, and convergence of the process simulation.

Table 5.2 Validation results for the round, chamfer and sharp tools.

	Numerical results (Tagiuri et al.)			**Experimental data** Same material properties			**Error %**		
Parameter	Edge radius (mm)	Chamfer angle (°)	Sharp angle (°)	Edge radius (mm)	Chamfer angle (°)	Sharp angle (°)	Edge radius (mm)	Chamfer angle (°)	Sharp angle (°)
Characteristics	0.03	35	25	0.025	35	25			
Cutting temperature (ºC) (Jacobus et al., 2000)	650	644	686	620	598	633	4.6%	7%	8 %
Cutting forces (N) (Altintas, 2000)	319	310	280	295	303	285	7.5 %	2 %	1.7%
Tool wear width (mm) (Jamel, 2012)	0.01	0.03	0.012	0.012	0.028	0.011	16%	6 %	8%
Residual stress Cutting (MPa) (Nasr, 2015)	1315	1312	1320	1260	1222	1243	4.18%	7%	5.8%

5.2.5 ANOVA and regression analysis

For the present study, the analysis of variance (ANOVA) was used to determine statistically significant cutting factors in relation to their effect on the dependent machining variables investigated, namely, temperature (T), cutting stress (σ), chip thickness (t_c) and tool wear depth (d_w). It involves examining the variability due to the difference of effects between various factors and their levels. The significance of the factors was determined through a comparison of their F-ratios with a *p*-value below 0.05 (95% confidence level). Only significant factors and their interactions were considered for establishing the empirical model.

To better comprehend the terms used in the tables provided in the ANOVA analysis of different variables discussed in this section, a brief terminology of these terms used in the tables presented will be appropriate. The term Variable refers to a property whose variation can be measured. Two types ae distinguished: Independent (X) and Dependent (Y) variables, where the latter depends on the former. Independent variables are selected or fixed by experimental design (DOE) which are hypothesized in a statistical model ($Y = X + \varepsilon$) capable of predicting their influence on the response variable(s). The hypothesis is then tested by calculating sums of squares to determine the variation in Y between levels of X, which exceeds the variation within the levels. An Error (ε in the statistical model) is the amount by which an observed variable differs from the value predicted by the model. The F-ratio is the statistic calculated by ANOVA which determines the significance of the hypothesis that Y depends on X. It is calculated as the ratio of the two mean squares MS[X] / MS[ε], and a large ratio indicates a significant effect of X. A critical value $p = 0.05$ is generally taken as marking an acceptable boundary of significance at a confidence interval of $\gtrsim$95%.

5.2.5.1 ANOVA for round tool geometry

From the DOE established previously for round tool geometry, three selected factors i.e., cutting speed (V), feed rate (f) and edge radius (r_c) with four levels each, were considered for the factorial design. The factorial design consisted of 64 tests with different non-randomized combinations between the factors. Table 5.3 presents the design matrix for the round geometry cutting tool.

Table 5.3 Design matrix for round geometry cutting tool

Factors	Level 1	Level 2	Level 3	Level 4
V: Cutting speed (m/min)	200	400	600	800
f: Feed rate (mm/rev)	0.15	0.2	0.25	0.3
r_c: Edge radius (mm)	0.03	0.05	0.07	0.09

The analysis of variance (ANOVA) results for cutting temperature, stress, chip thickness, wear depth and residual stress are displayed in Tables 5.4, 5.5, 5.6, 5.7 and 5.8, respectively, for the

round cutting tool. From the results obtained, it can be observed that the quadratic term of the cutting speed ($V * V$ or V^2) and the interaction between the speed and the feed rate ($V * f$) were the most significant terms affecting temperature. The ($V * V$) term has the greatest effect with an F-value of 25.77, followed by the interaction of cutting speed and feed rate ($V * f$) with its F-value of 14.14 (see Table 5.4). These terms were therefore selected for establishing the empirical model of the temperature. Furthermore, the cutting speed, the feed rate, the edge radius, and the interactions $V * r_c$, $f * f$, $f * r_c$ and $r_c * r_c$ were not significant, and were ignored in the model.

Table 5.4 Analysis of Variance (ANOVA) for Temperature, for Round Tool

Variable	SS	DF	MS	F-Ratio	*p*-Value
V: Cutting speed	4223.87	1	4223.87	0.28	0.5999
f: Feed rate	9654.06	1	9654.06	0.64	0.4285
r_c: Edge radius	1486.09	1	1486.09	0.10	0.7555
$V * V$	390953.	1	390953.	25.77	0.0000
$V * f$	219029.	1	219029.	14.44	0.0004
$V * r_c$	3869.9	1	3869.9	0.26	0.6156
$f * f$	27405.1	1	27405.1	1.81	0.1846
$f * r_c$	2624.67	1	2624.67	0.17	0.6791
$r_c * r_c$	2099.47	1	2099.47	0.14	0.7114
Error	819269.	54	15171.6		
Total	1480610	63			

For the stress, the cutting speed square term ($V * V$) displayed the highest F-value of 28.79, followed by cutting speed (V) with an F-value of 5.11 as seen from Table 5.5. These terms were then selected to establish the empirical model of the stress. Whereas, feed rate, edge radius, edge radius square and the interactions $V * r_c$, $f * f$, $f * r_c$ with no significant effects were removed.

For the chip thickness, and as may be seen from Table 5.6, the feed rate (f) was found to have the greatest effect, with an F-value of 30.35, followed by the edge radius (r_c) with an F-value of 8.89, and then by the edge radius square term ($r_c * r_c$) with its F-value of 7.39. These terms were selected to establish the empirical model for the chip thickness, while the other terms (V, $V * V$, $V * f$, $V * r_c$, $f * f$, $f * r_c$) being non-significant, were ignored in the development of the model.

Table 5.5 Analysis of Variance (ANOVA) for Stress, for Round tool

Source	SS	DF	MS	F-Ratio	*p*-Value
V: Cutting speed	25047.8	1	25047.8	5.11	0.0278
f: Feed rate	432.194	1	432.194	0.09	0.7677
r_c: Edge radius	1264.57	1	1264.57	0.26	0.6136
$V * V$	141157.	1	141157.	28.79	0.0000
$V * f$	2654.44	1	2654.44	0.54	0.4650
$V * r_c$	5.13816	1	5.13816	0.00	0.9743
$f * f$	28.0768	1	28.0768	0.01	0.9400
$f * r_c$	699.722	1	699.722	0.14	0.7071
$r_c * r_c$	131.36	1	131.36	0.03	0.8706
Error	264717.	54	4902.16		
Total	436137.	63			

SS: Sum of Squares; DF: Dependent variable level; MS: mean square

Table 5.6 Analysis of Variance (ANOVA) for Chip Thickness, for Round tool

Source	SS	DF	MS	F-Ratio	*p*-Value
V: Cutting speed	0.0	1	0.0	0.00	1.0000
f: Feed rate	11.7259	1	11.7259	30.35	0.0000
r_c: Edge radius	3.4362	1	3.4362	8.89	0.0043
$V * V$	3.05	1	0.0125	4.08	0.0570
$V * f$	2.08.	1	0.120	0.00	0.0870
$V * r_c$	4.1870	1	0.4870	0.00	0.784
$f * f$	0.009025	1	0.009025	0.02	0.8791
$f * r_c$	1.5021	1	1.5021	3.89	0.0538
$r_c * r_c$	2.8561	1	2.8561	7.39	0.0088
Error	20.8666	54	0.386419		
Total	40.396	63			

SS: Sum of Squares; DF: Dependent variable level; MS: mean square

For wear depth, the (cutting speed)^2 ($V*V$) was the most significant term with an F-value of 8.23, followed by the interaction ($V*f$) with its F-value of 4.39, as shown in Table 5.7. These terms were therefore selected to develop the empirical model of wear depth. The other factors ($V, f, r_c, f*f, r_c*r_c$, and the interactions $V*r_c, f*r_c$) being insignificant, were not considered in developing the empirical model.

Table 5.7 Analysis of Variance (ANOVA) for Wear Depth, for Round tool

Source	SS	DF	MS	F-Ratio	*p*-Value
V: Cutting speed	11.3289	1	11.3289	0.64	0.4273
f: Feed rate	0.0106953	1	0.0106953	0.00	0.9805
r_c: Edge radius	14.1078	1	14.1078	0.80	0.3760
$V * V$	145.655	1	145.655	8.23	0.0059
$V * f$	77.8233	1	77.8233	4.39	0.0407
$V * r_c$	0.0514156	1	0.0514156	0.00	0.9572
$f * f$	3.63379	1	3.63379	0.21	0.6524
$f * r_c$	7.57488	1	7.57488	0.43	0.5159
$r_c * r_c$	44.6391	1	44.6391	2.52	0.1182
Error	956.226	54	17.7079		
Total	1261.05	63			

SS: Sum of Squares; DF: Dependent variable level; MS: mean square

For residual stress, the ($V * V$) term displayed the highest F-value i.e., 25.77, followed by the interaction ($V * f$) with an F-value of 14.44, and the feed rate f (F-value of 0.64), as seen from Table 5.8. These terms were then selected to establish the empirical model of residual stress, while all other terms were neglected.

Table 5.8 Analysis of Variance (ANOVA) for Residual Stress, for Round tool

Source	SS	DF	MS	F-Ratio	*p*-Value
V: Cutting speed	2368.06	1	4189.01	0.28	0.5492
f: Feed rate	9654.06	1	9654.06	0.64	0.0000
r_c: Edge radius	1786.42	1	1789.42	0.10	0.7555
$V * V$	390953.	1	390953.	25.77	0.0000
$V * f$	229029.1	1	229029.1	14.44	0.0004
$V * r_c$	2674.89	1	3869.9	0.26	0.5156
$f * f$	29405.1	1	29405.1	1.81	0.1685
$f * r_c$	2624.67	1	2624.67	0.17	0.6791
$r_c * r_c$	2099.47	1	2099.47	0.14	0.9261
Error	819269.	54	16172.36		
Total	1480610	63			

SS: Sum of Squares; DF: Dependent variable level; MS: mean square

Figure 5.13 presents the Pareto diagram showing graphically the effects of the three parameters (cutting speed, feed rate and edge radius, and their interactions) on the temperature, stress, chip thickness and wear depth as investigated for the round cutting tool. It can be observed from Figure 5.13 that, with the exception of the interaction between feed rate and edge radius ($f * r_c$), which has a significant effect on chip thickness, the cutting speed square term parameter ($V * V$) had the greatest influence on temperature, stress and wear depth when using the round cutting tool.

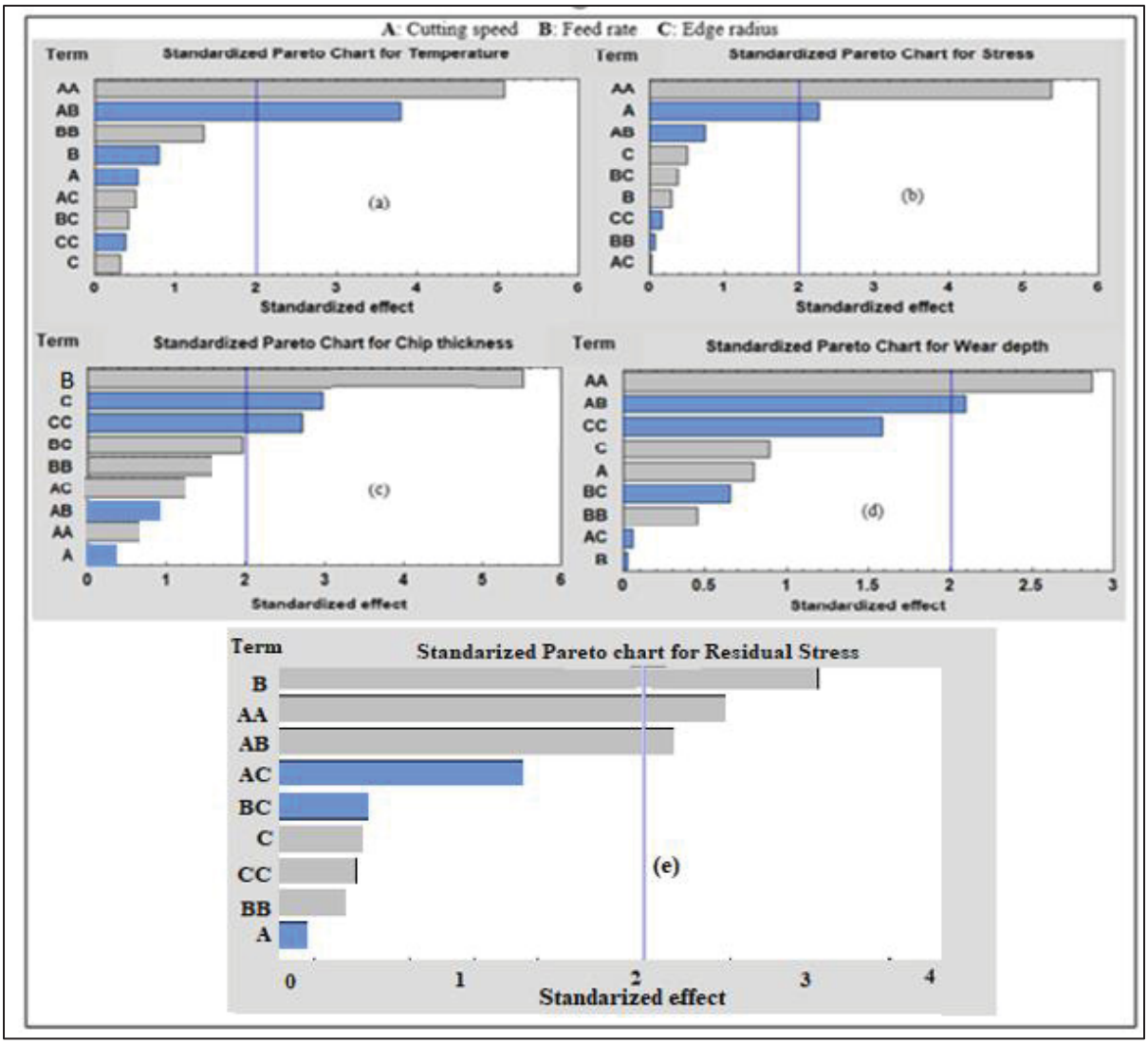

Figure 5.13 Pareto diagram of standardized effects for cutting round tool: (a) temperature; (b) effective stress; (c) chip thickness ;(d) wear depth ; and (e) residual stress

5.2.5.2 ANOVA

5.2.5.3 for chamfer tool geometry

For chamfer tool geometry, four selected factors, namely, cutting speed (V), feed rate (f), chamfer width (w_n) and chamfer angle (γ_n) with four levels each were used to design the matrix. The factorial design consists of 70 tests (where the 256 test combinations were reduced using

the Statgraphics program with different nonrandomized combinations between the factors. Table 5.9 presents the design matrix for the chamfer geometry-cutting tool.

Table 5.9 Design matrix for chamfer geometry cutting tool.

Factors	Level 1	Level 2	Level 3	Level 4
V: Cutting speed (m/min)	150	350	650	950
f: Feed rate (mm/rev)	0.15	0.2	0.25	0.3
w_n: Chamfer width (mm)	0.15	0.25	0.35	0.45
γ_n: Chamfer angle (º)	10	20	30	40

The analysis of variance (ANOVA) data obtained for cutting temperature, stress, chip thickness, wear depth and residual stress are shown in Tables 5.10, 5.11, 5.12, 5.13 and 5.14, respectively, for the chamfered cutting tool. From the results displayed in these tables, it may be noted that the cutting speed *V* appears to be the most influential parameter affecting the five dependent variables studied; the cutting speed square term (*V* * *V*) also appears to be a parameter of significant influence in four of these cases, with the exception of the chip thickness (Table 5.12), where the chamfer angle, γ_n , has the greatest influence on the chip thickness (given its *p*-value of 0.0001), followed by the (γ_n * γ_n) term, and then the cutting speed with a *p*-value of 0.0498 - barely within the limit of < 0.05. With respect to the temperature variable, a third factor, namely, the (γ_n * γ_n) term, is also influential, although its F-ratio is roughly half that of those for the *V* and (*V* * *V*) terms, while their p-values are all 0.0000. This is to be expected, as the temperature would be affected by the cutting speed and the chamfer angle simultaneously, since both would create friction in the work piece, which would increase its temperature.

Table 5.10 Analysis of Variance (ANOVA) for Temperature, for Chamfered Tool

Source	SS	DF	MS	F-Ratio	*p*-Value
V: Cutting speed	663363.	1	663363.	52.58	0.0000
f: Feed rate	363.221	1	363.221	0.03	0.8659
w_n: Chamfer width	708.321	1	708.321	0.06	0.8136
γ_n: Chamfer angle	37290.5	1	37290.5	2.96	0.0912
$V * V$	697341.	1	697341.	55.27	0.0000
$V * f$	3363.71	1	3363.71	0.27	0.6077
$V * w_n$	1631.02	1	1631.02	0.13	0.7206
$V * \gamma_n$	38811.7	1	38811.7	3.08	0.0850
$f * f$	59.7438	1	59.7438	0.00	0.9454
$f * w_n$	1913.67	1	1913.67	0.15	0.6984
$f * \gamma_n$	117.306	1	117.306	0.01	0.9235
$w_n * w_n$	50.2538	1	50.2538	0.00	0.9499
$w_n * \gamma_n$	424.748	1	424.748	0.03	0.8551
$\gamma_n * \gamma_n$	327231.	1	327231.	25.94	0.0000
Error	693915.	55	12616.6		
Total	2364800	69			

For the influence on the Stress parameter, as in the analysis of variance for the Temperature parameter (see Table 5.10), the Stress parameter is only affected by the cutting speed factors, V and ($V * V$), as seen from Table 5.11, and the chamfer angle has no influence upon or contribution to the stress.

Table 5.11 Analysis of Variance (ANOVA) for Stress, for Chamfered Tool

Source	SS	DF	MS	F-Ratio	*p*-Value
V: Cutting speed	252942.	1	252942.	194.22	0.0000
f: Feed rate	75.4921	1	75.4921	0.06	0.8106
w_n: Chamfer width	91.6302	1	91.6302	0.07	0.7918
γ_n: Chamfer angle	229.074	1	229.074	0.18	0.6766
V * *V*	136908.	1	136908.	105.12	0.0000
V * *f*	101.983	1	101.983	0.08	0.7807
V * w_n	75.4338	1	75.4338	0.06	0.8107
V * γ_n	693.939	1	693.939	0.53	0.4685
f * *f*	33.3928	1	33.3928	0.03	0.8734
f * w_n	340.284	1	340.284	0.26	0.6113
f * γ_n	10.8038	1	10.8038	0.01	0.9278
w_n * w_n	164.876	1	164.876	0.13	0.7233
w_n * γ_n	47.7067	1	47.7067	0.04	0.8489
γ_n * γ_n	3388.08	1	3388.08	2.60	0.1125
Error	71629.2	55	1302.35		
Total	444895.	69			

Moreover, as was mentioned earlier in an overall comparison of Tables 5.10 to 5.14, the chamfer angle, γ_n , had the greatest influence on the chip thickness with its *p*-value of 0.0001. This was followed by the (γ_n * γ_n) term, with a *p*-value of 0.0350, and then the cutting speed with a *p*-value of 0.0498, just within the acceptable limit criterion of < 0.05, as seen from Table 5.12. The F-ratios in the latter two cases are also similar, compared to the F-ratio (17.74) for the chamfer angle. By way of recapitulating, the F-ratio, which is the ratio of average variance between groups to that within groups, tells how much of a difference in the dependent variable there is between the groups. It can be statistically tested, and the p-value tells whether the F-ratio is statistically significant. If the p-value is less than the significance level, then this means that the sample data provides sufficient evidence that the regression model used fits the data better than a model with no independent variables. In other words, the independent variables proposed in the model improve the fit of the model.

Table 5.12 Analysis of Variance (ANOVA) for Chip thickness, for Chamfered Tool

Source	SS	DF	MS	F-Ratio	*p*-Value
V: Cutting speed	1.96914	1	1.96914	4.03	0.0498
f: Feed rate	0.0109061	1	0.0109061	0.02	0.8819
w_n: Chamfer width	0.178563	1	0.178563	0.36	0.5482
γ_n: Chamfer angle	8.67813	1	8.67813	17.74	0.0001
$V * V$	0.330884	1	0.330884	0.68	0.4144
$V * f$	0.00289092	1	0.00289092	0.01	0.9390
$V * w_n$	0.00552097	1	0.00552097	0.01	0.9158
$V * \gamma_n$	1.8796	1	1.8796	3.84	0.0551
$f * f$	0.0726436	1	0.0726436	0.15	0.7015
$f * w_n$	0.151439	1	0.151439	0.31	0.5802
$f * \gamma_n$	0.0189694	1	0.0189694	0.04	0.8446
$w_n * w_n$	0.098783	1	0.098783	0.20	0.6549
$w_n * \gamma_n$	0.0298254	1	0.0298254	0.06	0.8059
$\gamma_n * \gamma_n$	2.28565	1	2.28565	4.67	0.0350
Error	26.9071	55	0.48922		
Total	42.0653	69			

In the analysis of variance for the Wear depth dependent variable, for the chamfered tool, as shown in Table 5.13, the cutting speed (V), and the square of the chamfer angle term ($\boldsymbol{\gamma}_n * \boldsymbol{\gamma}_n$) have a considerable influence on the wear depth, as noted from their *p*-values. Of particular note is the very high F-ratio for the ($\boldsymbol{\gamma}_n * \boldsymbol{\gamma}_n$) term, which, together with its p-value of 0.0000, signifies its dominant influence on the wear depth.

Table 5.13 Analysis of Variance (ANOVA) for Wear Depth, for Chamfered Tool

Source	SS	DF	MS	F-Ratio	*p*-Value
V: Cutting speed	51.9268	1	51.9268	7.83	0.0071
f: Feed rate	0.0071101	1	0.0071101	0.00	0.9740
w_n: Chamfer width	0.000123539	1	0.000123539	0.00	0.9966
γ_n: Chamfer angle	46.9292	1	46.9292	7.07	0.0102
V * *V*	29.9346	1	29.9346	4.51	0.0382
V * *f*	0.0546841	1	0.0546841	0.01	0.9280
V * w_n	0.0525852	1	0.0525852	0.01	0.9294
V * γ_n	0.404875	1	0.404875	0.06	0.8058
f * *f*	0.000138196	1	0.000138196	0.00	0.9964
f * w_n	0.000801701	1	0.000801701	0.00	0.9913
f * γ_n	0.016715	1	0.016715	0.00	0.9601
w_n * w_n	0.0135079	1	0.0135079	0.00	0.9642
w_n * γ_n	0.0823197	1	0.0823197	0.01	0.9117
γ_n * γ_n	2257.11	1	2257.11	340.22	0.0000
Error	364.882	55	6.63423		
Total	2743.45	69			

From the analysis of variance for the Residual Stress for the chamfered tool, presented in Table 5.14, the cutting speed (V) and feed rate (f) have the greatest influence on the residual stress as evidenced from their high F-ratios and p-values of 0.0000. The next influential parameter is the (*V* * *V*) term with the same *p*-value of 0.0000 but an F-ratio that is roughly half that of the former two terms. The last factor which has some influence on the residual stress is the (*V* * *f*) term since its *p*-value of 0.0198 falls within the acceptable limit; however, the F-ratio is much lower in this case, i.e., 5.99. None of the other terms have any influence on the residual stress and were therefore not considered when developing the model for the residual stress,

Table 5.14 Analysis of Variance (ANOVA) for Residual Stress, for Chamfered Tool

Source	SS	DF	MS	F-Ratio	*p*-Value
V: Cutting speed	1804.76	1	1804.76	58.55	0.0000
f: Feed rate	1859.49	1	1859.49	60.32	0.0000
w_n: Chamfer width	0.474526	1	0.474526	0.02	0.9020
γ_n: Chamfer angle	2.31504	1	2.31504	0.08	0.7858
$V * V$	999.188	1	999.188	32.41	0.0000
$V * f$	184.749	1	184.749	5.99	0.0198
$V * w_n$	2.94233	1	2.94233	0.10	0.7593
$V * \gamma_n$	6.75669	1	6.75669	0.22	0.6427
$f * f$	38.4905	1	38.4905	1.25	0.2719
$f * w_n$	0.109204	1	0.109204	0.00	0.9529
$f * \gamma_n$	2.89709	1	2.89709	0.09	0.7611
$w_n * w_n$	30.4007	1	30.4007	0.99	0.3279
$w_n * \gamma_n$	8.50885	1	8.50885	0.28	0.6028
$\gamma_n * \gamma_n$	6.9942	1	6.9942	0.23	0.6370
Error	1017.25	33	30.8257		
Total	5982.48	47			

Figure 5.14 presents the Pareto diagram showing a graphic representation of the effects of the four parameters viz., cutting speed, feed rate, chamfer width and chamfer angle, and their interactions on the temperature, stress, chip thickness, wear depth and residual stress for the chamfer cutting tool. It may be seen from Figure 5.14 that the cutting speed, V, the cutting speed square term ($V * V$), the chamfer angle, γ_n , and the chamfer angle square term ($\gamma_n * \gamma_n$) were the most effective terms that influenced stress, temperature, chip thickness, wear depth, and residual stress, respectively, when employing the chamfer cutting tool.

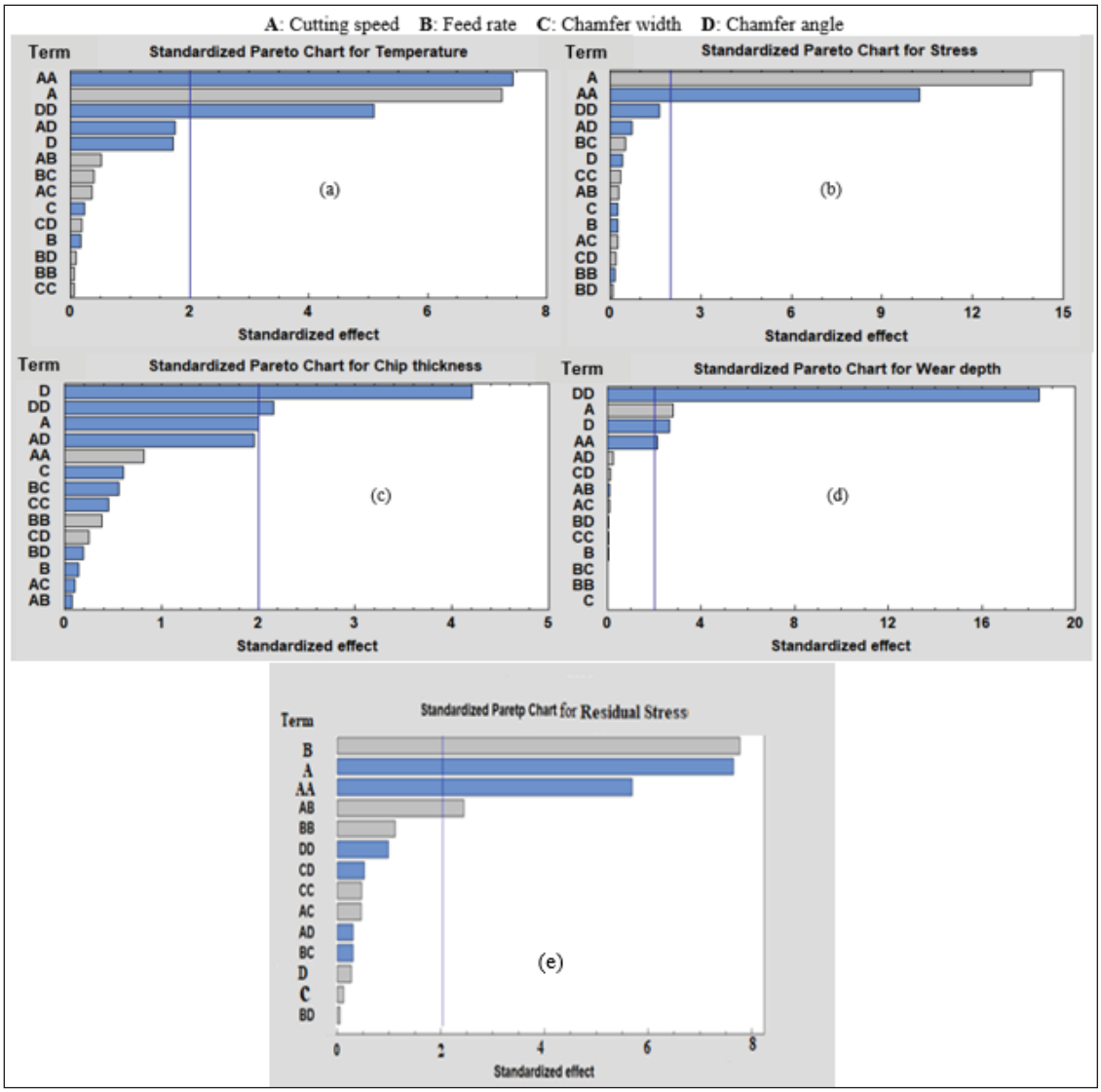

Figure 5.14 Pareto diagrams of standardized effects for chamfer cutting tool: (a) temperature (b) effective stress (c) chip thickness (d) wear depth (e) residual stress.

5.2.5.4 ANOVA for sharp tool geometry

For sharp tool geometry, the three selected factors (cutting speed (V), feed rate (f) and sharp angle (θ_n) had four levels each. The factorial design consists of 40 tests with different nonrandomized combinations between the factors. These factors were representative for obtaining accurate results. Tables 5.15 presents the design matrix for sharp geometry cutting tool.

Table 5.15 Design matrix for sharp geometry cutting tool

Factors	Level 1	Level 2	Level 3	Level 4
V: Cutting speed (m/min)	250	350	750	1000
f: Feed rate (mm/rev)	0.1	0.15	0.25	0.3
θ_n: Sharp angle (º)	30	40	50	60

The analysis of variance (ANOVA) of cutting temperature, stress, chip thickness, wear depth and residual stress are displayed in Tables 5.16, 5.17, 5.18, 5.19 and 5.20, respectively, for the sharp cutting tool. From the obtained results of ANOVA, it can be seen that the feed rate, f, and the cutting speed square term ($V * V$) were the two commonly observed main significant factors influencing temperature, stress, wear depth and residual stress, the only exception being the chip thickness, which was influenced solely by the cutting speed, V. These significant factors all had p-values less than 5%. In the case of the residual stress, in addition to the feed rate, f, the cutting speed square term ($V * V$), the cutting speed, V, a fourth significant factor, the ($V * f$) was also found to have a significant influence on the residual stress.

For the temperature, the feed rate has the strongest influence with a high F-ratio of 20.96, followed by the cutting speed square term ($V * V$) with an F-value of 5.06, as may be seen from Table 5.16. These terms were therefore selected to develop the empirical model for predicting the temperature. The other factors in the table, i.e., cutting speed, sharp angle and the interactions ($V * f$), ($V * \theta_n$), ($f * f$), ($f * \theta_n$) and ($\theta_n * \theta_n$) were not significant and so were ignored in the development of the model.

For the stress, the cutting speed square term ($V * V$) also has the greatest effect with an F-ratio of 9.45 and p-value of 0.0045, followed by the feed rate with an F-value of 4.28 and a p-value of 0.0472, as observed from Table 5.17. Therefore, these terms were considered for establishing the empirical model for stress. The remaining factors revealed no significance and were therefore discarded.

Table 5.16 Analysis of Variance (ANOVA) for Temperature for Sharp Tool

Source	SS	DF	MS	F-Ratio	*p*-Value
V: Cutting speed	2526.08	1	2526.08	1.71	0.2009
f: Feed rate	30971.1	1	30971.1	20.96	0.0001
θ_n: Sharp angle	475.643	1	475.643	0.32	0.5746
$V * V$	7473.4	1	7473.4	5.06	0.0320
$V * f$	506.853	1	506.853	0.34	0.5624
$V * \theta_n$	167.229	1	167.229	0.11	0.7389
$f * f$	2020.9	1	2020.9	1.37	0.2514
$f * \theta_n$	558.348	1	558.348	0.38	0.5433
$\theta_n * \theta_n$	147.411	1	147.411	0.10	0.7543
Error	44318.5	30	1477.28		
Total	89142.8	39			

Table 5.17 Analysis of Variance (ANOVA) for Stress, for Sharp Tool

Source	SS	DF	MS	F-Ratio	*p*-Value
V: Cutting speed	10161.4	1	10161.4	1.82	0.1875
f: Feed rate	23925.0	1	23925.0	4.28	0.0472
θ_n: Sharp angle	1302.55	1	1302.55	0.23	0.6327
$V * V$	52766.6	1	52766.6	9.45	0.0045
$V * f$	12235.8	1	12235.8	2.19	0.1493
$V * \theta_n$	5192.99	1	5192.99	0.93	0.3427
$f * f$	2583.51	1	2583.51	0.46	0.5017
$f * \theta_n$	22690.3	1	22690.3	4.06	0.0529
$\theta_n * \theta_n$	83.3739	1	83.3739	0.01	0.9036
Error	167581.	30	5586.03		
Total	320361.	39			

Table 5.18 reveals that only the cutting speed, V, has a significant influence on the chip thickness, with an F-ratio of 9.19 and a *p*-value of 0.0050. Thus, only this factor was considered

in developing the empirical model for chip thickness. All the other factors, viz., feed rate, sharp angle the interactions ($V*V$),($V*f$), ($V*\theta_n$), ($f*f$), ($f*\theta_n$) and ($\theta_n*\theta_n$) showed no significance and were not used in the development of the model.

Table 5.18 Analysis of Variance (ANOVA) for Chip thickness for sharp tool

Source	SS	DF	MS	F-Ratio	*p*-Value
V: Cutting speed	5.47631	1	5.47631	9.19	0.0050
f: Feed rate	0.484156	1	0.484156	0.81	0.3745
θ_n: Sharp angle	1.09896	1	1.09896	1.84	0.1845
$V * V$	0.134288	1	0.134288	0.23	0.6384
$V * f$	0.0320468	1	0.0320468	0.05	0.8182
$V * \theta_n$	0.292269	1	0.292269	0.49	0.4890
$f * f$	0.383508	1	0.383508	0.64	0.4286
$f * \theta_n$	0.854719	1	0.854719	1.43	0.2404
$\theta_n * \theta_n$	0.0635705	1	0.0635705	0.11	0.7462
Error	17.8706	30	0.595688		
Total	25.8474	39			

For wear depth, as Table 5.19 shows, the feed rate had the most significant effect on the wear depth, having an F-ratio of 20.78 and *p*-value of 0.0001, followed by the cutting speed square term ($V * V$), which exhibited an F-value of 5.82 (*p*-value 0.0221). These two terms were therefore used to develop the empirical model for wear depth. The other terms such as cutting speed, sharp angle and the interactions $V * f$, $V * \theta_n$, $f * f$, $f * \theta_n$ and $\theta_n * \theta_n$ were not significant and so were not considered in the development of the model.

Once again, it is interesting to note here, also, how a lower F-ratio increases the *p*-value to a level that approaches the acceptable limit of < 0.5, indicating the importance of the F-ratio in determining the influence of a specific parameter on the dependent variable being studied.

Table 5.19 Analysis of Variance (ANOVA) for Wear Depth for Sharp Tool

Source	SS	DF	MS	F-Ratio	*p*-Value
V: Cutting speed	0.00409301	1	0.00409301	0.00	0.9640
f: Feed rate	41.1318	1	41.1318	20.78	0.0001
θ_n: Sharp angle	3.79689	1	3.79689	1.92	0.1763
$V * V$	11.5271	1	11.5271	5.82	0.0221
$V * f$	2.49616	1	2.49616	1.26	0.2703
$V * \theta_n$	0.0076036	1	0.0076036	0.00	0.9510
$f * f$	1.62586	1	1.62586	0.82	0.3720
$f * \theta_n$	0.058184	1	0.058184	0.03	0.8650
$\theta_n * \theta_n$	3.0074	1	3.0074	1.52	0.2273
Error	59.38	30	1.97933		
Total	130.972	39			

The ANOVA results obtained for the residual stress reveal that four of the factors considered have a significant influence on this parameter, with three of them having p-values of 0.00001, and the fourth, a p-value of 0.0170. The feed rate has the greatest influence, with an F-ratio of 65.33, followed closely by the cutting speed with an F-value of 63.37, then by the cutting speed square term ($V * V$) with an F-value of 35.08, and lastly, by the interaction term ($V * f$), with a much lower F-ratio of 6.24. These four terms were therefore selected to develop the empirical model. Whereas the other terms were neglected since they were not significant, as seen from Table 5.20.

Table 5.20 Analysis of Variance (ANOVA) for Residual Stress for Sharp Tool

Source	SS	DF	MS	F-Ratio	*p*-Value
V: Cutting speed	1804.76	1	1804.76	63.37	0.0000
f: Feed rate	1860.5	1	1860.5	65.33	0.0000
θ_n: Sharp angle	0.204167	1	0.204167	0.01	0.9330
$V * V$	999.188	1	999.188	35.08	0.0000
$V * f$	177.625	1	177.625	6.24	0.0170
$V * \theta_n$	12.6737	1	12.6737	0.45	0.5087
$f * f$	42.6667	1	42.6667	1.50	0.2285
$f * \theta_n$	0.1	1	0.1	0.00	0.9531
$\theta_n * \theta_n$	2.52083	1	2.52083	0.09	0.7677
Error	1082.24	38	28.4801		
Total	5982.48	47			

Figure 5.15 illustrates the Pareto diagram showing the effects of the three parameters (cutting speed, feed rate and sharp angle) and their interactions on the temperature, stress, chip thickness, wear depth and residual stress for the sharp cutting tool. It can be seen from Figure 5.15 that the feed rate, the cutting speed, and the cutting speed square term ($V * V$) were the most effective factors with respect to temperature and wear depth, chip thickness, and stress, respectively, for the sharp cutting tool.

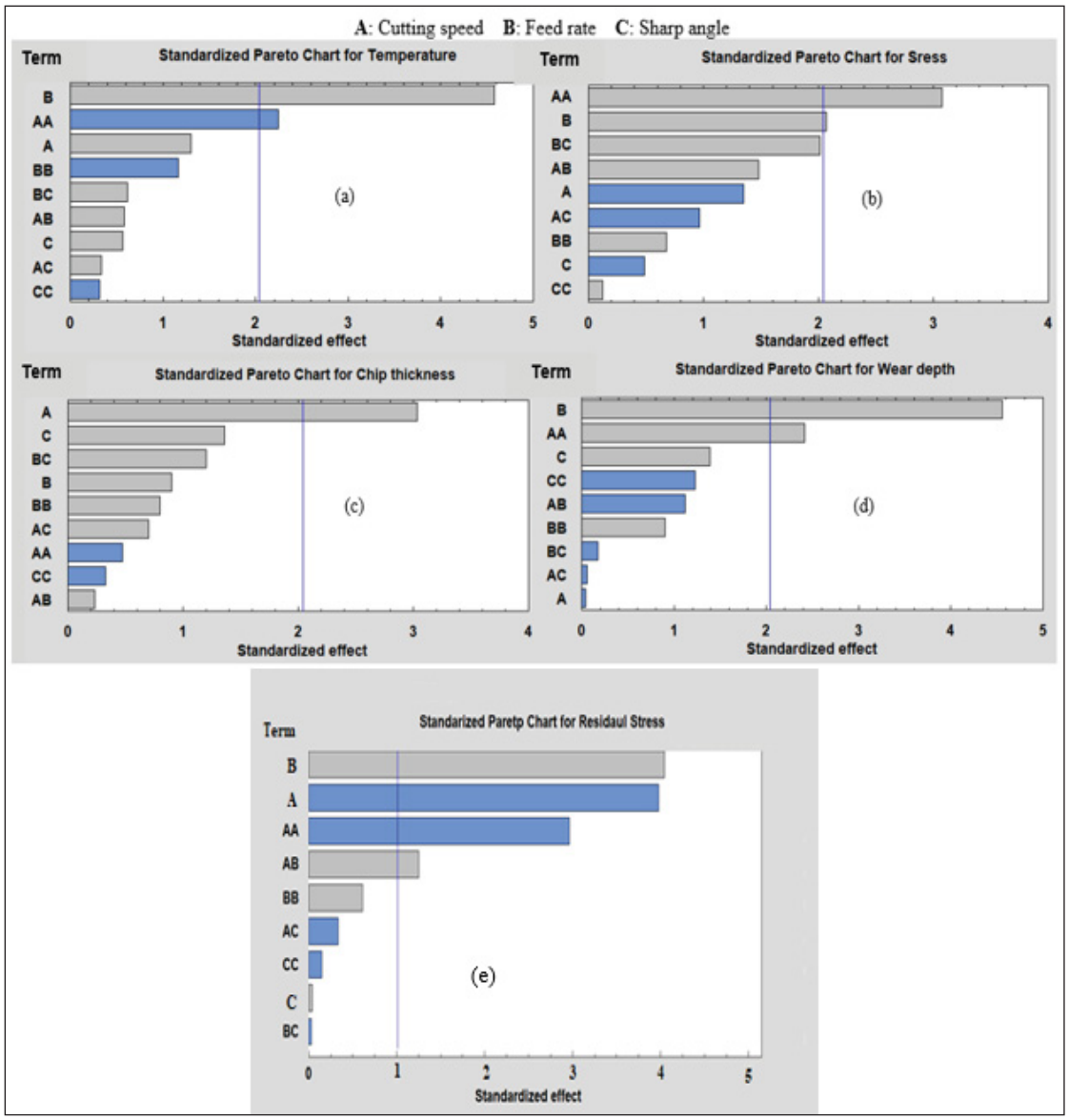

Figure 5.15 Pareto diagram of standardized effects for sharp cutting tool:
(a) temperature (b) effective stress (c) chip thickness (d) wear depth (e) residual stress

The ANOVA results obtained above may be summarized in terms of the important factors influencing the tested machining characteristics, namely, cutting temperature, effective stress, chip thickness, wear depth, and residual stress for the three different cutting tool designs studied. Table 5.21 presents the main parameters influencing the cutting process performance for each tool edge preparation.

Table 5.21 Summary of main parameters influencing the cutting process performance for each tool edge preparation

Process Performance Parameter	Round edge tool	Chamfered edge tool	Sharp edge tool
Cutting temperature	V^2 $(V \times f)$	V^2 V γ_n^2	f V^2
Cutting stress	V^2 V	V V^2	V^2 f
Deformed chip thickness	f r_c r_c^2	V γ_n γ_n^2	V
Tool wear depth	V^2 $(V \times f)$	γ_n γ_n^2 V V^2	f V^2
Residual stress	V^2 $(V \times f)$ f	f V V^2 $(V \times f)$	f V V^2 $(V \times f)$

The results obtained from the ANOVA tests may then expressed through mathematical and statistical equations using regression models to establish response functions fitting the available data. The following empirical models were obtained from statistical analysis:

For the round cutting tool, the regression equations for temperature and stress, chip thickness, wear depth, residual stress are presented in Equations (5.1), (5.2), (5.3), (5.4), and (5.5).

- Temperature = $64.07\ V^2 + 0.184\ Vf$ (5.1)
  $R^2 = 93\%$ R^2 Adjusted = 91%

- Stress = $0.24\ V - 75.63\ V^2$ (5.2)
  $R^2 = 92\ \%$ R^2 Adjusted = 90 %

- Chip Thickness = $14.04\ f - 0.0046\ r_c + 5.55\ r_c^2$ (5.3)
  $R^2 = 96.75\%$ R^2 Adjusted = 95%

- Wear Depth = $81.72\ V^2 + 22.07\ Vf$ (5.4)
  $R^2 = 92\ \%$ R^2 Adjusted = 91%

- Residual Stress = $71.85\ f + 72.84\ V^2 + 0.175\ V$
  $R^2 = 93\ \%$ R^2 Adjusted = 91% (5.5)

For the chamfer cutting tool, the regression equations for temperature, stress, chip thickness, wear depth, and residual stress are presented in Equations (5.6), (5.7), (5.8), (5.9) , and (5.10).

- Temperature = $1.65\ V + 2206.19\ f + 76.95\ V^2 - 4.920\ Vf$ (5.6)
  $R^2 = 96\ \%$ R^2 Adjusted = 94%

- Stress = $3.08\ V + 61.09\ V^2$ (5.7)
  $R^2 = 96\ \%$ R^2 Adjusted = 95%

- Chip Thickness = $0.029\ V - 0.0052\ \gamma_n + 3.048\ \gamma_n^2$ (5.8)
  $R^2 = 96\%$ R^2 Adjusted = 94%

- Wear Depth = $0.025\ V - 76.95\ V^2 + 0.0012\ \gamma_n + 2.051\gamma_n^2$ (5.9)
  $R^2 = 97\%$ R^2 Adjusted = 96%

- Residual Stress = $0.122\ V + 77.08\ f - 0.18\ Vf + 82.93\ V^2$ (5.10)
  $R^2 = 97\%$ R^2 Adjusted = 95%

For the sharp cutting tool, the regression equations for temperature, stress, chip thickness, wear depth, and residual stress are presented in Equations (5.11), (5.12), (5.13) ,(5.14), and (5.15)

- Temperature = $47.05\ f + 81.05 V^2$ (5.11)
  $R^2 = 94\%$ R^2 Adjusted = 93%

- Stress = $73.08\ V^2 + 2202.74\ f$ (5.12)
  $R^2 = 92\ \%$ R^2 Adjusted = 91%

- Chip Thickness = $0.025\ V$ (5.13)
  $R^2 = 93\%$ R^2 Adjusted = 92%

- Wear Depth = $35.85\ f + 84.32\ V^2$ (5.14)
  $R^2 = 93\%$ R^2 Adjusted = 91%

- Residual Stress = $0.057\ V + 71.05\ f - 0.148\ Vf + 66.08\ V^2$ (5.15)
  $R^2 = 94\%$ R^2 Adjusted = 93%

5.2.6 Response surface method analysis

Response surface methodology (RSM) is a convenient tool for visualizing the effects of selected factors on responses. The controlling variables are the input, and the output results are the response variables. The results are presented in the form of graphs or response surface plots and provide a clear picture of the variation of the response variable with the control factors.

In the present study, in order to predict the unknown response values with the corresponding cutting conditions as the controlling parameters, 3D statistical graphs or surface plot were produced to interpret the effects of the continuous parameters on the response values based on the fitted model.

For the three cutting tool geometries, the two factors considered were cutting speed and feed rate. Whereas the edge radius, the chamfer width and chamfer angle, and the sharp angle were kept constant at 0.03 mm, (0.35 mm; 20º), and 40º, respectively. Figures 5.16, 5.17 and 5.18 show the surface plots of the parametric effects on temperature, stress, chip thickness, wear depth and residual stress dependent variables for the round, chamfer, and sharp cutting tools, respectively.

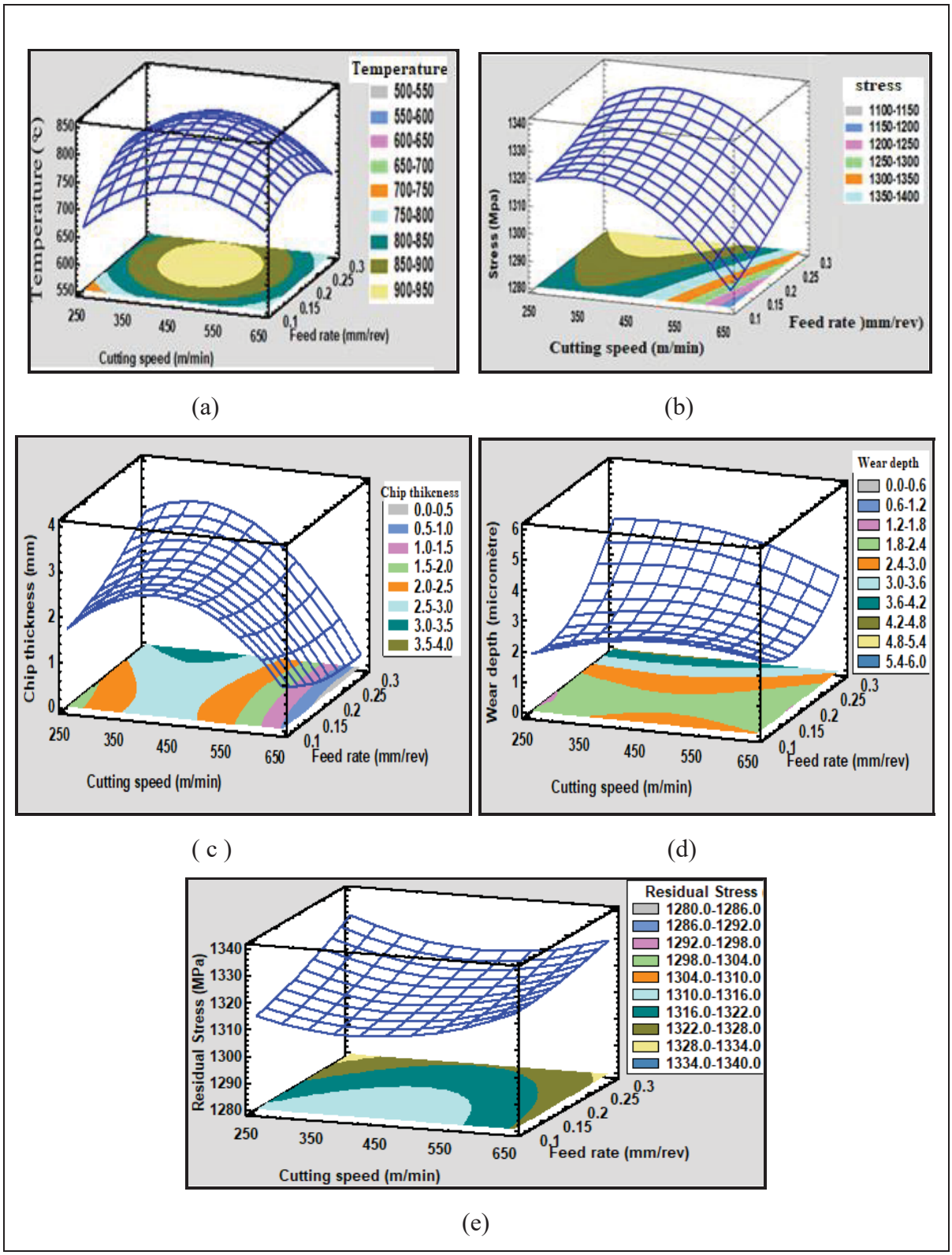

Figure 5.16 3D Surface plots of parametric effects on (a) temperature, (b) stress, (c) chip thickness and (d) wear depth for round cutting tool (Edge radius: 0.03 mm)

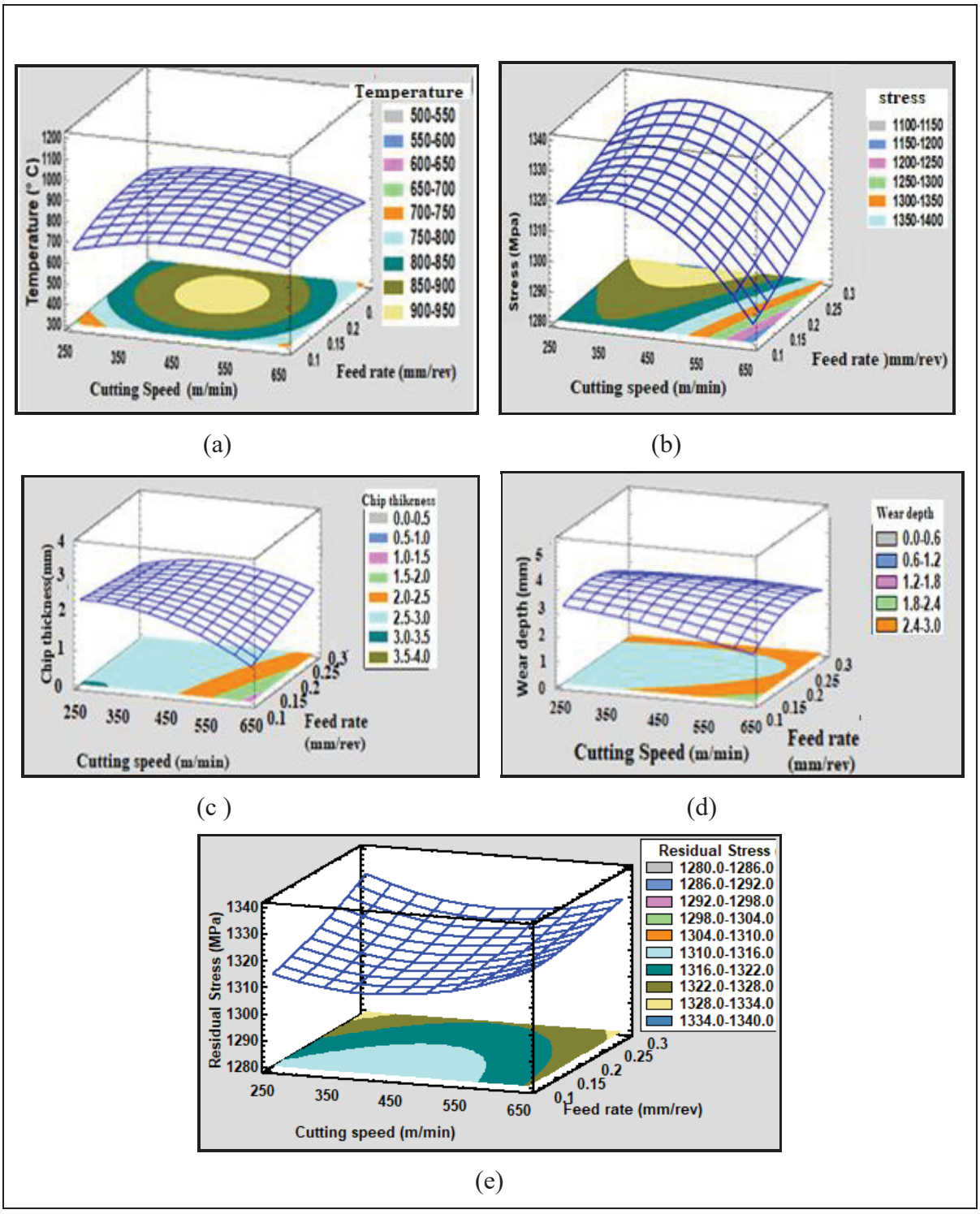

Figure 5.17 3D Surface plots of parametric effects on (a) temperature, (b) stress , (c) chip thickness and (d) wear depth (e) residual stress for cutting chamfer cutting tool (Chamfer width: 0.35 mm, Chamfer angle: 20º)

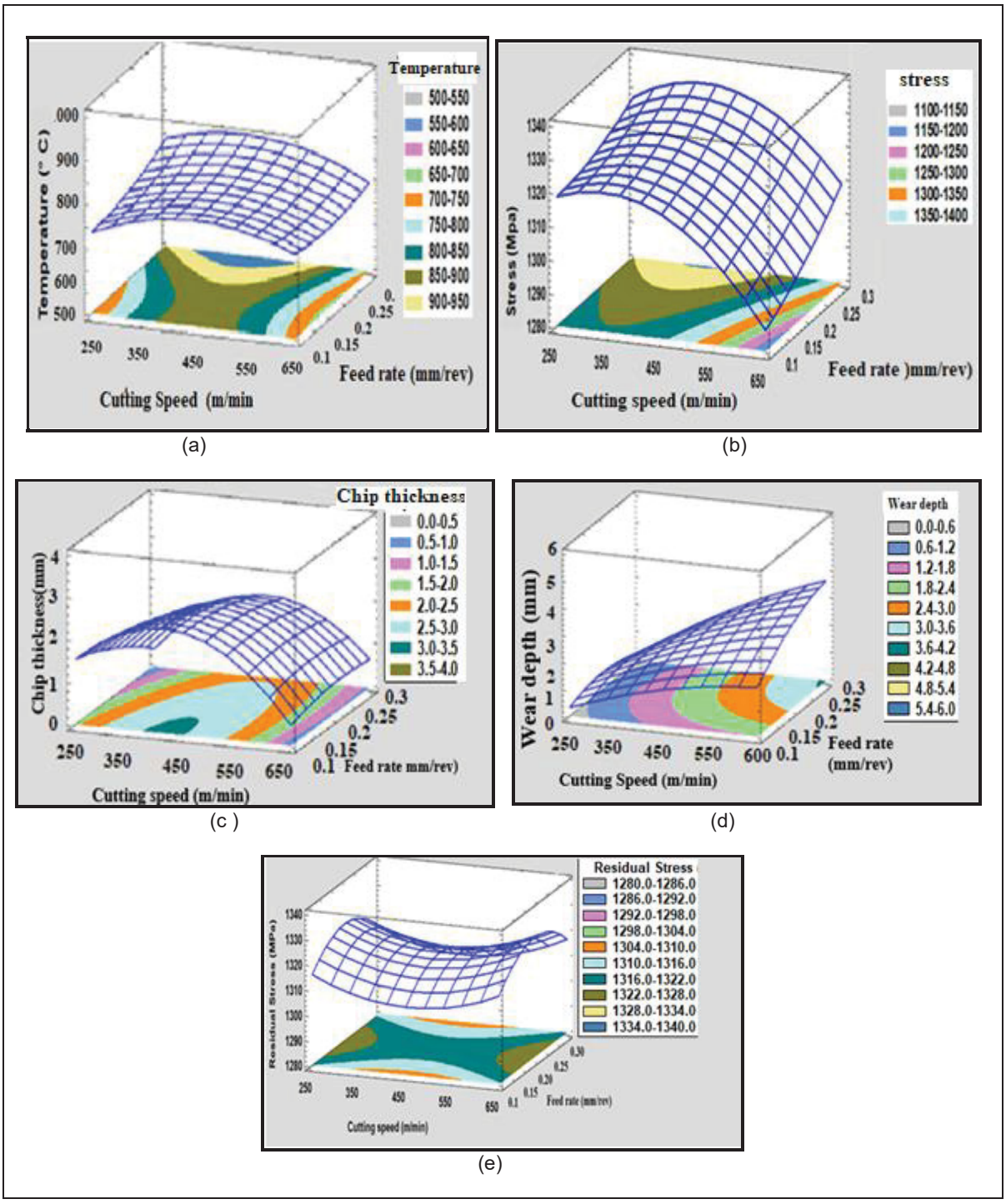

Figure 5.18 3D Surface plots of parametric effects on (a) temperature, (b) stress, (c) chip thickness and (d) wear depth (e) residual stress for sharp cutting tool (Sharp angle: 40º)

The response surface plots show how a specific dependent variable (represented along the Z-axis) varies continuously with two controlling parameters (plotted along the X and Y axes). They prove useful in optimization of processes and products through an understanding of the effect of the process variables on the factor or property in question.

5.3 Numerical determination of best output responses

In order to achieve a good cutting performance, the studied responses, the different tested parameters have to be optimized. Otherwise, it is about determining the parameter values corresponding to the minimum or the maximum of the variable output (responses). This technique was based on the fitted model developed previously using the response surface methodology (RSM). In the present study, the temperature, stress, chip thickness and tool wear should be minimized for cutting speed, feed rate, edge radius, chamfer width, chamfer angle and sharp angle. The numerical results of optimal responses were obtained using Statgraphics statistical analysis and are presented in Table 5.22 for the round, chamfer and sharp cutting tools.

Table 5.22 Numerical results of best responses for the three cutting tool designs (Round, chamfer and sharp)

Parameter						**Response**			
V (m/min)	f (mm/rev)	r_c (mm)	w_n (mm)	γ_n (º)	θ_n (º)	Variables	Round	Chamfer	Sharp
571	0.27	0.03	-	-	-	Temperature (ºC)	548	-	-
150	0.3	-	0.45	10	-		-	418	-
250	0.1	-	-	-	60		-	-	687
555	0.3	0.03	-	-	-	Stress (MPa)	1175	-	-
150	0.3	-	0.32	10	-		-	1108	-
794	0.1	-	-	-	60		-	-	1075
200	0.15	0.09	-	-	-	Chip thickness (mm)	1.05	-	-
150	0.3	-	0.17	20	-		-	2.97	-
250	0.13	-	-	-	60		-	-	1.12
385	0.15	0.03	-	-	-	Wear depth (μm)	0.99	-	-
695	0.15	-	0.45	24	-		-	18	-
553	0.1	-	-	-	30		-	-	0.46
300	0.2	0.03	-	-	-	Residual stress (MPa)	1355	-	
350	0.2	-	0.45	10	-		-	1450	
250	0.2	-	-	-	60		-	-	1330

From Table 5.22, the comparison between the results of the three different tool geometries revealed that a lower temperature was obtained for the chamfer cutting tool at low cutting speed, low chamfer angle, and high feed rate, high chamfer width. In order to obtain lower stress, the sharp cutting tool should be selected, using low feed rate, high sharp angle and a cutting speed of 794 m/min. Whereas, low cutting speed, low feed rate and high edge radius should be selected for the round cutting tool to obtain lower chip thickness.

For minimum of tool wear, it is preferable to choose the sharp cutting tool, using a low feed rate, a sharp angle of 30°and a cutting speed of 553 m/min. For residual stress, the minimum

values of 1330 MPa were also obtained for the sharp cutting tool at low cutting speed, high sharp angle, and the feed rate of 0.2 mm/rev.

A global optimization needs to be done later as in machining field a global optimization is often required. For example, obtain a better tool life, a good surface finish and a compressive stress, depending on the application targeted.

5.4 Conclusions

The present research studied numerically the effects of three cutting tool geometries (edge radius, chamfer width, chamfer angle, sharp angle) and the cutting parameters (cutting speed, feed rate) on cutting temperature, stress, chip thickness, wear depth and residual stress during orthogonal cutting of AISI1045 steel. The studied effects were evaluated statistically by performing the analysis of variance (ANOVA) in order to determine the factors influencing these machining properties. The results were further examined using statistical analysis and response surface analysis, followed by the optimization of the different parameters to identify good cutting tool preparation, which would correspond to good cutting performance.

From an analysis of the obtained results, the following may be concluded:

1. For the round edge tool, the quadratic term of the cutting speed (V^2) is a significant factor affecting the temperature, effective stress, tool wear and residual stress.

2. For the chamfer edge tool, the cutting speed is the important parameter that drives most of the studied machining characteristics.

3. For the sharp edge tool, the feed rate is the main factor influencing cutting temperature, effective stress, tool wear and residual stress.

4. The best cutting conditions for temperature are obtained at low cutting speed and high feed rate using a chamfered cutting tool comprising a low chamfer angle and high chamfer width.

The best cutting conditions when using a sharp cutting tool were obtained at a high cutting speed, low feed rate, and high sharp angle for the effective stress; at a cutting speed of 553 m/min, low feed rate and a sharp angle of 30° for the wear depth; and at low cutting speed, high sharp angle and a feed rate of 0.2 mm/rev for the residual stress.

GENERAL CONCLUSION

The present research work focused on investigating the effects of the various tool-edge preparation geometries and cutting parameters on the machining performance during orthogonal cutting of AISI 1045 steel. The cutting parameters were the cutting speed and the feed rate. The tool-edge geometries studied were round edge, chamfered edge and sharp edge. The studied machining characteristics were cutting temperature, cutting stress, chip thickness and wear depth. The study of the effects was realised numerically using 2D DEFORM software. Three research articles were produced from this thesis using the results presented in the Chapters 3, 4 and 5. From all the obtained results the main conclusions are given as follows:

- For a round tool, the cutting temperature, effective stress and wear width presented a linear behaviour with tool nose radius for all the studied cutting conditions.
- The numerical simulation results were validated experimentally and acceptable errors were obtained 4% to 8% for small nose radii and from 3% to 16% for large nose radii only for $r_c = 0.5$ mm.
- The numerical study of the effects of cutting round tool on the machining characteristics during orthogonal cutting of AISI 1045 steel showed that the cutting temperature, effective stress and wear width presented a linear behaviour with tool nose radius for small and large scales at all studied cutting condition.
- The numerical simulation results were validated experimentally (thanks to acceptable error)
- The interactive effects analysis between cutting parameters and tool geometries with the increase of tool nose radius and feed rate or cutting speed or rake angle showed and increase of cutting temperature and decrease of cutting stress but the tool wear showed an increase with the increase of cutting speed or rake angle and nose radius.

- The temperature for the large nose radii were higher than those for small nose radius, the contrary for cutting stress and little difference for tool wear.

- The combination of different of tool nose radius included small and large values with the cutting speed of 500 m/min affects strongly all the studied machining characteristics.
- The temperature, stress and wear depth increase with the increase of chamfer width and chamfer angle for chamfer tool and with sharp angle for sharp tool. Higher values obtained for widths w_n : 0.35, 0 and 45mm.
- The obtained results can provide valuable help in designing the tool edge microgeometry for better performance during machining.

CONTRIBUTION

The main contributions accomplished by the current research work can be summarized as follows:

- A 2D finite element model for the orthogonal cutting of AISI 1045 steel was developed to investigate the effects of edge radius, chamfer and sharp tool geometries and their interactions with cutting speed, feed rate, rake angle on machining forces, chip thickness temperature, residual stress, and tool wear.

- This research concept including the methodology can be applicable for other material categories and other cutting tool preparation designs. But the proper materials constitutive data must be determined and applied.

- The interactive effects between the cutting parameters and all studied cutting tool parameters (nose radius, chamfer width, chamfer angle, sharp angle, rake angle) of orthogonal cutting AISI 1045 steel were analysed statistically by ANOVA.

- The numerical comparison of the different parameters has helped to identify appropriate cutting tool preparation and the machining parameters that lead to good cutting performance.

The presented results can help designing new cutting-edge geometries without the need of time consuming and expensive machining tests.

RECOMMENDATION

Future research work related to this study will concentrate on the following aspects:

- Since most popular operations in industry involve oblique cutting. It is useful to perform 3D Finite element modeling of orthogonal cutting AISI 1045 steel for the interactive effects analysis between the parameters of different tool edge designs and the cutting parameters on the machining characteristics.

- An experimental work is required to further validate the different considered cutting tool edge designs and cutting parameters for 2D orthogonal cutting AISI 1045 steel, as function of different hardness and microstructures.

ANNEX I

FACTORIAL DESIGN FOR ROUND GEOMETRY CUTTING TOOL

Table A-I-1

Test Nº	Cutting speed (m/min)	Feed rate (mm/rev)	Edge radius (mm)	Test Nº	Cutting speed (m/min)	Feed rate (mm/rev)	Edge radius (mm)
1	200	0.15	0.03	33	600	0.15	0.03
2	200	0.15	0.05	34	600	0.15	0.05
3	200	0.15	0.07	35	600	0.15	0.07
4	200	0.15	0.09	36	600	0.15	0.09
5	200	0.2	0.03	37	600	0.2	0.03
6	200	0.2	0.05	38	600	0.2	0.05
7	200	0.2	0.07	39	600	0.2	0.07
8	200	0.2	0.09	40	600	0.2	0.09
9	200	0.25	0.03	41	600	0.25	0.03
10	200	0.25	0.05	42	600	0.25	0.05
11	200	0.25	0.07	43	600	0.25	0.07
12	200	0.25	0.09	44	600	0.25	0.09
13	200	0.3	0.03	45	600	0.3	0.03
14	200	0.3	0.05	46	600	0.3	0.05
15	200	0.3	0.07	47	600	0.3	0.07
16	200	0.3	0.09	48	600	0.3	0.09
17	400	0.15	0.03	49	800	0.15	0.03
18	400	0.15	0.05	50	800	0.15	0.05
19	400	0.15	0.07	51	800	0.15	0.07
20	400	0.15	0.09	52	800	0.15	0.09
21	400	0.2	0.03	53	800	0.2	0.03
22	400	0.2	0.05	54	800	0.2	0.05
23	400	0.2	0.07	55	800	0.2	0.07
24	400	0.2	0.09	56	800	0.2	0.09
25	400	0.25	0.03	57	800	0.25	0.03
26	400	0.25	0.05	58	800	0.25	0.05
27	400	0.25	0.07	59	800	0.25	0.07
28	400	0.25	0.09	60	800	0.25	0.09
29	400	0.3	0.03	61	800	0.3	0.03
30	400	0.3	0.05	62	800	0.3	0.05
31	400	0.3	0.07	63	800	0.3	0.07
32	400	0.3	0.09	64	800	0.3	0.09

ANNEX II

FACTORIAL DESIGN FOR CHAMFER GEOMETRY CUTTING TOOL

Table A-II-1

Test Nº	Cutting speed (m/min)	Feed rate (mm/rev)	Chamfer width (mm)	Chamfer angle	Test Nº	Cutting speed (m/min)	Feed rate (mm/rev)	Chamfer width (mm)	Chamfer angle (º)
1	150	0.15	0.15	10	36	650	0.15	0.15	20
2	150	0.15	0.25	20	37	650	0.15	0.25	10
3	150	0.15	0.35	30	38	650	0.15	0.35	40
4	150	0.15	0.45	40	39	650	0.15	0.45	30
5	150	0.2	0.15	30	40	650	0.2	0.15	40
6	150	0.2	0.25	40	41	650	0.2	0.25	30
7	150	0.2	0.35	10	42	650	0.2	0.35	20
8	150	0.2	0.45	20	43	650	0.2	0.45	10
9	150	0.25	0.15	40	44	650	0.25	0.15	10
10	150	0.25	0.25	10	45	650	0.25	0.25	40
11	150	0.25	0.35	20	46	650	0.25	0.35	30
12	150	0.25	0.45	30	47	650	0.25	0.45	20
13	150	0.3	0.15	20	48	650	0.3	0.15	30
14	150	0.3	0.25	30	49	650	0.3	0.25	20
15	150	0.3	0.35	20	50	650	0.3	0.35	10
16	150	0.3	0.35	40	51	650	0.3	0.45	40
17	150	0.3	0.45	10	52	950	0.15	0.15	40
18	350	0.15	0.15	20	53	950	0.15	0.25	30
19	350	0.15	0.15	30	54	950	0.15	0.35	10
20	350	0.15	0.25	40	55	950	0.15	0.45	20
21	350	0.15	0.35	20	56	950	0.2	0.15	20
22	350	0.15	0.45	10	57	950	0.2	0.25	10
23	350	0.2	0.15	10	58	950	0.2	0.25	20
24	350	0.2	0.25	20	59	950	0.2	0.35	30
25	350	0.2	0.35	40	60	950	0.2	0.45	40
26	350	0.2	0.45	30	61	950	0.25	0.15	30
27	350	0.25	0.15	20	62	950	0.25	0.25	20
28	350	0.25	0.25	30	63	950	0.25	0.35	40
29	350	0.25	0.35	10	64	950	0.25	0.45	10
30	350	0.25	0.45	10	65	950	0.25	0.45	30
31	350	0.25	0.45	40	66	950	0.3	0.15	10
32	350	0.3	0.15	40	67	950	0.3	0.25	40
33	350	0.3	0.25	10	68	950	0.3	0.35	10
34	350	0.3	0.35	30	69	950	0.3	0.35	20
35	350	0.3	0.45	20	70	950	0.3	0.45	30

ANNEX III

FACTORIAL DESIGN FOR SHARP GEOMETRY CUTTING TOOL

Table A-III-1

Test Nº	Cutting speed	Feed rate (mm/rev)	Sharp angle	Test Nº	Cutting speed	Feed rate (mm/rev)	Sharp angle
1	250	0.1	30	21	500	0.3	60
2	250	0.1	60	22	750	0.1	30
3	250	0.15	30	23	750	0.1	40
4	250	0.15	40	24	750	0.1	60
5	250	0.15	50	25	750	0.15	50
6	250	0.25	40	26	750	0.15	60
7	250	0.25	50	27	750	0.25	30
8	250	0.25	60	28	750	0.25	50
9	250	0.3	40	29	750	0.3	30
10	250	0.3	60	30	750	0.3	40
11	500	0.1	40	31	750	0.3	50
12	500	0.1	50	32	1000	0.1	30
13	500	0.1	60	33	1000	0.1	50
14	500	0.15	30	34	1000	0.15	30
15	500	0.15	40	35	1000	0.15	60
16	500	0.15	60	36	1000	0.25	30
17	500	0.25	40	37	1000	0.25	40
18	500	0.25	50	38	1000	0.25	60
19	500	0.3	30	39	1000	0.3	40
20	500	0.3	50	40	1000	0.3	50

APPENDIX I

PUBLICATION LIST

JOURNAL PUBLICATIONS

- Zakaria Ahmed M. Tagiuri, Thien-My Dao, Agnes Marie Samuel, Victor Songmene. A Numerical Model for Predicting the Effect of Tool Nose Radius on Machining Process Performance during Orthogonal Cutting of AISI 1045 Steel. Materials 2022, 15, 3369
- Zakaria Ahmed M. Tagiuri, Thien-My Dao, Agnes Marie Samuel, Victor Songmene. Numerical prediction of the performance of chamfered and sharp cutting tools during orthogonal cutting of AISI 1045 steel. Processes 2022, 10, 2171

LIST OF BIBLIOGRAPHICAL REFERENCES

Afrasiabi, M., Saelzer, J., Berger, S., Iovkov, I., Klippel, H., Röthlin, M., Zabel, A., Biermann, D., & Wegener, K. (2021). A numerical-experimental study on orthogonal cutting of aisi 1045 steel and ti6al4v alloy: Sph and fem modeling with newly identified friction coefficients. *Metals*, *11*(11). https://doi.org/10.3390/met11111683

Altintas, Y. (2012). *Manufacturing Automation: Metal Cutting Mechanics, Machine Tool Vibrations, and CNC Design (2nd ed.). Cambridge: Cambridge University Press. doi:10.1017/CBO9780511843723*.

Al-zkeri, I., Rech, J., Altan, T., Hamdi, H., & Valiorgue, F. (2009). Optimization of the cutting edge geometry of coated carbide tools in dry turning of steels using a finite element analysis. *Mach. Sci. Technol.*, *13*(April), 36–51. https://doi.org/10.1080/10910340902776051

Aouici, H., Yallese, M. A., Fnides, B., Chaoui, K., & Mabrouki, T. (2011). Modeling and optimization of hard turning of X38CrMoV5 ’ 1 steel with CBN tool : Machining parameters effects on flank wear and surface roughness †. *Journal of Mechanical Science and Technology*, *25*(11), 2843–2851. https://doi.org/10.1007/s12206

Avallone et al. (2018). Machining Processes and Machine Tools. *Marks Standard Handbook for Mechanical Engineers*, *16*, 1–75.

Azom.(2000). *AISI 1045 Carbon Steel (UNS G10450). In properties data.* Https://Www.Azom.Com/Article.Aspx?ArticleID=9153.Accessed July 7,2022. Boothroyd, G., & Knight, W. A. (2006). *Fundamentals of machining and machine tools (3rd ed.).Boca Raton, Flor.: CRC/Taylor and Francis.*

Bassett E, Ko¨ hler J, Denkena B (2012) On the Honed Cutting Edge and its Side Effects During Orthogonal Turning Operations of AISI1045 with Coated WC-Co Inserts. CIRP *Journal of Manufacturing Science and Technology* 5:108–126.

Bordin, F. M., & Zeilmann, R. P. (2014). Effect of the Cutting Edge Preparation on the Surface Integrity after Dry Drilling *Procedia CIRP*,*13*,103–107. https://doi.org/10.1016/J.PROCIR.2014.04.018

Bouzakisa, K.-D., Michailidis, N., Skordaris, G., Kombogiannis, S., Hadjiyiannis, S., Efstathiou, K., Erkens, G., Rambadt, S., & Wirth, I. (2002). Effect of the Cutting Edge Radius and its Manufacturing Procedure , on the Milling Performance of PVD Coated Ceme ... *CIRP Annals - Manufacturing Technology*, *51*(1), 61–64.

Chaofeng, L., Zengqiang, W., Guang, Z., & Lei, L. (2015). *The effect of cutting speed on residual stresses when orthogonal Workpiece Tool*. *01035*, 1–4. https://doi.org/10.1051/epjconf/20159401035

Cheng, X., Jin, S., Liao, T., & Jiang, F. (2017). Optimizing the geometric parameters of chamfered edge for rough machining Fe – Cr – Ni stainless steel. *Int.J. Adv. Manuf. Technol.*, *91*(1–4), 137–146. https://doi.org/10.1007/s00170-016-9736-4

Cheng, X., Zha, X., & Jiang, F. (2016). Optimizing the geometric parameters of cutting edge for rough machining Fe-Cr-Ni stainless steel. *The International Journal of Advanced Manufacturing Technology*, *85*(1–4), 683–693. https://doi.org/10.1007/s00170-015-7892-6

Childs, T., Maekawa, K., Obikawa, T., & Yamane, Y. (2000). *Metal Machining : Theory and Applications. Book published by Arnold in Great Britain*.

Chowdhury, M. A., Khalil, M. K., Nuruzzaman, D. M., & Rahaman, M. L. (2011). The effect of sliding speed and normal load on friction and wear property of aluminum. *International Journal of Mechanical and Mechanics Engineering*, *11*(1), 53–57.

Daoud, M., Chatelain, J. F., & Bouzid, A. (2015). Effect of rake angle on Johnson-Cook material constants and their impact on cutting process parameters of Al2024-T3 alloy machining simulation. *International Journal of Advanced Manufacturing Technology*, *81*(9–12), 1987–1997. https://doi.org/10.1007/s00170-015-7179-y

Davoudinejad, A., & Noordin, M. Y. (2014). Effect of cutting edge preparation on tool performance in hard-turning of DF-3 tool steel with ceramic tools. *Journal of Mechanical Science and Technology*, *28*(11), 4727–4736. https://doi.org/10.1007/s12206-014-1039-9

Denkena, B., & Biermann, D. (2014). Cutting edge geometries. *CIRP Annals - Manufacturing Technology*, *63*(2), 631–653. https://doi.org/10.1016/j.cirp.2014.05.009

Denkena, B., Merklein, M., Bach, F.-W., Bouzakis, K.-D., & Toenshoff, M. G. and H.-K. (2010). Cutting Edge Preparation by Means of Abrasive Brushing. *Key Engineering Materials*, *438*, 1–7.

E D'Errico, G., Sante, B., & Emanuele, G. (1998). Tool-life reliability of cermet inserts in milling tests. *Journal of Materials Processing Technology*, *77*(1–3), 337–343.

El-Hossainy, T. M., El-Zoghby, A. A., Badr, M. A., Maalawi, K. Y., & Nasr, M. F. (2010). Cutting Parameter Optimization when Machining Different Materials Cutting Parameter Optimization when Machining Different Materials. *Mater. Manuf. Processes*, *25*(931134518), 1101–1114. https://doi.org/10.1080/10426914.2010.480998

Elgnemi, T., Songmene, V., Kouam, J., Jun, M. B. G., & Agnes Marie, S. (2021). *Experimental Investigation on Dry Routing of CFRP Composite :*

Emamian, A. (2017). the Effect of Tool Edge Radius on Cutting Conditions Based on updated Lagrangian formulation in finite element method. *Master Dissertation, McMaster University, Canada*, 104.

Engineering ToolBox. (2003). *Convective Heat Transfer*. [Online] Https://Www.Engineeringtoolbox.Com/Convective-Heat-Transfer-D_430.Html. Accessed June 12 2022.

Gao, P., Liang, Z., Wang, X., Li, S., & Zhou, T. (2018). Effects of different chamfered cutting edges of micro end mill on cutting performance. *International Journal of Advanced Manufacturing Technology*, *96*(1–4), 1215–1224. https://doi.org/10.1007/s00170-018-1640-7

Gregório, A. V. L., Silva, T. E. F., Reis, A. P., de Jesus, A. M. P., & Rosa, P. A. R. (2022). A Methodology for Tribo-Mechanical Characterization of Metallic Alloys under Extreme Loading and Temperature Conditions Typical of Metal Cutting Processes. *Journal of Manufacturing and Materials Processing*, *6*(2). https://doi.org/10.3390/jmmp6020046

Jacobus, K., DeVor, R. E., & Kapoor, S. G. (2000). Machining-induced residual stress: Experimentation and modeling. *Journal of Manufacturing Science and Engineering, Transactions of the ASME*, *122*(1), 20-31. https://doi.org/10.1115/1.538906

Jamel, R. S. (2012). 3-D Finite Element Analysis Of Effect Cutting Edge Geometry on Cutting Forces , Effective Stress , Temperature And Tool Wear In Turning. *J. Kerbala Univ.*, *10*(2).

Jaspers, S. P. F. C., Dautzenberg, J. H., & Taminiau, D. A. (1998). Temperature measurement in orthogonal metal cutting. *International Journal of Adv. Manufacture Technology*, *14*, 7–12.

Javidikia, M., Sadeghifar, M., Songmene, V., & Jahazi, M. (2020). On the impacts of tool geometry and cutting conditions in straight turning of aluminum alloys 6061-T6: an experimentally validated numerical study. *International Journal of Advanced Manufacturing Technology*, *106*(9–10), 4547–4565. https://doi.org/10.1007/s00170-020-04945-3

Jiang, L., & Wang, D. (2019). Finite-element-analysis of the effect of different wiper tool edge geometries during the hard turning of AISI 4340 steel. *Simul. Model. Pract. Theory*, *94*, 250–263.

Kalpakjian, S., & Schmid, S. R. (2009). *Chapter 21: Fundamentals of Machining ,part IV: Machining processes and Machine tools.Manufacturing Engineering and Technology,Sixth Edition,p.556*.

Khalili, K., & Safaei, M. (2009). FEM analysis of edge preparation for chamfered tools. *International Journal of Material Forming*, *2*(4), 217–224. https://doi.org/10.1007/s12289-009-0405-0

Li, B. (2012). A review of tool wear estimation using theoretical analysis and numerical simulation technologies. *International Journal of Refractory Metals and Hard Materials*, *35*, 143–151. https://doi.org/10.1016/j.ijrmhm.2012.05.006

Liao, T., Jiang, T., Yan, L., & Cheng, X. (2017). Optimizing the geometric parameters of cutting edge for finishing machining of Fe-Cr-Ni stainless steel. *Int. J. Adv .Manuf. Technol.*, *88*(5–8), 2061–2073. https://doi.org/10.1007/s00170-016-8895-7

Makadia, A. J., & Nanavati, J. I. (2014). Analysis of Surface Roughness in Turning with Coated Carbide Cutting Tools : Prediction Model and Cutting Conditions Optimization Analysis of Surface Roughness in Turning with Coated Carbide Cutting Tools : Prediction Model and Cutting Conditions Optimiza. *5th International & 26th All India Manufacturing Technology, Design and Research Conference.IIT Guwahati Assam, India.*, *December 2014*, 20-1,20-6.

Marinov, V. (2018). *ME 364 Manufacturing Technology, Lecture notes: Cutting forces,p.71*.
Özel, T., & Zeren, E. (2007). Finite element modeling the influence of edge roundness on the stress and temperature fields induced by high-speed machining. *Adv. Manuf. Technol.*, *35*(February), 255–267. https://doi.org/10.1007/s00170-006-0720-2

Marcos Guilherme Carvalho Braulio Barbosa1 (2021) . Effect of cutting parameters and cutting edge preparation on milling of VP20TS steel

Nasr, M.N.A.; Ng, E.-G. (2007). Elbestawi, M.A. Modelling the effects of tool-edge radius on residual stresses when orthogonal cutting AISI 316L. Int. J. Mach. Tools Manuf. 2007, 47, 401–411.

Ozlu , E. (2008). *Analytical modeling of cutting process mechanics and dynamics for simulation of industrial machining operations* [Ph.D.]. Sabanci University, Turkey. PDF4PRO,amp.(n.d.) *Machining Processes, IME 240*.

Qasim, A., Nisar, S., Shah, A., Khalid, M. S., & Sheikh, M. A. (2015). Optimization of process parameters for machining of AISI-1045 steel using Taguchi design and ANOVA. *Simulation Modelling Practice and Theory*, *59*, 36–51.

Ren, H., & Altintas, Y. (2000). Mechanics of machining with chamfered tools. *Journal of Manufacturing Science and Engineering, Transactions of the ASME*, *122*(4), 650–659. https://doi.org/10.1115/1.1286368

Rodríguez, C. (2009). Cutting edge preparation of precision cutting tools by applying micro-abrasive jet machining and brushing. In *Ph.D. Thesis,, Kassel University, Kassel, Germany*. http://books.google.com/books?hl=en&lr=&id=NfRFEgFRmD4C&oi=fnd&pg=PA1&dq=Cutting+edge+preparation+of+precision+cutting+tools+by+applying+micro-abrasive+jet+machining+and+brushing&ots=Gg-zYmpGzY&sig=q4ztuTawKtjrVKvtbx4ZHTPCho4%5Cnhttp://books.google.com/bo

Shnfir, M. (2020). Effect of Tool Edge Preparation and Hardness of Workpiece on Machinability of AISI 1045 Steel. In *Ph.D. Thesis, École de Technologie Supérieure, Montréal, Canada*.

Shnfir, M., Olufayo, O. A., & Jomaa, W. (2019). Machinability Study of Hardened 1045 Steel When Milling with Ceramic Cutting Inserts. *Materials*, *12*, 3974.

Shravankumar, C., & Kodli, B. S. (2013). A Finite Element Analysis of Orthogonal Machining Using Different Tool Edge Geometries and End Relief Angles. *Int. J. Eng. Res. Technol.*, *2*(10), 39–45.

Tagiuri, Z. A. M., Dao, T., Samuel, A. M., & Songmene, V. (2022). A Numerical Model for Predicting the Effect of Tool Nose Radius on Machining Process Performance during Orthogonal. *Materials*, *15*(9), 3369.

Tiffe, M., Aßmuth, R., Saelzer, J., & Biermann, D. (2019). Investigation on cutting edge preparation and FEM assisted optimization of the cutting edge micro shape for machining of nickel-base alloy. *Prod. Eng.*, *13*, 459–467.
Töenshoff, H. K., & Denkena, B. (2013). Basics of cutting and abrasive processes. *Lecture Notes in Production Engineering (2013 Ed.)*.

Ucun, I., Aslantas, K., & Ucan, I. (2011). Finite Element Modeling of Machining of AISI 1045 With Ceramic Cutting Tool. *JoMFT*, *4*(1), 1–17.

Uhlmann, E., Oberschmidt, D., Kuche, Y., Löwenstein, A., & Winker, I. (2016). Effects of Different Cutting Edge Preparation Methods on Micro Milling Performance. *Procedia CIRP*, *46*, 352–355. https://doi.org/10.1016/J.PROCIR.2016.04.004
Umbert, S. M. (2017). *Cutting Forces in Turning Operations. Bachelor's thesis, Norwegian University of Science and Technology*.

Wan, L., Wang, D., & Gao, Y. (2015). Investigations on the effects of different tool edge geometries in the finite element simulation of machining. *Strojniski Vestnik/Journal of Mechanical Engineering*, *61*(3), 157–166. https://doi.org/10.5545/sv-jme.2014.2051

Wang, W., Saifullah, M. K., Aßmuth, R., Biermann, D., Arif, A. F. M., & Veldhuis, S. C. (2020). Effect of edge preparation technologies on cutting edge properties and tool performance. *International Journal of Advanced Manufacturing Technology*, *106*(5–6), 1823–1838. https://doi.org/10.1007/s00170-019-04702-1

Xingzhong, Z., Jiajun, L., Baoliang, Z., Hezhou, M., & Zhenbi, L. (1999). Wear behavior of Si 3 N 4 ceramic cutting tool material against stainless steel in dry and water-lubricated conditions. *Ceram. Int.*, *25*, 309–315.

Yen, Y.-C., Jain, A., & Altan, T. (2004). A finite element analysis of orthogonal machining using different tool edge geometries. *Journal of Materials Processing Technology*, *146*(1), 72–81.

Yen, Y. C., Jain, A., & Altan, T. (2004). A finite element analysis of orthogonal machining using different tool edge geometries. *Journal of Materials Processing Technology*, *146*(1), 72–81. https://doi.org/10.1016/S0924-0136(03)00846-X

Zakaria, T. (2019). *Understanding of Cutting Tool Edge Preparation and Their Impacts on Machining Process Performance. DGA1031 Exam report,ETS: Montréal, QC, Canada*.

Zhuang, K., Stief, P., Dantan, J., Etienne, A., & Siadat, A. (2020). Effect of cutting edge microgeometry on surface roughness and white layer France and white layer Effect of cutting edge microgeometry on surface roughness in turning AISI steel in turning AISI 52100 steel. *Procedia CIRP*, *87*, 53–58. https://doi.org/10.1016/j.procir.2020.02.079

Zhuang, K., Weng, J., Zhu, D., & Ding, H. (2018). Analytical modeling and experimental validation of cutting forces considering edge effects and size effects with round chamfered ceramic tools. *J. Manuf. Sci. Eng.*, *140*(8). https://doi.org/081012.